

**NASA  
Reference  
Publication  
1105**

June 1983

# Rolling-Element Bearings

Bernard J. Hamrock  
and William J. Anderson

NASA  
RP  
1105  
c.1



LOAN COPY: RETURN TO  
AFWL TECHNICAL LIBRARY  
KIRTLAND AFB, N.M.

**NASA**



25th Anniversary  
1958-1983

**NASA  
Reference  
Publication  
1105**

1983

TECH LIBRARY KAFB, NM



0063242

# Rolling-Element Bearings

**Bernard J. Hamrock**  
*Lewis Research Center  
Cleveland, Ohio*

**William J. Anderson**  
*Bearings and Lubrication  
North Olmsted, Ohio*

**NASA**  
National Aeronautics  
and Space Administration

Scientific and Technical  
Information Branch

ERRATA

NASA RP-1105

Rolling-Element Bearings

B.J. Hamrock and W.J. Anderson

Page 1, definition of  $F$  should read as follows:

$F$  Load on element, N

Page 1, definition of  $R$  should read as follows:

$R$  Effective radius of curvature, m

Page 2, definition of delta ( $\delta$ ) should read as follows:

$\delta$  Total race deflection including deformation and clearance takeup, m

Page 20, equation (44), based on ESDU 78035 (1978, as revised 1995) should read as follows:

$$\delta = \frac{2WR_x}{\pi} \left[ \ln\left(\frac{4r_{ax}}{b}\right) + \ln\left(\frac{4r_{bx}}{b}\right) - 1 \right] \quad (44)$$

Page 20, equation (47) should read as follows:

$$K_1 = \frac{\pi IE'}{2} \frac{1}{\left[ \ln\left(\frac{4r_{ax}}{b}\right) + \ln\left(\frac{4r_{bx}}{b}\right) - 1 \right]} \quad (47)$$

Issued February 2011

# Contents

	Page
Symbols.....	1
1. Introduction.....	2
1.1 Historical Overview.....	2
1.2 Conformal and Nonconformal Surfaces.....	3
1.3 Bearing Selection.....	3
2. Bearing Types.....	4
2.1 Ball Bearings.....	5
2.2 Roller Bearings.....	7
3. Geometry.....	8
3.1 Geometry of Ball Bearings.....	8
3.2 Geometry of Roller Bearings.....	12
4. Kinematics.....	13
5. Materials and Manufacturing Processes.....	15
5.1 Ferrous Alloys.....	16
5.2 Ceramics.....	16
6. Separators.....	17
7. Contact Stresses and Deformations.....	17
7.1 Elliptical Contacts.....	17
7.2 Rectangular Contacts.....	20
8. Static Load Distribution.....	20
8.1 Load Deflection Relationships.....	20
8.2 Radially Loaded Ball and Roller Bearings.....	20
8.3 Thrust-Loaded Ball Bearings.....	22
8.4 Preloading.....	24
9. Rolling Friction and Friction in Bearings.....	25
9.1 Rolling Friction.....	25
9.2 Friction Losses in Rolling-Element Bearings.....	27
10. Lubricants and Lubrication Systems.....	27
10.1 Solid Lubrication.....	27
10.2 Liquid Lubrication.....	28
11. Elastohydrodynamic Lubrication.....	29
11.1 Relevant Equations.....	29
11.2 Dimensionless Grouping.....	30



11.3 Minimum-Film-Thickness Formula .....	30
11.4 Pressure and Film Thickness Plots .....	31
12. Rolling Bearing Fatigue Life .....	32
12.1 Contact Fatigue Theory .....	32
12.2 The Weibull Distribution.....	32
12.3 Lundberg-Palmgren Theory.....	33
12.4 The AFBMA Method .....	35
12.5 Life Adjustment Factors .....	35
13. Dynamic Analyses and Computer Codes .....	36
13.1 Quasi-Static Analyses .....	36
13.2 Dynamic Analyses .....	37
14. Applications .....	37
14.1 Cylindrical Roller Bearing Problem .....	37
14.2 Radial Ball Bearing Problem .....	39
References .....	42

Rolling-element bearings are a precision, yet simple, machine element of great utility. In this report we draw together the current understanding of rolling-element bearings. A brief history of rolling-element bearings is reviewed in the Introduction, and subsequent sections are devoted to describing the types of rolling-element bearings, their geometry and kinematics, as well as the materials they are made from and the manufacturing processes they involve. The organization of this report is such that unloaded and unlubricated rolling-element bearings are considered in the first six sections, loaded but unlubricated rolling-element bearings are considered in sections 7 to 9, and loaded and lubricated rolling-element bearings are considered in sections 10 to 14. The recognition and understanding of elastohydrodynamic lubrication, covered briefly in sections 11, 12, and 14, represents one of the major developments in rolling-element bearings in the last 18 years.

## Symbols

$B$	Total conformity of bearing	$F_t$	Applied thrust load, N
$b$	Semiminor axis of roller contact, m	$\mathcal{F}$	Elliptic integral of first kind
$C$	Dynamic load capacity, N	$\bar{\mathcal{F}}$	Approximate elliptic integral of first kind
$c_1, \dots, c_4$	Constants	$f$	Race conformity ratio
$D$	Distance between race curvature centers, m	$f_a$	rms surface finish of rolling element
$\bar{D}$	Material factor	$f_b$	rms surface finish of race
$D_x$	Diameter of contact ellipse along $x$ axis, m	$f_c$	Coefficient dependent on materials and bearing type (table 14)
$D_y$	Diameter of contact ellipse along $y$ axis, m	$G$	Dimensionless materials parameter, $\xi E'$
$d$	Rolling-element diameter	$\bar{G}$	Speed effect factor
$d_a$	Overall diameter of bearing (fig. 5), m	$H$	Dimensionless film thickness, $h/R_x$
$d_b$	Bore diameter, mm	$\bar{H}$	Misalignment factor
$d_e$	Pitch diameter, m	$H_{\min}$	Dimensionless minimum film thickness
$d_i$	Inner-race diameter, m	$h$	Film thickness, m
$d_o$	Outer-race diameter, m	$J$	Number of stress cycles
$E$	Modulus of elasticity, N/m <sup>2</sup>	$K$	Load-deflection constant
$E'$	Effective elastic modulus, $2 \left/ \left( \frac{1 - \nu_a^2}{E_a} + \frac{1 - \nu_b^2}{E_b} \right) \right., \text{ N/m}^2$	$K_1$	Load-deflection constant for roller bearing
$\bar{E}$	Metallurgical processing factor	$K_{1.5}$	Load-deflection constant for ball bearing
$\varepsilon$	Elliptic integral of second kind	$k$	Ellipticity parameter, $D_y/D_x$
$\bar{\varepsilon}$	Approximate elliptic integral of second kind	$\bar{k}$	Approximate ellipticity parameter
$e$	Percentage of error	$L$	Fatigue life
$\bar{F}$	Lubrication factor	$L_A$	Adjusted fatigue life
$F$	Applied load, N	$L_{10}$	Fatigue life where 90 percent of bearing population will endure
$F'$	Load per unit length, N/m	$L_{50}$	Fatigue life where 50 percent of bearing population will endure
$F_e$	Bearing equivalent load, N	$l$	Bearing length, m
$F_r$	Applied radial load, N	$l_r$	Roller effective length, m
		$l_t$	Roller length, m
		$l_v$	Length dimension in stressed volume, m
		$M$	Probability of failure
		$m$	Number of rows of rolling elements
		$N$	Rotational speed, rpm
		$n$	Number of rolling elements
		$P$	Dimensionless pressure, $p/E'$
		$P_d$	Diametral clearance, m
		$P_e$	Free endplay, m
		$p$	Pressure, N/m <sup>2</sup>
		$q$	Constant, $\pi/2 - 1$
		$R$	Curvature sum, m
		$R_x$	Effective radius in $x$ direction, m
		$R_y$	Effective radius in $y$ direction, m
		$r$	Race curvature radius, m
		$r_a$	Ball radius, m
		$r_c$	Roller corner radius, m
		$r_y$	Radius of roller in $y$ direction, m
		$S$	Probability of survival
		$s$	Shoulder height, m



$T$	Tangential force, N
$U$	Dimensionless speed parameter, $u\eta_0/E'R_x$
$u$	Mean surface velocity in direction of motion, $(u_a+u_b)/2$ , m/s
$V$	Stressed volume, $m^3$
$v$	Elementary volume, $m^3$
$W$	Dimensionless load parameter, $F/E'R_x^2$
$X, Y$	Factors for calculation of equivalent load
$x, y, z$	Coordinate system
$Z$	Constant defined by eq. (58)
$Z_o$	Depth of maximum shear stress, m
$\alpha$	Radius ratio, $R_y/R_x$
$\beta$	Contact angle, deg
$\beta'$	Iterated value of contact angle, deg
$\beta_f$	Free or initial contact angle, deg
$\Gamma$	Curvature difference
$\delta$	Total elastic deformation, m
$\bar{\delta}$	Approximate total elastic deformation, m
$\xi$	Pressure-viscosity coefficient of lubrication, $m^2/N$
$\eta$	Absolute viscosity at gage pressure, N s/m <sup>2</sup>
$\eta_0$	Viscosity at atmospheric pressure, N s/m <sup>2</sup>
$\theta$	Angle used to define shoulder height
$\Lambda$	Film parameter (ratio of film thickness to composite surface roughness)
$\mu$	Coefficient of rolling friction
$\nu$	Poisson's ratio
$\rho$	Lubricant density, N s <sup>2</sup> /m <sup>4</sup>
$\rho_0$	Density at atmospheric pressure, N s <sup>2</sup> /m <sup>4</sup>
$\sigma_{max}$	Maximum Hertzian stress, N/m <sup>2</sup>
$\gamma_0$	Maximum shear stress, N/m <sup>2</sup>
$\psi$	Angular location
$\psi_l$	Limiting value of $\psi$
$\omega$	Angular velocity, rad/s
$\omega_B$	Angular velocity of rolling-element-race contact, rad/s
$\omega_b$	Angular velocity of rolling element about its own center, rad/s
$\omega_c$	Angular velocity of rolling element about shaft center, rad/s

Subscripts:

$a$	Solid $a$
$b$	Solid $b$
$i$	Inner race
$o$	Outer race
$x, y, z$	Coordinate system

Superscript:

$(\bar{\quad})$	Approximate
-----------------	-------------

## 1. Introduction

The purpose of a bearing is to provide relative positioning and rotational freedom while transmitting a load between two structures, usually a shaft and a housing. The basic form and concept of the rolling-element bearing are simple. If loads are to be transmitted between surfaces in relative motion in a machine, the action can be facilitated in a most effective manner if rolling elements are interposed between the sliding members. The frictional resistance encountered in sliding is then largely replaced by the much smaller resistance associated with rolling, although the arrangement is inevitably afflicted with high stresses in the restricted regions of effective load transmission.

### 1.1 Historical Overview

The precision rolling-element bearing of the twentieth century is a product of exacting technology and sophisticated science. It is simple in form and concept and yet very effective in reducing friction and wear in a wide range of machinery. The spectacular development of numerous forms of rolling-element bearings in the twentieth century is well known and documented, but it is possible to trace the origins and development of these vital machine elements to periods long before there was a large industrial demand for such devices and certainly long before there were adequate machine tools for their effective manufacture in large quantities. A complete historical development of rolling-element bearings is given in Hamrock and Dowson (1981), and therefore only some of its conclusions are presented here.

The influence of general technological progress on the development of rolling-element bearings, particularly those concerned with the movement of heavy stone building blocks and carvings, road vehicles, precision instruments, water-raising equipment, and windmills is discussed in Hamrock and Dowson (1981). The concept of rolling-element bearings emerged in embryo form in Roman times, faded from the scene during the Middle Ages, was revived during the Renaissance, developed steadily in the seventeenth and eighteenth centuries for various applications, and was firmly established for individual road carriage bearings during the Industrial Revolution. Toward the end of the nineteenth century, the great merit of ball bearings for bicycles promoted interest in the manufacture of accurate steel balls. Initially, the balls were turned from bar on special lathes, with individual general machine manufacturing companies making their own bearings. Growing demand

for both ball and roller bearings encouraged the formation of specialist bearing manufacturing companies at the turn of the century and thus laid the foundations of a great industry. The advent of precision grinding techniques and the availability of improved materials did much to confirm the future of the new industry.

The essential features of most forms of modern rolling-element bearings were therefore established by the second half of the nineteenth century, but it was the formation of specialist, precision-manufacturing companies in the early years of the twentieth century that finally established rolling-element bearings as a most valuable, high-quality, readily available machine component. The availability of ball and roller bearings in standard sizes has had a tremendous impact on machine design throughout the twentieth century. Such bearings still provide a challenging field for further research and development, and many engineers and scientists are currently engaged in exciting and demanding research projects in this area. In many cases, new and improved materials or enlightened design concepts have extended the life and range of application of rolling-element bearings, yet in other respects much remains to be done in explaining the extraordinary operating characteristics of bearings that have served our technology so very well for almost a century. Recent developments in the understanding and analysis of one important aspect of rolling-element performance—the lubrication mechanism in small, highly stressed conjunctions between the rolling element and the rings or races—is considered in the elastohydrodynamic lubrication section.

### 1.2 Conformal and Nonconformal Surfaces

Hydrodynamic lubrication is generally characterized by surfaces that are conformal. That is, the surfaces fit snugly into each other with a high degree of geometrical conformity, as shown in figure 1, so that the load is carried over a relatively large area. Furthermore, the

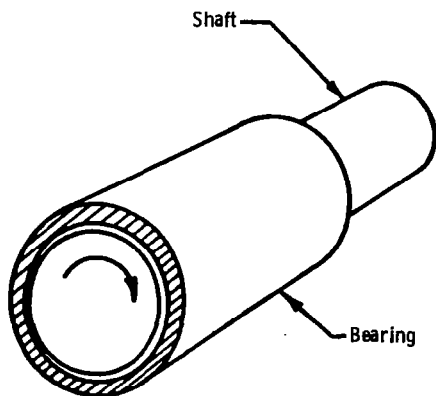


Figure 1.—Conformal surfaces as shown in sliding surface bearing.

load-carrying surface area remains essentially constant while the load is increased. Fluid-film journal and slider bearings exhibit conformal surfaces. In journal bearings, the radial clearance between the shaft and bearing is typically one-thousandth of the shaft diameter; in slider bearings, the inclination of the bearing surface to the runner is typically one part in a thousand.

Many machine elements have contacting surfaces that *do not* conform to each other very well, as shown in figure 2 for a rolling-element bearing. The full burden of the load must then be carried by a very small contact area. In general, the contact areas between nonconformal surfaces enlarge considerably with increasing load, but they are still small when compared with the contact areas between conformal surfaces. Some examples of these nonconformal surfaces are mating gear teeth, cams and followers, and rolling-element bearings, as shown in figure 2.

The load per unit area in conformal bearings is relatively low, typically only  $1 \text{ MN/m}^2$  and seldom over  $7 \text{ MN/m}^2$ . By contrast, the load per unit area in nonconformal contacts, such as those that exist in ball bearings, will generally exceed  $700 \text{ MN/m}^2$  even at modest applied loads. These high pressures result in elastic deformation of the bearing materials such that elliptical contact areas are formed for oil film generation and load support. The significance of the high contact pressures is that they result in a considerable increase in fluid viscosity. Inasmuch as viscosity is a measure of a fluid's resistance to flow, this increase greatly enhances the lubricant's ability to support load without being squeezed out of the contact zone.

### 1.3 Bearing Selection

Ball bearings are used in many kinds of machines and devices with rotating parts. The designer is often confronted with decisions on whether a rolling-element or hydrodynamic bearing should be used in a particular

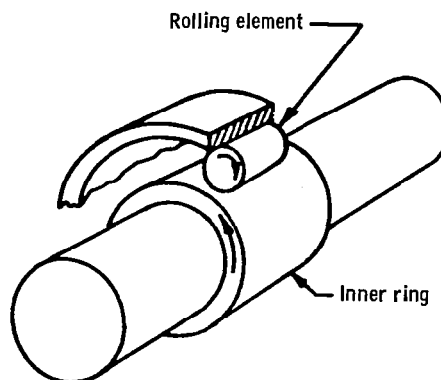


Figure 2.—Nonconformal surfaces as shown in a rolling-element bearing.



application. The following characteristics make ball bearings *more desirable* than hydrodynamic bearings in many situations:

- (1) Low starting and good operating friction
- (2) The ability to support combined radial and thrust loads
- (3) Less sensitivity to interruptions in lubrication
- (4) No self-excited instabilities
- (5) Good low-temperature starting

Within reasonable limits, changes in load, speed, and operating temperature have but little effect on the satisfactory performance of ball bearings.

The following characteristics make ball bearings *less desirable* than hydrodynamic bearings:

- (1) Finite fatigue life subject to wide fluctuations
- (2) Larger space required in the radial direction
- (3) Low damping capacity
- (4) Higher noise level
- (5) More severe alignment requirements
- (6) Higher cost

Each type of bearing has its particular strong points, and care should be taken in choosing the most appropriate type of bearing for a given application.

Useful guidance on the important issue of bearing selection has been presented by the Engineering Science Data Unit (ESDU 1965, 1967). These Engineering Science Data Unit documents provide an excellent guide to the selection of the type of journal or thrust bearing most likely to give the required performance when considering the load, speed, and geometry of the bearing. The following types of bearings were considered:

- (1) Rubbing bearings, where the two bearing surfaces rub together (e.g., unlubricated bushings made from materials based on nylon, polytetrafluoroethylene, also known as PTFE, and carbon)
- (2) Oil-impregnated porous metal bearings, where a porous metal bushing is impregnated with lubricant and thus gives a self-lubricating effect (as in sintered-iron and sintered-bronze bearings)
- (3) Rolling-element bearings, where relative motion is facilitated by interposing rolling elements between stationary and moving components (as in ball, roller, and needle bearings)
- (4) Hydrodynamic film bearings, where the surfaces in relative motion are kept apart by pressures generated hydrodynamically in the lubricant film

Figure 3, reproduced from the Engineering Science Data Unit publication (1965), gives a guide to the typical load that can be carried at various speeds, for a nominal life of 10 000 hr at room temperature, by journal bearings of various types on shafts of the diameters quoted. The heavy curves indicate the preferred type of journal bearing for a particular load, speed, and diameter and thus divide the graph into distinct regions. From figure 3 it is observed that rolling-element bearings are

preferred at lower speeds and hydrodynamic oil film bearings are preferred at higher speeds. Rubbing bearings and oil-impregnated porous metal bearings are not preferred for any of the speeds, loads, or shaft diameters considered. Also, as the shaft diameter is increased, the transitional point at which hydrodynamic bearings are preferred over rolling-element bearings moves to the left.

The applied load and speed are usually known, and this enables a preliminary assessment to be made of the type of journal bearing most likely to be suitable for a particular application. In many cases, the shaft diameter will already have been determined by other considerations, and figure 3 can be used to find the type of journal bearing that will give adequate load capacity at the required speed. These curves are based on good engineering practice and commercially available parts. Higher loads and speeds or smaller shaft diameters are possible with exceptionally high engineering standards or specially produced materials. Except for rolling-element bearings, the curves are drawn for bearings with a width equal to the diameter. A medium-viscosity mineral oil lubricant is assumed for the hydrodynamic bearings.

Similarly, figure 4, reproduced from the Engineering Science Data Unit publication (1967), gives a guide to the typical maximum load that can be carried at various speeds for a nominal life of 10 000 hr at room temperature by thrust bearings of various diameters quoted. The heavy curves again indicate the preferred type of bearing for a particular load, speed, and diameter and thus divide the graph into major regions. As with the journal bearing results (fig. 3), the hydrodynamic bearing is preferred at higher speeds and the rolling-element bearing is preferred at lower speeds. A difference between figures 3 and 4 is that at very low speeds there is a portion of the latter figure in which the rubbing bearing is preferred. Also, as the shaft diameter is increased, the transitional point at which hydrodynamic bearings are preferred over rolling-element bearings moves to the left. Note also from this figure that oil-impregnated porous metal bearings are not preferred for any of the speeds, loads, or shaft diameters considered.

## 2. Bearing Types

A great variety of both designs and size ranges of ball and roller bearings are available to the designer. The intent of this report is not to duplicate the complete descriptions given in manufacturers' catalogs, but rather to present a guide to representative bearing types along with the approximate range of sizes available. Tables 1 to 9 illustrate some of the more widely used bearing types. In addition, there are numerous types of specialty bearings available; space does not permit a complete cataloging of all available bearings. Size ranges are given in metric units. Traditionally, most rolling-element

bearings have been manufactured to metric dimensions, precluding the efforts toward a metric standard.

In addition to bearing types and approximate size ranges available, tables 1 to 9 also list approximate relative load-carrying capabilities, both radial and thrust, and where relevant, approximate tolerances to misalignment.

Rolling bearings are an assembly of several parts – an inner race, an outer race, a set of balls or rollers, and a cage or separator. The cage or separator maintains even spacing of the rolling elements. A cageless bearing, in which the annulus is packed with the maximum rolling-element complement, is called a full-complement bearing. Full-complement bearings have high load capacity but lower speed limits than bearings equipped

with cages. Tapered-roller bearings are an assembly of a cup, a cone, a set of tapered rollers, and a cage.

### 2.1 Ball Bearings

Ball bearings are used in greater quantity than any other type of rolling bearing. For an application where the load is primarily radial with some thrust load present, one of the types in table 1 can be chosen. A Conrad, or deep-groove, bearing has a ball complement limited by the number of balls that can be packed into the annulus between the inner and outer races with the inner race resting against the inside diameter of the outer race. A stamped and riveted two-piece cage, piloted on the ball set, or a machined two-piece cage, ball piloted or race

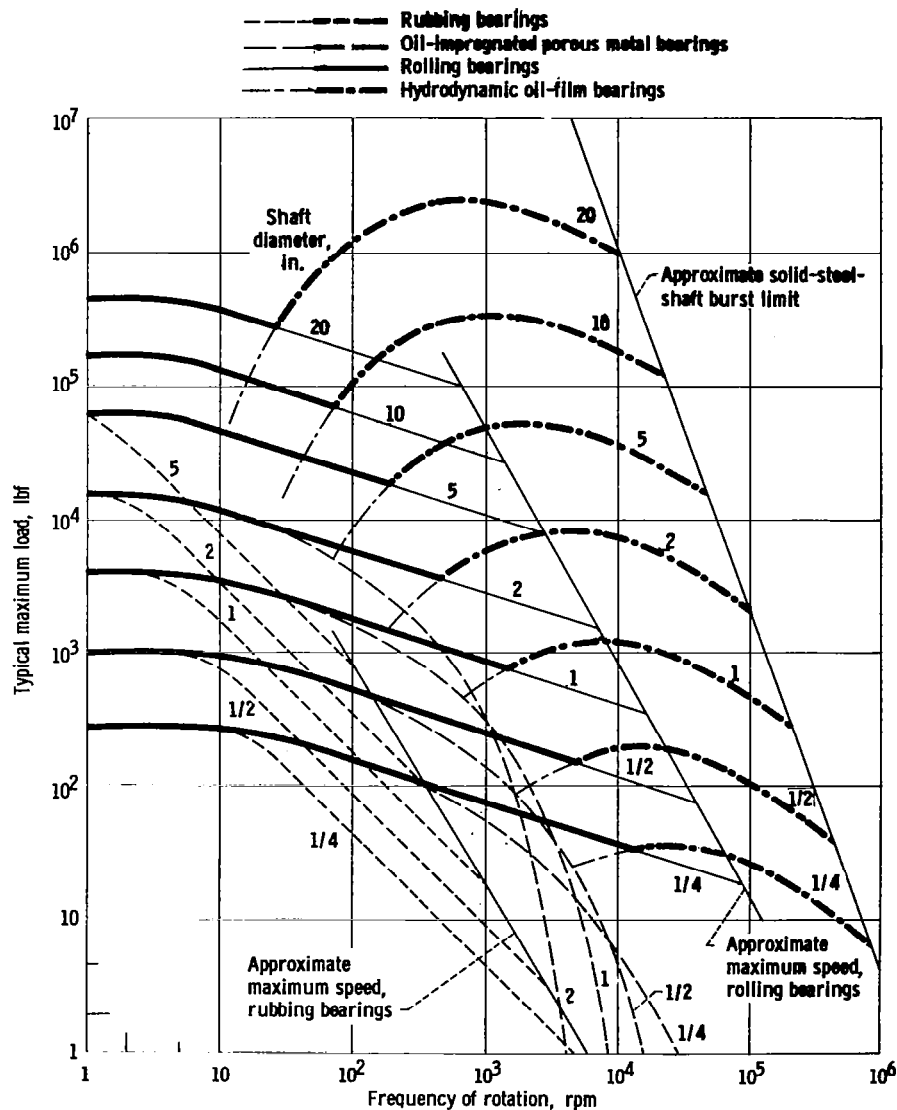


Figure 3.—General guide to journal bearing type. (Except for roller bearings, curves are drawn for bearings with width equal to diameter. A medium-viscosity mineral oil lubricant is assumed for hydrodynamic bearings.) (From Engineering Science Data Unit, 1965.)

piloted, is almost always used in a Conrad bearing. The only exception is a one-piece cage with open-sided pockets that is snapped into place. A filling-notch bearing has both inner and outer races notched so that a ball complement limited only by the annular space between the races can be used. It has low thrust capacity because of the filling notch.

The self-aligning internal bearing shown in table 1 has an outer-race ball path ground in a spherical shape so that it can accept high levels of misalignment. The self-aligning external bearing has a multipiece outer race with a spherical interface. It too can accept high misalignment and has higher capacity than the self-aligning internal bearing. However, the external self-aligning bearing is somewhat less self-aligning than its internal counterpart because of friction in the multipiece outer race.

Representative angular-contact ball bearings are illustrated in table 2. An angular-contact ball bearing has a two-shouldered ball groove in one race and a single-shouldered ball groove in the other race. Thus it is capable of supporting only a unidirectional thrust load. The cutaway shoulder allows assembly of the bearing by snapping over the ball set after it is positioned in the cage and outer race. This also permits use of a one-piece, machined, race-piloted cage that can be balanced for high-speed operation. Typical contact angles vary from 15° to 25°.

Angular-contact ball bearings are used in duplex pairs mounted either back to back or face to face as shown in table 2. Duplex bearing pairs are manufactured so that they "preload" each other when clamped together in the housing and on the shaft. The use of preloading provides

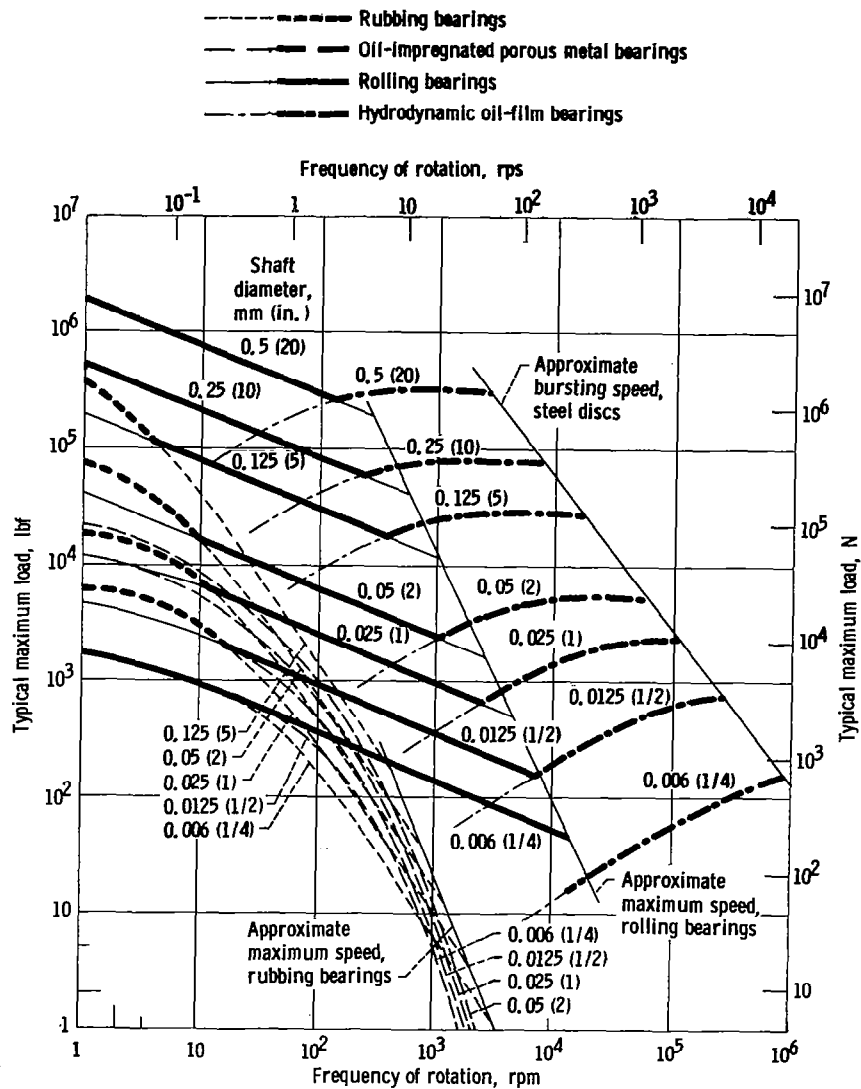


Figure 4. — General guide to thrust bearing type. (Except for roller bearings, curves are drawn for typical ratios of inside to outside diameter. A medium-viscosity mineral oil lubricant is assumed for hydrodynamic bearings.) (From Engineering Science Data Unit, 1967.)

stiffer shaft support and helps prevent bearing skidding at light loads. Proper levels of preload can be obtained from the manufacturer. A duplex pair can support bidirectional thrust load. The back-to-back arrangement offers more resistance to moment or overturning loads than does the face-to-face arrangement.

Where thrust loads exceed the capability of a simple bearing, two bearings can be used in tandem, with both bearings supporting part of the thrust load. Three or more bearings are occasionally used in tandem, but this is discouraged because of the difficulty in achieving good load sharing. Even slight differences in operating temperature will cause a maldistribution of load sharing.

The split-ring bearing shown in table 2 offers several advantages. The split ring (usually the inner) has its ball groove ground as a circular arc with a shim between the ring halves. The shim is then removed when the bearing is assembled so that the split-ring ball groove has the shape of a gothic arch. This reduces the axial play for a given radial play and results in more accurate axial positioning of the shaft. The bearing can support bidirectional thrust loads but must not be operated for prolonged periods of time at predominantly radial loads. This results in three-point ball-race contact and relatively high frictional losses. As with the conventional angular-contact bearing, a one-piece precision-machined cage is used.

Ball thrust bearings ( $90^\circ$  contact angle), table 3, are used almost exclusively for machinery with vertically oriented shafts. The flat-race bearing allows eccentricity of the fixed and rotating members. An additional bearing must be used for radial positioning. It has low load capacity because of the very small ball-race contacts and consequent high Hertzian stress. Grooved-race bearings have higher load capacities and are capable of supporting low-magnitude radial loads. All of the pure thrust ball bearings have modest speed capability because of the  $90^\circ$  contact angle and the consequent high level of ball spinning and frictional losses.

## 2.2 Roller Bearings

Cylindrical roller bearings, table 4, provide purely radial load support in most applications. An *N* or *U* type of bearing will allow free axial movement of the shaft relative to the housing to accommodate differences in thermal growth. An *F* or *J* type of bearing will support a light thrust load in one direction; and a *T* type of bearing, a light bidirectional thrust load.

Cylindrical roller bearings have moderately high radial load capacity as well as high speed capability. Their speed capability exceeds that of either spherical or tapered-roller bearings. A commonly used bearing combination for support of a high-speed rotor is an angular-contact ball bearing or duplex pair and a cylindrical roller bearing.

As explained in the following section on bearing

geometry, the rollers in cylindrical roller bearings are seldom pure cylinders. They are crowned or made slightly barrel shaped, to relieve stress concentrations of the roller ends when any misalignment of the shaft and housing is present.

Cylindrical roller bearings may be equipped with one- or two-piece cages, usually race piloted. For greater load capacity, full-complement bearings can be used, but at a significant sacrifice in speed capability.

Spherical roller bearings, tables 5 to 7, are made as either single- or double-row bearings. The more popular bearing design uses barrel-shaped rollers. An alternative design employs hourglass-shaped rollers. Spherical roller bearings combine very high radial load capacity with modest thrust load capacity (with the exception of the thrust type) and excellent tolerance to misalignment. They find widespread use in heavy-duty rolling mill and industrial gear drives, where all of these bearing characteristics are requisite.

Tapered-roller bearings, table 8, are also made as single- or double-row bearings with combinations of one- or two-piece cups and cones. A four-row bearing assembly with two- or three-piece cups and cones is also available. Bearings are made with either a standard angle for applications in which moderate thrust loads are present or with a steep angle for high thrust capacity. Standard and special cages are available to suit the application requirements.

Single-row tapered-roller bearings must be used in pairs because a radially loaded bearing generates a thrust reaction that must be taken by a second bearing. Tapered-roller bearings are normally set up with spacers designed so that they operate with some internal play. Manufacturers' engineering journals should be consulted for proper setup procedures.

Needle roller bearings, table 9, are characterized by compactness in the radial direction and are frequently used without an inner race. In the latter case the shaft is hardened and ground to serve as the inner race. Drawn cups, both open and closed end, are frequently used for grease retention. Drawn cups are thin walled and require substantial support from the housing. Heavy-duty roller bearings have relatively rigid races and are more akin to cylindrical roller bearings with long-length-to-diameter-ratio rollers.

Needle roller bearings are more speed limited than cylindrical roller bearings because of roller skewing at high speeds. A high percentage of needle roller bearings are full-complement bearings. Relative to a caged needle bearing, these have higher load capacity but lower speed capability.

There are many types of specialty bearings available other than those discussed here. Aircraft bearings for control systems, thin-section bearings, and fractured-ring bearings are some of the more widely used bearings

among the many types manufactured. A complete coverage of all bearing types is beyond the scope of this report.

Angular-contact ball bearings and cylindrical roller bearings are generally considered to have the highest speed capabilities. Speed limits of roller bearings are discussed in conjunction with lubrication methods. The lubrication system employed has as great an influence on bearing limiting speed as does the bearing design.

### 3. Geometry

The operating characteristics of a rolling-element bearing depend greatly on the diametral clearance of the bearing. This clearance varies for the different types of bearings discussed in the preceding section. In this section, the principal geometrical relationships governing the operation of unloaded rolling-element bearings are developed. This information will be of vital interest when such quantities as stress, deflection, load capacity, and life are considered in subsequent sections. Although bearings rarely operate in the unloaded state, an understanding of this section is vital to the appreciation of the remaining sections.

#### 3.1 Geometry of Ball Bearings

**Pitch diameter and clearance.**—The cross section through a radial, single-row ball bearing shown in figure 5 depicts the radial clearance and various diameters. The pitch diameter  $d_e$  is the mean of the inner- and outer-race contact diameters and is given by

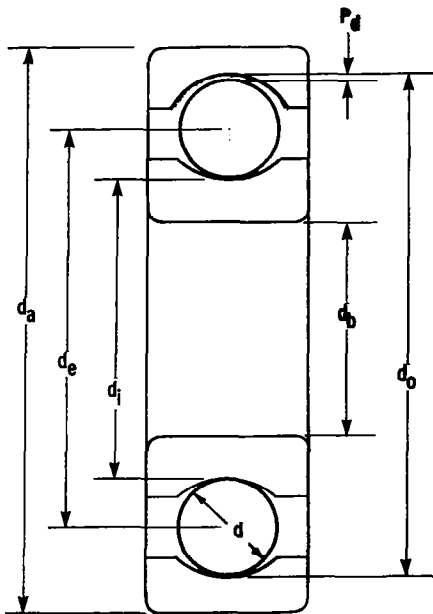


Figure 5.—Cross section through radial, single-row ball bearing.

$$d_e = d_i + \frac{1}{2}(d_o - d_i)$$

or

$$d_e = \frac{1}{2}(d_o + d_i) \quad (1)$$

Also from figure 5, the diametral clearance denoted by  $P_d$  can be written as

$$P_d = d_o - d_i - 2d \quad (2)$$

Diametral clearance may therefore be thought of as the maximum distance that one race can move diametrically with respect to the other when no measurable force is applied and both races lie in the same plane. Although diametral clearance is generally used in connection with single-row radial bearings, equation (2) is also applicable to angular-contact bearings.

**Race conformity.**—Race conformity is a measure of the geometrical conformity of the race and the ball in a plane passing through the bearing axis, which is a line passing through the center of the bearing perpendicular to its plane and transverse to the race. Figure 6 is a cross section of a ball bearing showing race conformity, expressed as

$$f = r/d \quad (3)$$

For perfect conformity, where the radius of the race is equal to the ball radius,  $f$  is equal to 1/2. The closer the race conforms to the ball, the greater the frictional heat within the contact. On the other hand, open-race curvature and reduced geometrical conformity, which reduce friction, also increase the maximum contact stresses and consequently reduce the bearing fatigue life. For this reason, most ball bearings made today have race conformity ratios in the range  $0.51 \leq f \leq 0.54$ , with  $f = 0.52$  being the most common value. The race conformity ratio for the outer race is usually made slightly larger than that for the inner race to compensate for the closer conformity in the plane of the bearing between the outer race and ball than between the inner race and ball. This tends to equalize the contact stresses

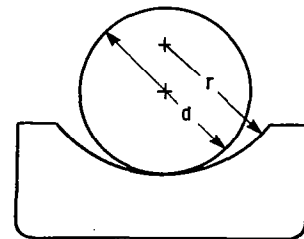


Figure 6.—Cross section of ball and outer race, showing race conformity.

at the inner- and outer-race contacts. The difference in race conformities does not normally exceed 0.02.

**Contact angle.**— Radial bearings have some axial play since they are generally designed to have a diametral clearance, as shown in figure 7(a). This implies a free-contact angle different from zero. Angular-contact bearings are specifically designed to operate under thrust loads. The clearance built into the unloaded bearing, along with the race conformity ratio, determines the bearing free-contact angle. Figure 7(b) shows a radial bearing with contact due to the axial shift of the inner and outer rings when no measurable force is applied.

Before the free-contact angle is discussed, it is important to define the distance between the centers of curvature of the two races in line with the center of the ball in both figures 7(a) and (b). This distance—denoted by  $x$  in figure 7(a) and by  $D$  in figure 7(b)—depends on race radius and ball diameter. Denoting quantities referred to the inner and outer races by subscripts  $i$  and  $o$ , respectively, we see from figures 7(a) and (b) that

$$\frac{P_d}{4} + d + \frac{P_d}{4} = r_o - x + r_i$$

or

$$x = r_o + r_i - d - P_d/2$$

and

$$d = r_o - D + r_i$$

or

$$D = r_o + r_i - d \quad (4)$$

From these equations, we can write

$$x = D - P_d/2$$

This distance, shown in figure 7(b), will be useful in defining the contact angle.

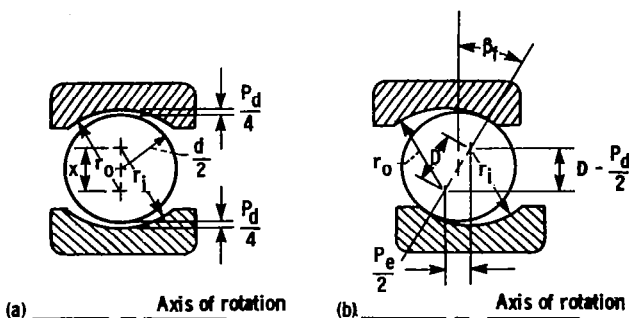


Figure 7.—Cross section of radial ball bearing, showing ball-race contact due to axial shift of inner and outer rings. (a) Initial position. (b) Shifted position.

By using equation (3), we can write equation (4) as

$$D = Bd \quad (5)$$

where

$$B = f_o + f_i - 1 \quad (6)$$

The quantity  $B$  in equation (6) is known as the total conformity ratio and is a measure of the combined conformity of both the outer and inner races to the ball. Calculations of bearing deflection in later sections depend on the quantity  $B$ .

The free-contact angle  $\beta_f$  (fig. 7(b)) is defined as the angle made by a line through the points of contact of the ball and both races with a plane perpendicular to the bearing axis of rotation when no measurable force is applied. Note that the centers of curvature of both the outer and inner races lie on the line defining the free-contact angle. From figure 7(b), the expression for the free-contact angle can be written as

$$\cos \beta_f = \frac{D - P_d/2}{D} \quad (7)$$

By using equations (2) and (4), we can write equation (7) as

$$\beta_f = \cos^{-1} \left[ \frac{r_o + r_i - \frac{1}{2}(d_o - d_i)}{r_o + r_i - d} \right] \quad (8)$$

Equation (8) shows that if the size of the balls is increased and everything else remains constant, the free-contact angle is decreased. Similarly, if the ball size is decreased, the free-contact angle is increased.

From equation (7), the diametral clearance  $P_d$  can be written as

$$P_d = 2D(1 - \cos \beta_f) \quad (9)$$

This is an alternative definition of the diametral clearance given in equation (2).

**Endplay.**—Free endplay  $P_e$  is the maximum axial movement of the inner race with respect to the outer when both races are coaxially centered and no measurable force is applied. Free endplay depends on total curvature and contact angle, as shown in figure 7(b), and can be written as

$$P_e = 2D \sin \beta_f \quad (10)$$

The variation of free-contact angle and endplay with the ratio  $P_d/2d$  is shown in figure 8 for four values of total conformity normally found in single-row ball bearings. Eliminating  $\beta_f$  in equations (9) and (10) enables the establishment of the following relationships between free endplay and diametral clearance:

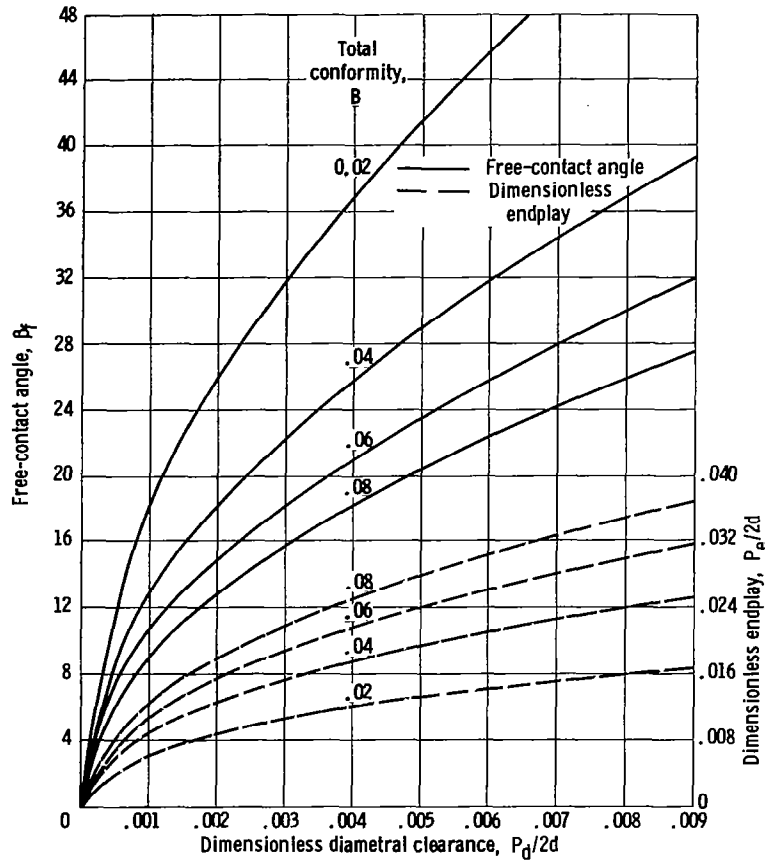


Figure 8. — Free-contact angle and endplay as function of  $P_d/2d$  for four values of total conformity.

$$P_d = 2D - [(2D)^2 - P_e^2]^{1/2}$$

$$P_e = (4DP_d - P_d^2)^{1/2}$$

**Shoulder height.** — The shoulder height of ball bearings is illustrated in figure 9. Shoulder height, or race depth, is the depth of the race groove measured from the shoulder to the bottom of the groove and is denoted by  $s$  in figure 9. From this figure, the equation defining the shoulder height can be written as

$$s = r(1 - \cos \theta) \quad (11)$$

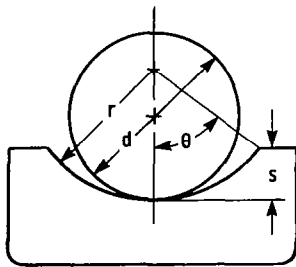


Figure 9. — Shoulder height in ball bearing.

The maximum possible diametral clearance for complete retention of the ball-race contact within the race under zero thrust load is given by

$$(P_d)_{\max} = 2Ds/r$$

**Curvature sum and difference.** — The undeformed geometry of contacting solids in a ball bearing can be represented by two ellipsoids. The two solids with different radii of curvature in a pair of principal planes ( $x$  and  $y$ ) passing through the contact between the solids make contact at a single point under the condition of zero applied load. Such a condition is called point contact and is shown in figure 10, where the radii of curvature are denoted by  $r$ 's. It is assumed that convex surfaces, as shown in figure 10, exhibit positive curvature and concave surfaces, negative curvature. Therefore, if the center of curvature lies within the solids, the radius of curvature is positive; if the center of curvature lies outside the solids, the radius of curvature is negative. It is important to note that if coordinates  $x$  and  $y$  are chosen such that

$$\frac{1}{r_{ax}} + \frac{1}{r_{bx}} > \frac{1}{r_{ay}} + \frac{1}{r_{by}} \quad (12)$$

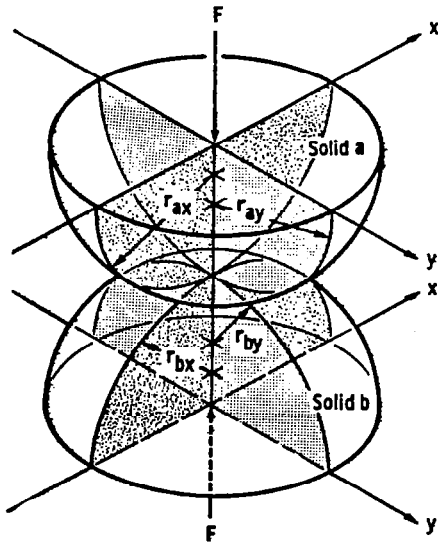


Figure 10. — Geometry of contacting elastic solids.

coordinate  $x$  then determines the direction of the semiminor axis of the contact area when a load is applied and  $y$ , the direction of the semimajor axis. The direction of motion is always considered to be along the  $x$  axis.

A cross section of a ball bearing operating at a contact angle  $\beta$  is shown in figure 11. Equivalent radii of curvature for both inner- and outer-race contacts in, and normal to, the direction of rolling can be calculated from this figure. The radii of curvature for the *ball-inner-race contact* are

$$r_{ax} = r_{ay} = d/2 \quad (13)$$

$$r_{bx} = \frac{d_e - d \cos \beta}{2 \cos \beta} \quad (14)$$

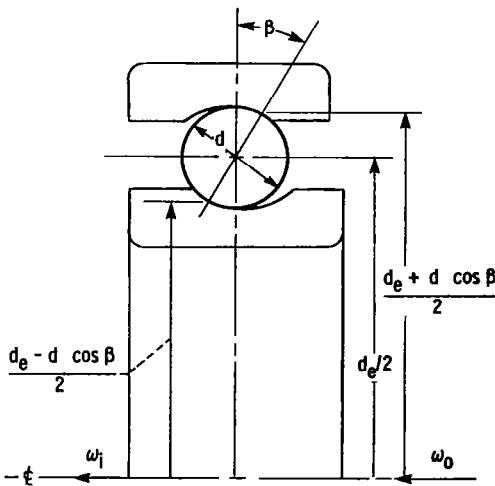


Figure 11. — Cross section of ball bearing.

$$r_{by} = -f_i d = -r_i \quad (15)$$

The radii of curvature for the *ball-outer-race contact* are

$$r_{ax} = r_{ay} = d/2 \quad (16)$$

$$r_{bx} = \frac{d_e + d \cos \beta}{2 \cos \beta} \quad (17)$$

$$r_{by} = -f_o d = -r_o \quad (18)$$

In equations (14) and (17),  $\beta$  is used instead of  $\beta_f$  since these equations are also valid when a load is applied to the contact. By setting  $\beta = 0^\circ$ , equations (13) to (18) are equally valid for radial ball bearings. For thrust ball bearings,  $r_{bx} = \infty$  and the other radii are defined as given in the preceding equations.

The curvature sum and difference, which are quantities of some importance in the analysis of contact stresses and deformations, are

$$\frac{1}{R} = \frac{1}{R_x} + \frac{1}{R_y} \quad (19)$$

$$\Gamma = R \left( \frac{1}{R_x} - \frac{1}{R_y} \right) \quad (20)$$

where

$$\frac{1}{R_x} = \frac{1}{r_{ax}} + \frac{1}{r_{bx}} \quad (21)$$

$$\frac{1}{R_y} = \frac{1}{r_{ay}} + \frac{1}{r_{by}} \quad (22)$$

$$\alpha = R_y / R_x$$

Equations (21) and (22) effectively redefine the problem of two ellipsoidal solids approaching one another in terms of an equivalent ellipsoidal solid of radii  $R_x$  and  $R_y$  approaching a plane. From the radius-of-curvature expressions, the radii  $R_x$  and  $R_y$  for the contact example discussed earlier can be written for the *ball-inner-race contact* as

$$R_x = \frac{d(d_e - d \cos \beta)}{2d_e} \quad (23)$$

$$R_y = \frac{f_i d}{2f_i - 1} \quad (24)$$

and for the *ball-outer-race contact* as

$$R_x = \frac{d(d_e + d \cos \beta)}{2d_e} \quad (25)$$



$$R_y = \frac{f_o d}{2f_o - 1} \quad (26)$$

### 3.2 Geometry of Roller Bearings

The equations developed for the pitch diameter  $d_e$  and diametral clearance  $P_d$  for ball bearings in equations (1) and (2), respectively, are directly applicable for roller bearings.

**Crowning.**—To prevent high stresses at the edges of the rollers in cylindrical roller bearings, the rollers are usually crowned as shown in figure 12. A fully crowned roller is shown in figure 12(a) and a partially crowned roller, in figure 12(b). In this figure the crown curvature is greatly exaggerated for clarity. The crowning of rollers also gives the bearing protection against the effects of slight misalignment. For cylindrical rollers,  $r_{ay}/d \approx 10^2$ . In contrast, for spherical rollers in spherical roller bearings, as shown in figure 12(a),  $r_{ay}/d \approx 4$ . In figure 12 it is observed that the roller effective length  $l_r$  is the length presumed to be in contact with the races under loading. Generally the roller effective length can be written as

$$l_r = l_t - 2r_c$$

where  $r_c$  is the roller corner radius or the grinding undercut, whichever is larger.

**Race conformity.**—Race conformity applies to roller bearings much like it applies to ball bearings. It is a measure of the geometrical conformity of the race and the roller. Figure 13 shows a cross section of a spherical roller bearing. From this figure the race conformity can be written as

$$f = r/2r_{ay}$$

In this equation if subscripts  $i$  or  $o$  are subscripted for  $f$  and  $r$ , we obtain the values for the race conformity for the inner- and outer-race contacts.

**Free endplay and contact angle.**—Cylindrical roller bearings have a contact angle of zero and may take thrust load only by virtue of axial flanges. Tapered-roller bearings must be subjected to a thrust load or the inner and outer rings (the cone and cup) will not remain assembled; therefore tapered-roller bearings do not exhibit free diametral play. Radial spherical roller bearings are, however, normally assembled with free diametral play and hence exhibit free endplay. The diametral play  $P_d$  for a spherical roller bearing is the same as that obtained for ball bearings as expressed in equation (2). This diametral play as well as endplay is shown in figure 14 for a spherical roller bearing. From this figure we can write that

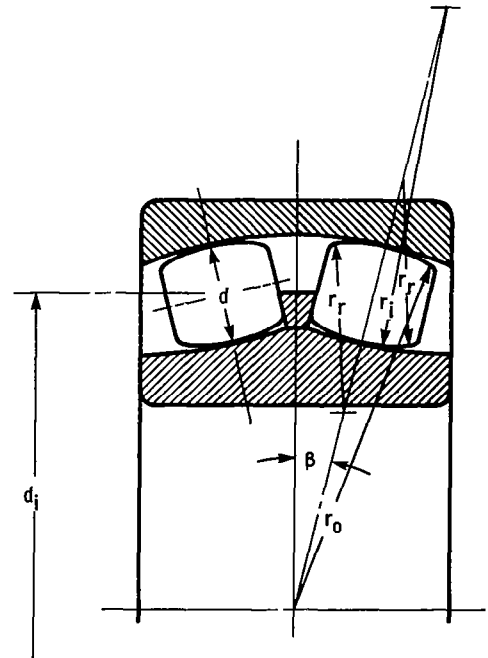


Figure 13.—Spherical roller bearing geometry.

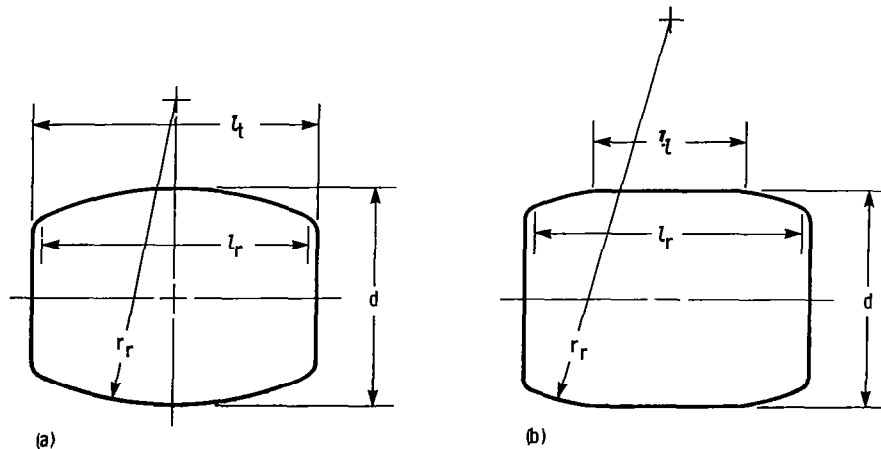


Figure 12.—Spherical and cylindrical rollers. (a) Spherical roller (fully crowned). (b) Cylindrical roller (partially crowned).

$$r_o \cos \beta = \left( r_o - \frac{P_d}{2} \right) \cos \gamma$$

or

$$\beta = \cos^{-1} \left[ \left( 1 - \frac{P_d}{2r_o} \right) \cos \gamma \right]$$

Also from figure 14 the free endplay can be written as

$$P_e = 2r_o(\sin \beta - \sin \gamma) + P_d \sin \gamma$$

**Curvature sum and difference.** – The same procedure will be used for defining the curvature sum and difference for roller bearings as was used for ball bearings. For spherical roller bearings, as shown in figure 13, the radii of curvature for the *roller-inner-race contact* can be written as

$$r_{ax} = d/2$$

$$r_{ay} = f_i(r_i/2)$$

$$r_{bx} = \frac{(d_e - d \cos \beta)}{2 \cos \beta}$$

$$r_{by} = -2f_i r_{ay}$$

For the spherical roller bearing shown in figure 13 the radii of curvature for the *roller-outer-race contact* can be written as

$$r_{ax} = d/2$$

$$r_{ay} = f_o(r_o/2)$$

$$r_{bx} = -\frac{(d_e + d \cos \beta)}{2 \cos \beta}$$

$$r_{by} = -2f_o r_{ay}$$

Knowing the radii of curvature for the respective contact condition, we can write the curvature sum and difference directly from equations (19) and (20). Furthermore, the radius-of-curvature expressions  $R_x$  and  $R_y$  for spherical roller bearings can be written for the *roller-inner-race contact* as

$$R_x = \frac{d(d_e - d \cos \beta)}{2d_e} \quad (27)$$

$$R_y = \frac{2r_{ay}f_i}{2f_i - 1} \quad (28)$$

and for the *roller-outer-race contact* as

$$R_x = \frac{d(d_e + d \cos \beta)}{2d_e} \quad (29)$$

$$R_y = \frac{2r_{ay}f_o}{2f_o - 1} \quad (30)$$

## 4. Kinematics

The relative motions of the separator, the balls or rollers, and the races of rolling-element bearings are important to understanding their performance. The relative velocities in a ball bearing are somewhat more complex than those in roller bearings, the latter being analogous to the specialized case of a zero- or fixed-value-contact-angle ball bearing. For that reason the ball bearing is used as an example here to develop approximate expressions for relative velocities. These are useful for rapid but reasonably accurate calculation of elastohydrodynamic film thickness, which can be used with surface roughnesses to calculate the lubrication life factor.

The precise calculation of relative velocities in a ball bearing in which speed or centrifugal force effects, contact deformations, and elastohydrodynamic traction effects are considered requires a large computer to numerically solve the relevant equations. The reader is referred to the growing body of computer codes discussed in section 13 for precise calculations of bearing

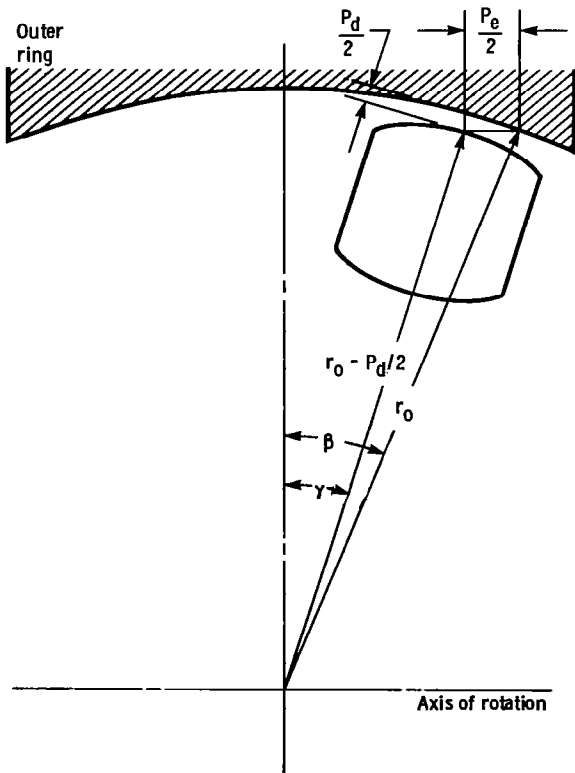


Figure 14.—Schematic diagram of spherical roller bearing, showing diametral play and endplay.

performance. Such a treatment is beyond the scope of this section. However, approximate expressions that yield answers with accuracies satisfactory for many situations are available.

When a ball bearing operates at high speeds, the centrifugal force acting on the ball creates a divergency of the inner- and outer-race contact angles, as shown in figure 15, in order to maintain force equilibrium on the ball. For the most general case of rolling and spinning at both inner- and outer-race contacts, the rolling and spinning velocities of the ball are as shown in figure 16.

The equations for ball and separator angular velocity for all combinations of inner- and outer-race rotation were developed by Jones (1964). Without introducing additional relationships to describe the elasto-hydrodynamic conditions at both ball-race contacts, however, the ball-spin-axis orientation angle  $\theta$  cannot be obtained. As mentioned, this requires a lengthy numerical solution except for the two extreme cases of

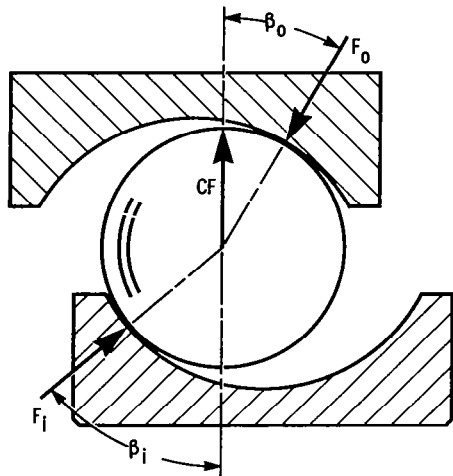


Figure 15.—Contact angles in a ball bearing at appreciable speeds.

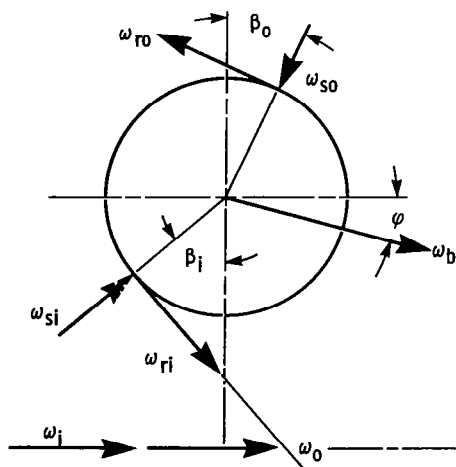


Figure 16.—Angular velocities of a ball.

outer- or inner-race control. These are illustrated in figure 17.

Race control assumes that pure rolling occurs at the controlling race, with all of the ball spin occurring at the other race contact. The orientation of the ball rotational axis is then easily determinable from bearing geometry. Race control probably occurs only in dry bearings or dry-film-lubricated bearings where Coulomb friction conditions exist in the ball-race contact ellipses, the moment-resisting spin will always be greater at one of the race contacts. Pure rolling will occur at the race contact with the higher magnitude moment-resisting spin. This is usually the inner race at low speeds and the outer race at high speeds.

In oil-lubricated bearings in which elasto-hydrodynamic films exist in both ball-race contacts, rolling with spin occurs at both contacts. Therefore precise ball motions can only be determined through use of a computer analysis. We can approximate the situation with a reasonable degree of accuracy, however, by assuming that the ball rolling axis is normal to the line drawn through the centers of the two ball-race contacts. This is shown in figure 11.

The angular velocity of the separator or ball set  $\omega_c$  about the shaft axis can be shown to be (Anderson, 1970)

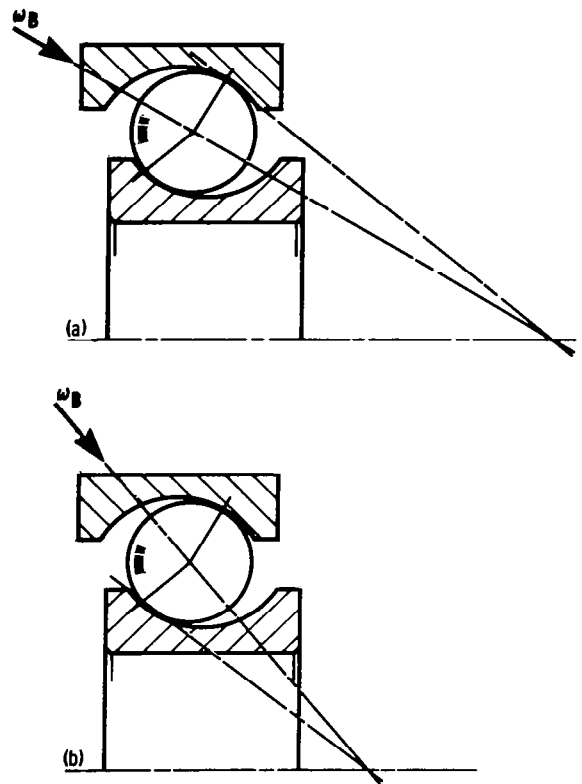


Figure 17.—Ball spin axis orientations for outer- and inner-race control. (a) Outer-race control. (b) Inner-race control.

$$\begin{aligned}\omega_c &= \frac{(v_i + v_o)/2}{d_e/2} \\ &= \frac{1}{2} \left[ \omega_i \left( 1 - \frac{d \cos \beta}{d_e} \right) + \omega_o \left( 1 + \frac{d \cos \beta}{d_e} \right) \right] \quad (31)\end{aligned}$$

where  $v_i$  and  $v_o$  are the linear velocities of the inner and outer contacts. The angular velocity of a ball about its own axis  $\omega_b$  is

$$\begin{aligned}\omega_b &= \frac{v_i - v_o}{d_e/2} \\ &= \frac{d_e}{2d} \left[ \omega_i \left( 1 - \frac{d \cos \beta}{d_e} \right) - \omega_o \left( 1 + \frac{d \cos \beta}{d_e} \right) \right] \quad (32)\end{aligned}$$

To calculate the velocities of the ball-race contacts, which are required for calculating elastohydrodynamic film thicknesses, it is convenient to use a coordinate system that rotates at  $\omega_c$ . This fixes the ball-race contacts relative to the observer. In the rotating coordinate system the angular velocities of the inner and outer races become

$$\begin{aligned}\omega_{ir} &= \omega_i - \omega_c = \left( \frac{\omega_i - \omega_o}{2} \right) \left( 1 + \frac{d \cos \beta}{d_e} \right) \\ \omega_{or} &= \omega_o - \omega_c = \left( \frac{\omega_o - \omega_i}{2} \right) \left( 1 - \frac{d \cos \beta}{d_e} \right)\end{aligned}$$

The surface velocities entering the *ball-inner-race contact* for pure rolling are

$$u_{ai} = u_{bi} = \left( \frac{d_e - d \cos \beta}{2} \right) \omega_{ir} \quad (33)$$

or

$$u_{ai} = u_{bi} = \frac{d_e(\omega_i - \omega_o)}{4} \left( 1 - \frac{d^2 \cos^2 \beta}{d_e^2} \right) \quad (34)$$

and those at the *ball-outer-race contact* are

$$u_{ao} = u_{bo} = \left( \frac{d_e + d \cos \beta}{2} \right) \omega_{or}$$

or

$$u_{ao} = u_{bo} = \frac{d_e(\omega_o - \omega_i)}{4} \left( 1 - \frac{d^2 \cos^2 \beta}{d_e^2} \right) \quad (35)$$

For a cylindrical roller bearing,  $\beta = 0^\circ$  and equations (31), (32), (34), and (35) become, if  $d$  is roller diameter,

$$\omega_c = \frac{1}{2} \left[ \omega_i \left( 1 - \frac{d}{d_e} \right) + \omega_o \left( 1 + \frac{d}{d_e} \right) \right]$$

$$\begin{aligned}\omega_R &= \frac{d_e}{2d} \left[ \omega_i \left( 1 - \frac{d}{d_e} \right) + \omega_o \left( 1 + \frac{d}{d_e} \right) \right] \\ u_{ai} = u_{bi} &= \frac{d_e(\omega_i - \omega_o)}{4} \left( 1 - \frac{d^2}{d_e^2} \right) \\ u_{ao} = u_{bo} &= \frac{d_e(\omega_o - \omega_i)}{4} \left( 1 - \frac{d^2}{d_e^2} \right)\end{aligned} \quad (36)$$

For a tapered-roller bearing, equations directly analogous to those for a ball bearing can be used if  $d$  is the average diameter of the tapered roller,  $d_e$  is the diameter at which the geometric center of the rollers is located, and  $\omega$  is the angle as shown in figure 18.

## 5. Materials and Manufacturing Processes

Until about 1955, rolling-element bearing materials technology did not receive much attention from materials scientists. Bearing materials were restricted to SAE 52100 and some carburizing grades such as AISI 4320 and AISI 9310, which seemed to be adequate for most bearing applications, despite the limitation in temperature of about  $176^\circ \text{C}$  ( $350^\circ \text{F}$ ) for 52100 steel. A minimum acceptable hardness of Rockwell C 58 should be specified. Experiments indicate that fatigue life increases with increasing hardness.

The advent of the aircraft gas turbine engine, with its need for advanced rolling-element bearings, provided the major impetus for advancements in rolling-element bearing materials technology. Increased temperatures, higher speeds and loads, and the need for greater durability and reliability all served as incentives for the development and evaluation of a broad range of new

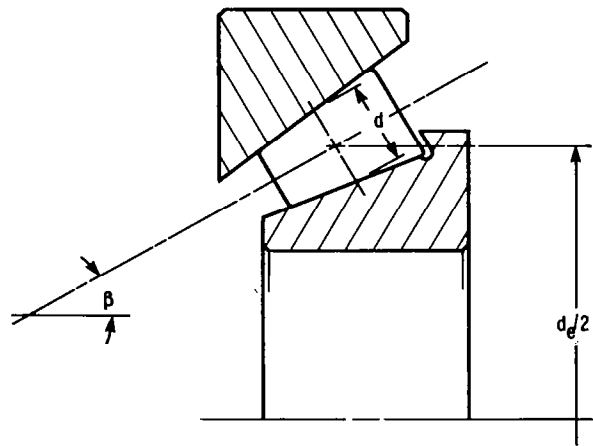


Figure 18. — Simplified geometry for tapered-roller bearing.

materials and processing methods. The combined research efforts of bearing manufacturers, engine manufacturers, and Government agencies over the past three decades have resulted in startling advances in rolling-element bearing life and reliability and in performance. The discussion here is brief in scope. For a comprehensive treatment of the research status of current bearing technology and current bearing designs, refer to Bamberger et al. (1980).

### 5.1 Ferrous Alloys

The need for higher temperature capability led to the evaluation of a number of available molybdenum and tungsten alloy tool steels as bearing materials (table 10). These alloys have excellent high-temperature hardness retention. Such alloys melted and cast in an air environment, however, were generally deficient in fatigue resistance because of the presence of nonmetallic inclusions. Vacuum processing techniques can reduce or eliminate these inclusions. Techniques used include vacuum induction melting (VIM) and vacuum arc remelting (VAR). These have been extensively explored, not only with the tool steels now used as bearing materials, but with SAE 52100 and some of the carburizing steels as well. Table 10 lists a fairly complete array of ferrous alloys, both fully developed and experimental, from which present-day bearings are fabricated. AISI M-50, usually VIM-VAR or consumable electrode vacuum melted (CEVM) processed, has become a very widely used quality bearing material. It is usable at temperatures to 315° C (600° F), and it is usually assigned a materials life factor of 3 to 5 (section 12.5). T-1 tool steel has also come into fairly wide use, mostly in Europe, in bearings. Its hot hardness retention is slightly superior to that of M-50 and approximately equal to that of M-1 and M-2. These alloys retain adequate hardness to about 400° C (750° F).

Surface-hardened or carburized steels are used in many bearings where, because of shock loads or cyclic bending stresses, the fracture toughness of the through-hardened steels is inadequate. Some of the newer materials being developed, such as CBS 1000 and Vasco X-2 have hot hardness retention comparable to that of the tool steels (fig. 19). They too are available as ultraclean, vacuum-processed materials and should offer adequate resistance to fatigue. Carburized steels may become of increasing importance in ultra-high-speed applications. Bearings with through-hardened steel races are currently limited to approximately 2.5 million  $d_b N$  (where  $d_b$  is bore diameter in millimeters and  $N$  is rotational speed in rpm) because, at higher  $d_b N$  values, fatigue cracks propagate through the rotating race as a result of the excessive hoop stress present (Bamberger, et al., 1976).

In applications where the bearings are not lubricated with conventional oils and protected from corrosion at all

times, a corrosion-resistant alloy should be used. Dry-film-lubricated bearings, bearings cooled by liquefied cryogenic gases, and bearings exposed to corrosive environments such as very high humidity and salt water are applications where corrosion-resistant alloys should be considered. Of the alloys listed in table 10, both 440C and AMS5749 are readily available in vacuum-melted heats.

In addition to improved melting practice, forging and forming methods that result in improved resistance to fatigue have been developed. Experiments indicate that fiber or grain flow parallel to the stressed surface is superior to fiber flow that intersects the stressed surface (Bamberger, 1970; Zaretsky and Anderson, 1966). Forming methods that result in more parallel grain flow are now being used in the manufacture of many bearings, especially those used in high-load applications.

### 5.2 Ceramics

Experimental bearings have been made from a variety of ceramics including alumina, silicon carbide, titanium carbide, and silicon nitride. The use of ceramics as bearing materials for specialized applications will probably continue to grow for several reasons. These include

(1) High-temperature capability—Because ceramics can exhibit elastic behavior to temperatures beyond 1000° C (1821° F), they are an obvious choice for extreme-temperature applications.

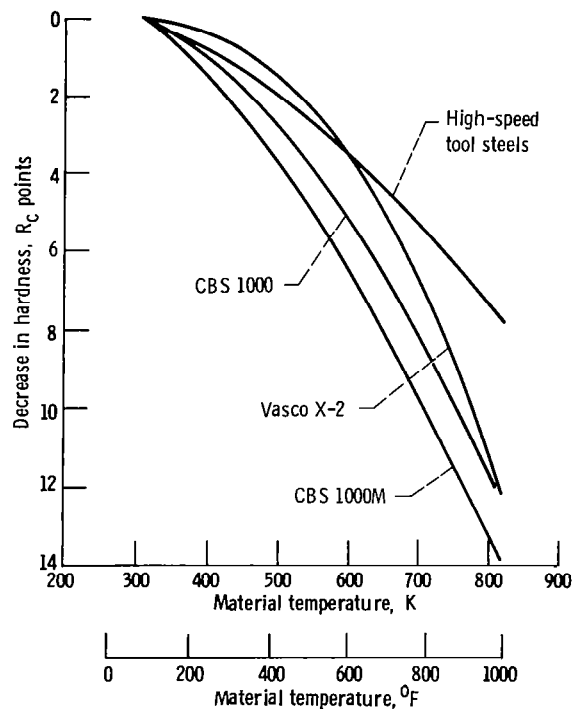


Figure 19.—Hot hardness of CBS 1000, CBS 1000M, Vasco X-2, and high-speed tool steels. (From Anderson and Zaretsky, 1975.)

(2) Corrosion resistance—Ceramics are essentially chemically inert and able to function in many environments hostile to ferrous alloys.

(3) Low density—This can be translated into improved bearing capacity at high speeds, where centrifugal effects predominate.

(4) Low coefficient of thermal expansion—Under conditions of severe thermal gradients, ceramic bearings exhibit less drastic changes in geometry and internal play than do ferrous alloy bearings.

At the present time, silicon nitride is being actively developed as a bearing material (Sibley, 1982; Cundill and Giordano, 1982). Silicon nitride bearings have exhibited fatigue lives comparable to and, in some instances, superior to that of high-quality vacuum-melted M-50 (Sibley, 1982). Two problems remain: (1) quality control and precise nondestructive inspection techniques to determine acceptability and (2) cost. Improved hot isostatic compaction, metrology, and finishing techniques are all being actively pursued. However, silicon nitride bearings must still be considered experimental.

## 6. Separators

Ball and roller bearing separators, sometimes called cages or retainers, are bearing components that, although never carrying load, are capable of exerting a vital influence on the efficiency of the bearing. In a bearing without a separator, the rolling elements contact each other during operation and in so doing experience severe sliding and friction. The primary function of a separator is to maintain the proper distance between the rolling elements and to ensure proper load distribution and balance within the bearing. Another function of the separator is to maintain control of the rolling elements in such a manner as to produce the least possible friction through sliding contact. Furthermore, a separator is necessary for several types of bearings to prevent the rolling elements from falling out of the bearing during handling. Most separator troubles occur from improper mounting, misaligned bearings, or improper (inadequate or excessive) clearance in the rolling-element pocket.

The materials used for separators vary according to the type of bearing and the application. In ball bearings and some sizes of roller bearings, the most common type of separator is made from two strips of carbon steel that are pressed and riveted together. Called ribbon separators, they are the least expensive to manufacture and are entirely suitable for many applications. They are also lightweight and usually require little space.

The design and construction of angular-contact ball bearings allow the use of a one-piece separator. The simplicity and inherent strength of one-piece separators

permit their fabrication from many desirable materials. Reinforced phenolic and bronze are the two most commonly used materials. Bronze separators offer strength and low-friction characteristics and can be operated at temperatures to 230° C (450° F). Machined, silver-plated ferrous alloy separators are used in many demanding applications. Because reinforced cotton-base phenolic separators combine the advantages of low weight, strength, and nongalling properties, they are used for such high-speed applications as gyro bearings. In high-speed bearings, lightness and strength are particularly desirable since the stresses increase with speed but may be greatly minimized by reduction of separator weight. A limitation of phenolic separators, however, is that they have a allowable maximum temperature of about 135° C (275° F).

## 7. Contact Stresses and Deformations

The loads carried by rolling-element bearings are transmitted through the rolling element from one race to the other. The magnitude of the load carried by an individual rolling element depends on the internal geometry of the bearing and the location of the rolling element at any instant. A load-deflection relationship for the rolling-element-race contact is developed in this section. The deformation within the contact is a function of, among other things, the ellipticity parameter and the elliptic integrals of the first and second kinds. Simplified expressions that allow quick calculations of the stresses and deformations to be made easily from a knowledge of the applied load, the material properties, and the geometry of the contacting elements are presented in this section.

### 7.1 Elliptical Contacts

When two elastic solids are brought together under a load, a contact area develops, the shape and size of which depend on the applied load, the elastic properties of the materials, and the curvatures of the surfaces. When the two solids shown in figure 10 have a normal load applied to them, the shape of the contact area is elliptical, with  $D_y$  being the diameter in the  $y$  direction (transverse direction) and  $D_x$  being the diameter in the  $x$  direction (direction of motion). For the special case where  $r_{ax}=r_{ay}$  and  $r_{bx}=r_{by}$ , the resulting contact is a circle rather than an ellipse. Where  $r_{ay}$  and  $r_{by}$  are both infinity, the initial line contact develops into a rectangle when load is applied.

The contact ellipses obtained with either a radial or a thrust load for the ball-inner-race and ball-outer-race contacts in a ball bearing are shown in figure 20. Inasmuch as the size and shape of these contact areas are highly significant in the successful operation of rolling

elements, it is important to understand their characteristics.

The ellipticity parameter  $k$  is defined as the elliptical-contact diameter in the  $y$  direction (transverse direction) divided by the elliptical-contact diameter in the  $x$  direction (direction of motion) or  $k = D_y/D_x$ . If equation (12) is satisfied and  $\alpha \geq 1$ , the contact ellipse will be oriented so that its major diameter will be transverse to the direction of motion, and consequently  $k \geq 1$ . Otherwise, the major diameter would lie along the direction of motion with both  $\alpha \leq 1$  and  $k \leq 1$ . Figure 21 shows the ellipticity parameter and the elliptic integrals of the first and second kinds for a range of the curvature ratio ( $\alpha = R_y/R_x$ ) usually encountered in concentrated contacts.

**Simplified solutions for  $\alpha \geq 1$ .** — The classical Hertzian solution requires the calculation of the ellipticity parameter  $k$  and the complete elliptic integrals of the first and second kinds  $\mathcal{F}$  and  $\mathcal{E}$ . This entails finding a solution to a transcendental equation relating  $k$ ,  $\mathcal{F}$ , and  $\mathcal{E}$  to the geometry of the contacting solids. This is usually accomplished by some iterative numerical procedure, as described by Hamrock and Anderson (1973), or with the aid of charts, as shown by Jones (1946). Hamrock and Brewe (1982) provide a shortcut to the classical Hertzian solution for the local stress and deformation of two elastic bodies in contact. The shortcut is accomplished by using simplified forms of the ellipticity parameter and the complete elliptic integrals, expressing them as functions of the geometry. The results of Hamrock and Brewe's (1982) work are summarized here.

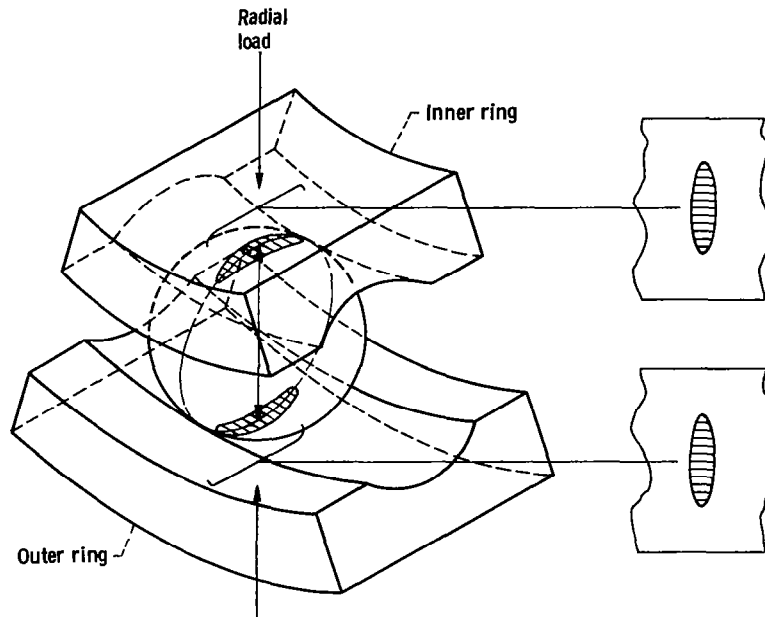


Figure 20. — Contact areas in a ball bearing.

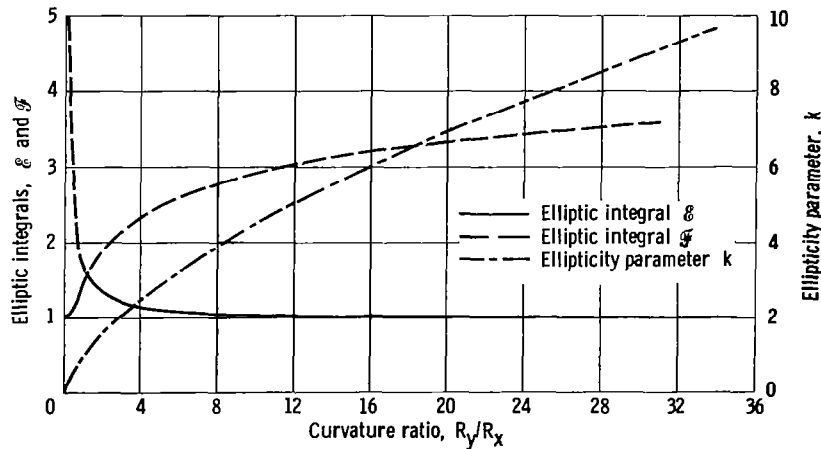


Figure 21. — Ellipticity parameter and elliptic integrals of first and second kinds as function of curvature ratio.

Table 11 shows various values of radius-of-curvature ratios and corresponding values of  $k$ ,  $\mathfrak{F}$ , and  $\mathfrak{E}$  obtained from the numerical procedure given in Hamrock and Anderson (1973). For the set of pairs of data  $\{(k_i, \alpha_i), i=1, 2, \dots, 26\}$ , a power fit using linear regression by the method of least squares resulted in the following equation:

$$\bar{k} = \alpha^{2/\pi} \quad \text{for } \alpha \geq 1 \quad (37)$$

The asymptotic behavior of  $\mathfrak{E}$  and  $\mathfrak{F}$  ( $\alpha \rightarrow 1$  implies  $\mathfrak{E} \rightarrow \mathfrak{F} \rightarrow \pi/2$ , and  $\alpha \rightarrow \infty$  implies  $\mathfrak{F} \rightarrow \infty$  and  $\mathfrak{E} \rightarrow 1$ ) was suggestive of the type of functional dependence that  $\mathfrak{E}$  and  $\mathfrak{F}$  might follow. As a result, an inverse and a logarithmic curve fit were tried for  $\mathfrak{E}$  and  $\mathfrak{F}$ , respectively. The following expressions provided excellent curve fits:

$$\bar{\mathfrak{E}} = 1 + q/\alpha \quad \text{for } \alpha \geq 1 \quad (38)$$

$$\bar{\mathfrak{F}} = \pi/2 + q \ln \alpha \quad \text{for } \alpha \geq 1 \quad (39)$$

where  $q = \pi/2 - 1$ . Values of  $\bar{k}$ ,  $\bar{\mathfrak{E}}$ , and  $\bar{\mathfrak{F}}$  are presented in table 11 and compared with the numerically determined values of  $k$ ,  $\mathfrak{E}$ , and  $\mathfrak{F}$ . Table 11 also gives the percentage of error determined as

$$e = \frac{(\bar{z} - z) 100}{z}$$

$$z = \{k, \mathfrak{E}, \mathfrak{F}\}$$

$$\bar{z} = \{\bar{k}, \bar{\mathfrak{E}}, \bar{\mathfrak{F}}\}$$

When the ellipticity parameter  $k$  (eq. (37)), the elliptic integrals of the first and second kinds (eqs. (39) and (38)), the normal applied load  $F$ , Poisson's ratio  $\nu$ , and the modulus of elasticity  $E$  of the contacting solids are known, we can write the major and minor axes of the contact ellipse and the maximum deformation at the center of the contact, from the analysis of Hertz (1881), as

$$D_y = 2 \left( \frac{6\bar{k}^2\bar{\mathfrak{E}}FR}{\pi E'} \right)^{1/3} \quad (40)$$

$$D_x = 2 \left( \frac{6\bar{\mathfrak{E}}FR}{\pi\bar{k}E'} \right)^{1/3} \quad (41)$$

$$\delta = \bar{\mathfrak{F}} \left[ \left( \frac{9}{2\bar{\mathfrak{E}}R} \right) \left( \frac{F}{\pi\bar{k}E'} \right)^2 \right]^{1/3} \quad (42)$$

$$E' = \frac{2}{\frac{1-\nu_a^2}{E_a} + \frac{1-\nu_b^2}{E_b}} \quad (43)$$

In these equations,  $D_y$  and  $D_x$  are proportional to  $F^{1/3}$  and  $\delta$  is proportional to  $F^{2/3}$ .

The maximum Hertzian stress at the center of the contact can also be determined by using equations (40) and (41).

$$\sigma_{\max} = 6F/\pi D_x D_y$$

**Simplified solutions for  $\alpha \leq 1$ .**—Table 12 gives the simplified equations for  $\alpha < 1$  as well for  $\alpha \geq 1$ . Recall that  $\alpha \geq 1$  implies  $k \geq 1$  and equation (12) is satisfied and  $\alpha < 1$  implies  $k < 1$  and equation (12) is not satisfied. It is important to make the proper evaluation of  $\alpha$  since it has a great significance in the outcome of the simplified equations. Figure 22 shows three diverse situations in which the simplified equations can be usefully applied. The locomotive wheel on a rail (fig. 22(a)) illustrates an example in which the ellipticity parameter  $k$  and the radius ratio  $\alpha$  are less than 1. The ball rolling against a flat plate (fig. 22(b)) provides pure circular contact (i.e.,  $\alpha = k = 1.0$ ). Figure 22(c) shows how the contact ellipse is formed in the ball-outer-ring contact of a ball bearing. Here the semimajor axis is normal to the direction of rolling and consequently  $\alpha$  and  $k$  are greater than 1. Table 13 uses this figure to show how the degree of conformity affects the contact parameters.

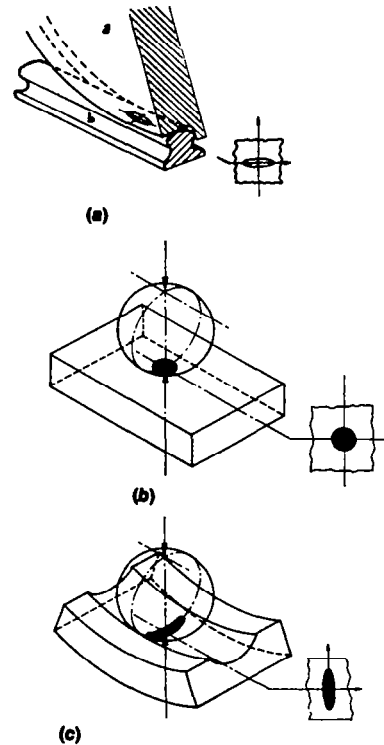


Figure 22. — Three degrees of conformity. (a) Wheel on rail. (b) Ball on plane. (c) Ball-outer-race contact.



## 7.2 Rectangular Contacts

For this situation the contact ellipse discussed in the preceding section is of infinite length in the transverse direction ( $D_y \rightarrow \infty$ ). This type of contact is exemplified by a cylinder loaded against a plate, a groove, or another, parallel, cylinder or by a roller loaded against an inner or outer ring. In these situations the contact semiwidth is given by

$$b = R_x \sqrt{8W/\pi}$$

where the dimensionless load

$$W = F'/E'R_x$$

and  $F'$  is the load per unit length along the contact. The maximum deformation for a rectangular contact can be written as (ESDU, 1978)

$$\delta = \frac{2WR_x}{\pi} \left[ \frac{2}{3} + \ln\left(\frac{4r_{ax}}{b}\right) + \ln\left(\frac{4r_{bx}}{b}\right) \right] \quad (44)$$

The maximum Hertzian stress in a rectangular contact can be written as

$$\sigma_{\max} = E' \sqrt{W/2\pi}$$

## 8. Static Load Distribution

Having defined a simple analytical expression for the deformation in terms of load in the previous section, it is possible to consider how the bearing load is distributed among the rolling elements. Most rolling-element bearing applications involve steady-state rotation of either the inner or outer race or both; however, the speeds of rotation are usually not so great as to cause ball or roller centrifugal forces or gyroscopic moments of significant magnitudes. In analyzing the loading distribution on the rolling elements, it is usually satisfactory to ignore these effects in most applications. In this section the load deflection relationships for ball and roller bearings are given, along with radial and thrust load distributions of statically loaded rolling elements.

### 8.1 Load Deflection Relationships

For an elliptical contact, the load deflection relationship given in equation (42) can be written as

$$F = K_{1.5} \delta^{3/2} \quad (45)$$

where

$$K_{1.5} = \pi k E' \sqrt{2\mathcal{E}R/9\mathcal{F}^3} \quad (46)$$

Similarly for a rectangular contact, equation (44) gives

$$F = K_1 \delta$$

where

$$K_1 = \left( \frac{\pi E'}{2} \right) \frac{1}{\left[ \frac{2}{3} + \ln\left(\frac{4r_{ax}}{b}\right) + \ln\left(\frac{4r_{bx}}{b}\right) \right]} \quad (47)$$

In general then,

$$F = K_j \delta^j \quad (48)$$

in which  $j=1.5$  for ball bearings and 1.0 for roller bearings. The total normal approach between two races separated by a rolling element is the sum of the deformations under load between the rolling element and both races. Therefore

$$\delta = \delta_o + \delta_i \quad (49)$$

where

$$\delta_o = \left[ F/(K_j)_o \right]^{1/j} \quad (50)$$

$$\delta_i = \left[ F/(K_j)_i \right]^{1/j} \quad (51)$$

Substituting equations (49) to (51) into equation (48) gives

$$K_j = \frac{1}{\left\{ \left[ \frac{1}{(K_j)_o} \right]^{1/j} + \left[ \frac{1}{(K_j)_i} \right]^{1/j} \right\}^j}$$

Recall that  $(K_j)_o$  and  $(K_j)_i$  are defined by equations (46) and (47) for elliptical and rectangular contacts, respectively. From these equations we observe that  $(K_j)_o$  and  $(K_j)_i$  are functions of only the geometry of the contact and the material properties. The radial and thrust load analyses are presented in the following two sections and are directly applicable for radially loaded ball and roller bearings and thrust-loaded ball bearings.

### 8.2 Radially Loaded Ball and Roller Bearings

A radially loaded rolling element with radial clearance  $P_d$  is shown in figure 23. In the concentric position shown in figure 23(a), a uniform radial clearance between the rolling element and the races of  $P_d/2$  is evident. The application of a small radial load to the shaft causes the

inner ring to move a distance  $P_d/2$  before contact is made between a rolling element located on the load line and the inner and outer races. At any angle, there will still be a radial clearance  $c$  that, if  $P_d$  is small as compared with the radius of the tracks, can be expressed with adequate accuracy by

$$c = (1 - \cos \psi) P_d / 2$$

On the load line where  $\psi = 0$ , the clearance is zero; but when  $\psi = 90^\circ$  the clearance retains its initial value of  $P_d/2$ .

The application of further load will cause elastic deformation of the balls and the elimination of clearance around an arc  $2\psi_c$ . If the interference or total elastic compression on the load line is  $\delta_{\max}$ , the corresponding elastic compression of the ball  $\delta_\psi$  along a radius at angle  $\psi$  to the load line will be given by

$$\delta_\psi = (\delta_{\max} \cos \psi - c) = \left( \delta_{\max} + \frac{P_d}{2} \right) \cos \psi - \frac{P_d}{2}$$

This assumes that the races are rigid. Now, it is clear from figure 23(c) that  $(\delta_{\max} + P_d/2)$  represents the total relative radial displacement of the inner and outer races.

Hence

$$\delta_\psi = \delta \cos \psi - P_d/2 \tag{52}$$

The relationship between load and elastic compression along the radius at angle  $\psi$  to the load vector is given by equation (48) as

$$F_\psi = K_j \delta_\psi^j$$

Substituting equation (52) into this equation gives

$$F_\psi = K_j (\delta \cos \psi - P_d/2)^j$$

For static equilibrium, the applied load must equal the sum of the components of the rolling-element loads parallel to the direction of the applied load.

$$F_r = \sum F_\psi \cos \psi$$

therefore

$$F_r = K_j \sum (\delta \cos \psi - P_d/2)^j \cos \psi \tag{53}$$

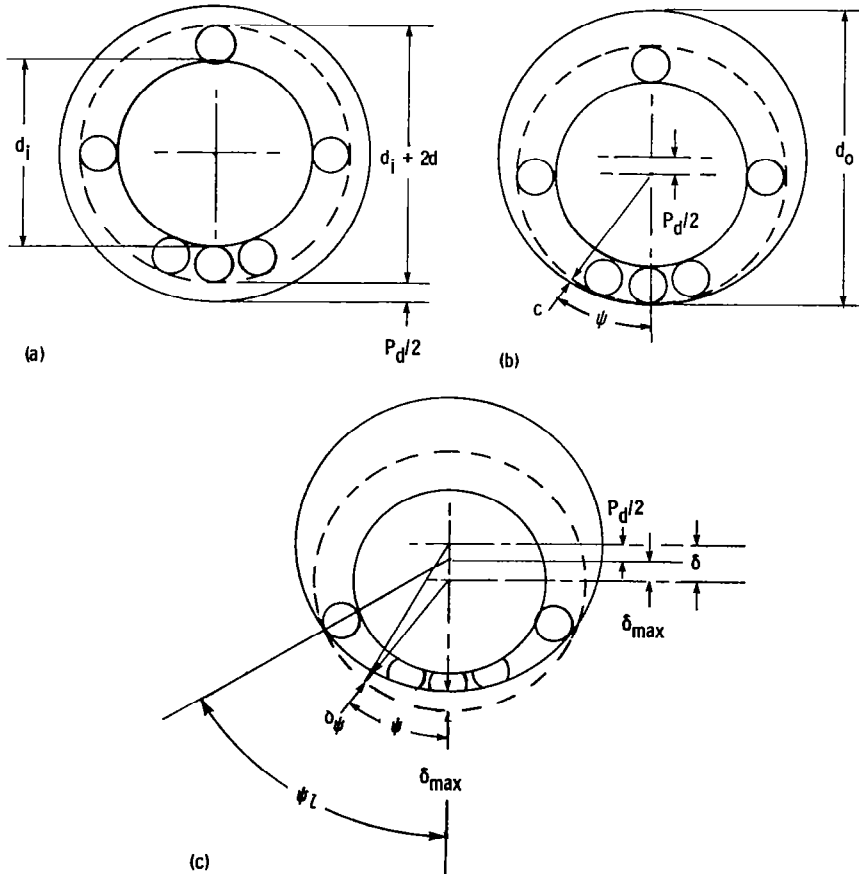


Figure 23. — Radially loaded rolling-element bearing. (a) Concentric arrangement. (b) Initial contact. (c) Interference.

The angular extent of the bearing arc  $2\psi_l$  in which the rolling elements are loaded is obtained by setting the root expression in equation (53) equal to zero and solving for  $\psi$ .

$$\psi_l = \cos^{-1}(P_d/2\delta)$$

The summation in equation (53) applies only to the angular extent of the loaded region. This equation can be written for a *roller bearing* as

$$F_r = \left( \psi_l - \frac{P_d}{2\delta} \sin \psi_l \right) n K_1 \delta / 2\pi \quad (54)$$

and similarly in integral form for a *ball bearing* as

$$F_r = \frac{n}{\pi} K_{1.5} \delta^{3/2} \int_0^{\psi_l} \left( \cos \psi - \frac{P_d}{2\delta} \right)^{3/2} \cos \psi \, d\psi$$

The integral in the equation can be reduced to a standard elliptic integral by the hypergeometric series and the beta function. If the integral is numerically evaluated directly, the following approximate expression is derived:

$$\int_0^{\psi_l} \left( \cos \psi - \frac{P_d}{2\delta} \right)^{3/2} \cos \psi \, d\psi = 2.491 \left\{ \left[ 1 + \left( \frac{P_d/2\delta - 1}{1.23} \right)^2 \right]^{1/2} - 1 \right\}$$

This approximate expression fits the exact numerical solution to within  $\pm 2$  percent for a complete range of  $P_d/2\delta$ .

The load carried by the most heavily loaded ball is obtained by substituting  $\psi = 0^\circ$  in equation (53) and dropping the summation sign

$$F_{\max} = K_j \delta^j \left( 1 - \frac{P_d}{2\delta} \right)^j \quad (55)$$

Dividing the maximum ball load (eq. (55)) by the total radial load for a *roller bearing* (eq. (54)) gives

$$F_r = \frac{\left( \psi_l - \frac{P_d}{2\delta} \sin \psi_l \right) n F_{\max} / 2\pi}{(1 - P_d/2\delta)} \quad (56)$$

and similarly for a *ball bearing*

$$F_r = n F_{\max} / Z \quad (57)$$

where

$$Z = \frac{\pi(1 - P_d/2\delta)^{3/2}}{2.491 \left\{ \left[ 1 + \left( \frac{1 - P_d/2\delta}{1.23} \right)^2 \right]^{1/2} - 1 \right\}} \quad (58)$$

For *roller bearings* when the diametral clearance  $P_d$  is zero, equation (56) gives

$$F_r = n F_{\max} / 4 \quad (59)$$

For *ball bearings* when the diametral clearance  $P_d$  is zero, the value of  $Z$  in equation (57) becomes 4.37. This is the value derived by Stribeck (1901) for ball bearings of zero diametral clearance. The approach used by Stribeck was to evaluate the finite summation for various numbers of balls. He then derived the celebrated Stribeck equation for static load-carrying capacity by writing the more conservative value of 5 for the theoretical value of 4.37:

$$F_r = n F_{\max} / 5 \quad (60)$$

In using equation (60), it should be remembered that  $Z$  was considered to be a constant and that the effects of clearance and applied load on load distribution were not taken into account. However, these effects were considered in obtaining equation (57).

### 8.3 Thrust-Loaded Ball Bearings

The static-thrust-load capacity of a ball bearing may be defined as the maximum thrust load that the bearing can endure before the contact ellipse approaches a race shoulder, as shown in figure 24, or the load at which the allowable mean compressive stress is reached, whichever is smaller. Both the limiting shoulder height and the mean

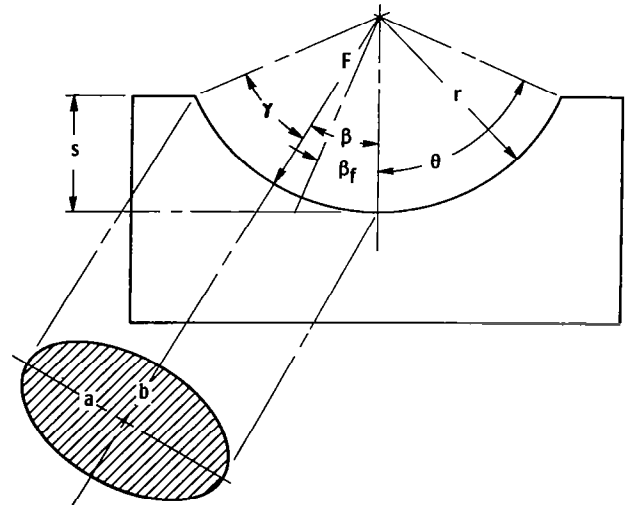


Figure 24. — Contact ellipse in bearing race.

compressive stress must be calculated to find the static-thrust-load capacity.

The contact ellipse in a bearing race under a load is shown in figure 24. Each ball is subjected to an identical thrust component  $F_t/n$ , where  $F_t$  is the total thrust load. The initial contact angle before the application of a thrust load is denoted by  $\beta_f$ . Under load the normal ball thrust load  $F$  acts at the contact angle  $\beta$  and is written as

$$F = F_t/n \sin \beta \quad (61)$$

A cross section through an angular-contact bearing under a thrust load  $F_t$  is shown in figure 25. From this figure, the contact angle after the thrust load has been applied can be written as

$$\beta = \cos^{-1} \left( \frac{D - P_d/2}{D + \delta} \right) \quad (62)$$

The initial contact angle was given in equation (7). Using that equation and rearranging terms in equation (62) give, solely from geometry (fig. 25),

$$\delta = D \left( \frac{\cos \beta_f}{\cos \beta} - 1 \right)$$

$$\delta = \delta_o + \delta_i$$

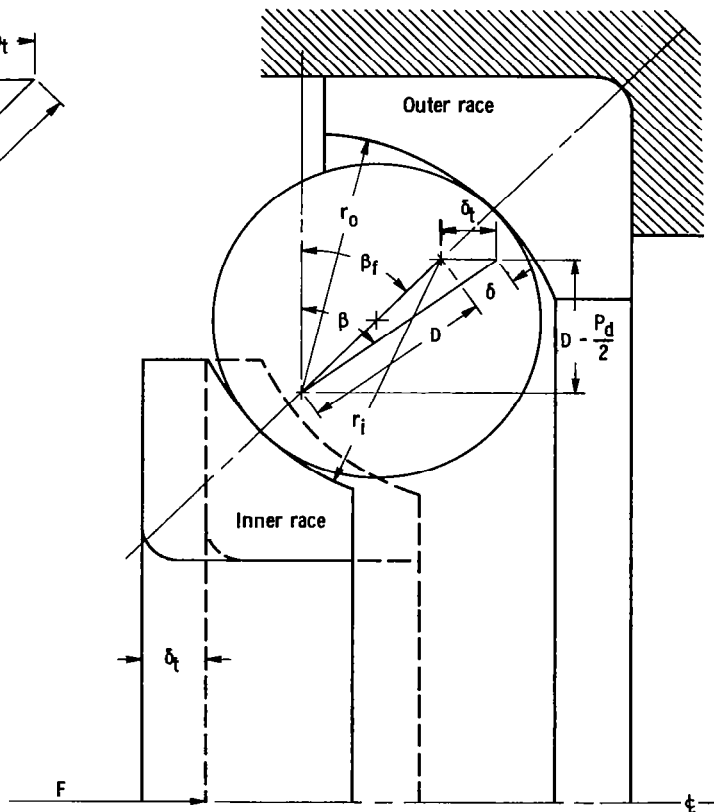
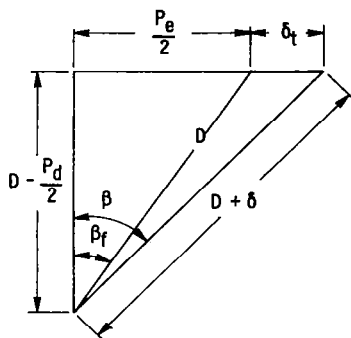


Figure 25. — Angular-contact ball bearing under thrust load.

$$\delta = \left[ \frac{F}{(K_j)_o} \right]^{1/j} + \left[ \frac{F}{(K_j)_i} \right]^{1/j}$$

$$K_j = \frac{1}{\left\{ \left[ \frac{1}{(K_j)_o} \right]^{1/j} + \left[ \frac{1}{(K_j)_i} \right]^{1/j} \right\}^j}$$

$$K_j = \frac{1}{\left[ \frac{4.5 \bar{\mathfrak{F}}_o^3}{\pi \bar{k}_o E'_o (R_o \bar{\mathfrak{E}}_o)^{1/2}} \right]^{2/3} + \left[ \frac{4.5 \bar{\mathfrak{F}}_i^3}{\pi \bar{k}_i E'_i (R_i \bar{\mathfrak{E}}_i)^{1/2}} \right]^{2/3}} \quad (63)$$

$$F = K_j D^{3/2} \left( \frac{\cos \beta_f}{\cos \beta} - 1 \right)^{3/2} \quad (64)$$

where

$$K_{1.5} = \pi \bar{k} E' \left( \frac{R \bar{\mathfrak{E}}}{4.5 \bar{\mathfrak{F}}^3} \right)^{1/2} \quad (65)$$

and  $k$ ,  $\bar{\varepsilon}$ , and  $\bar{\mathfrak{F}}$  are given by equations (37), (38), and (39), respectively.

From equations (61) and (64), we can write

$$\left. \begin{aligned} \frac{F_t}{n \sin \beta} &= F \\ \frac{F_t}{n K_j D^{3/2}} &= \sin \beta \left( \frac{\cos \beta_f}{\cos \beta} - 1 \right)^{3/2} \end{aligned} \right\} \quad (66)$$

This equation can be solved numerically by the Newton-Raphson method. The iterative equation to be satisfied is

$$\beta' - \beta = \frac{\frac{F_t}{n K_{1.5} D^{3/2}} - \sin \beta \left( \frac{\cos \beta_f}{\cos \beta} - 1 \right)^{3/2}}{\cos \beta \left( \frac{\cos \beta_f}{\cos \beta} - 1 \right)^{3/2} + \frac{3}{2} \cos \beta_f \tan^2 \beta \left( \frac{\cos \beta_f}{\cos \beta} - 1 \right)^{1/2}} \quad (67)$$

In this equation convergence is satisfied when  $\beta' - \beta$  becomes essentially zero.

When a thrust load is applied, the shoulder height is limited to the distance by which the pressure-contact ellipse can approach the shoulder. As long as the following inequality is satisfied, the pressure-contact ellipse will not exceed the shoulder height limit:

$$\theta > \beta + \sin^{-1}(D_y/fd)$$

From figure 9 and equation (11), the angle used to define the shoulder height  $\theta$  can be written as

$$\theta = \cos^{-1}(1 - s/fd)$$

From figure 7, the axial deflection  $\delta_t$  corresponding to a thrust load can be written as

$$\delta_t = (D + \delta) \sin \beta - D \sin \beta_f \quad (68)$$

Substituting equation (63) into equation (68) gives

$$\delta_t = \frac{D \sin(\beta - \beta_f)}{\cos \beta}$$

Having determined  $\beta$  from equation (67) and  $\beta_f$  from equation (49), we can easily evaluate the relationship for  $\delta_t$ .

## 8.4 Preloading

The use of angular-contact bearings as duplex pairs preloaded against each other is discussed in section 2.1. As shown in table 2 duplex bearing pairs are used in either back-to-back or face-to-face arrangements. Such bearings are usually preloaded against each other by providing what is called "stickout" in the manufacture of the bearing. This is illustrated in figure 26 for a bearing pair used in a back-to-back arrangement. The magnitude of the stickout and the bearing design determine the level of preload on each bearing when the bearings are clamped together as in figure 26. The magnitude of preload and the load deflection characteristics for a given bearing pair can be calculated by using equations (7), (45), (61), (63), (64), (65), and (66).

The relationship of initial preload, system load, and final load for bearings  $a$  and  $b$  is shown in figure 27. The load deflection curve follows the relationship  $\delta = KF^{2/3}$ . When a system thrust load  $F_t$  is imposed on the bearing pairs, the magnitude of load on bearing  $b$  increases while that on bearing  $a$  decreases until the difference equals the system load. The physical situation demands that the *change* in each bearing deflection be the same ( $\Delta a = \Delta b$  in fig. 27). The increments in bearing load, however, are *not* the same. This is important because it always requires a system thrust load far greater than twice the preload before one bearing becomes unloaded. Prevention of bearing unloading, which can result in skidding and early failure, is an objective of preloading.

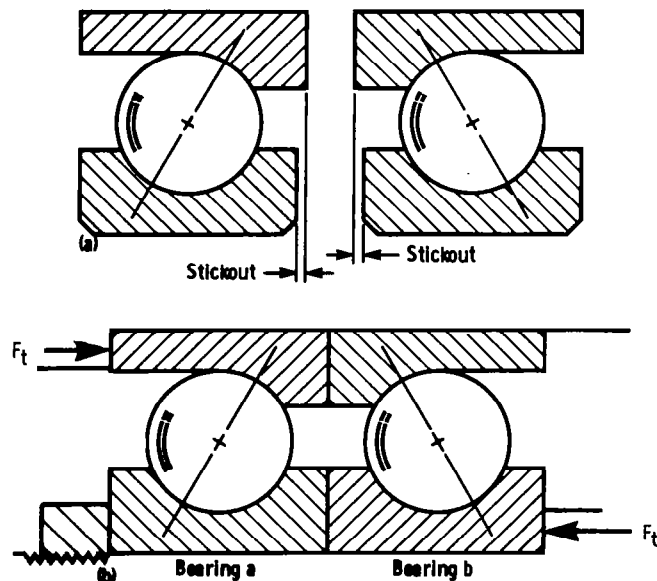


Figure 26.—Angular-contact bearings in back-to-back arrangement, shown individually as manufactured and as mounted with preload. (a) Separated. (b) Mounted and preloaded.

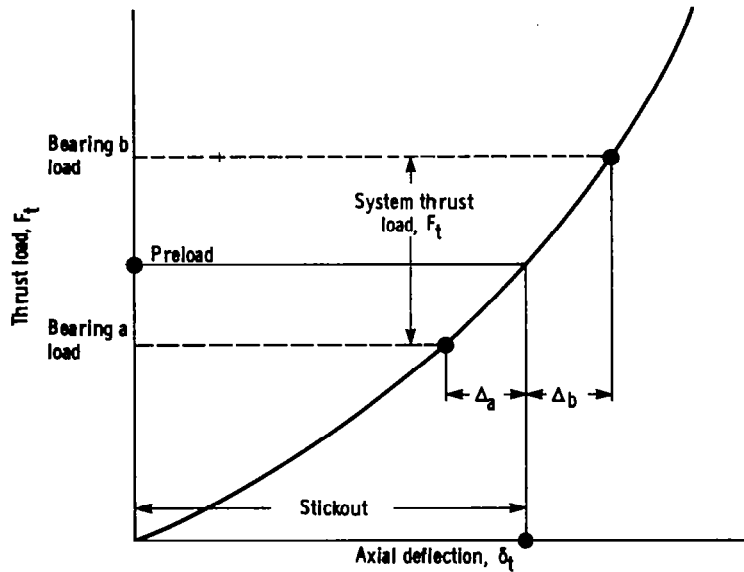


Figure 27. — Thrust load-axial deflection curve for a typical ball bearing.

## 9. Rolling Friction and Friction in Bearings

### 9.1 Rolling Friction

The concepts of rolling friction are important generally in understanding the behavior of machine elements in rolling contact and particularly because rolling friction influences the overall behavior of rolling-element bearings. The theories of Reynolds (1875) and Heathcote (1921) attempted to explain rolling friction in terms of the energy required to overcome the interfacial slip that occurs because of the curved shape of the contact area. As shown in figure 28, the ball rolls about the  $y$  axis and makes contact with the groove from  $a$  to  $b$ . If the groove

is fixed, then for zero slip over the contact area, no point within the area should have a velocity in the direction of rolling. The surface of the contact area is curved, however, so that points  $a$  and  $b$  are at different radii from the  $y$  axis than are points  $c$  and  $d$ . For a rigid ball, points  $a$  and  $b$  must have different velocities with respect to the  $y$  axis than do points  $c$  and  $d$  because the velocity of any point on the ball relative to the  $y$  axis equals the angular velocity times the radius from the  $y$  axis. Slip must occur at various points over the contact area unless the body is so elastic that yielding can take place in the contact area to prevent this interfacial slip. The theory of Reynolds and later Heathcote assumed that this interfacial slip took place and that the forces required to make a ball roll were those required to overcome the friction due to this

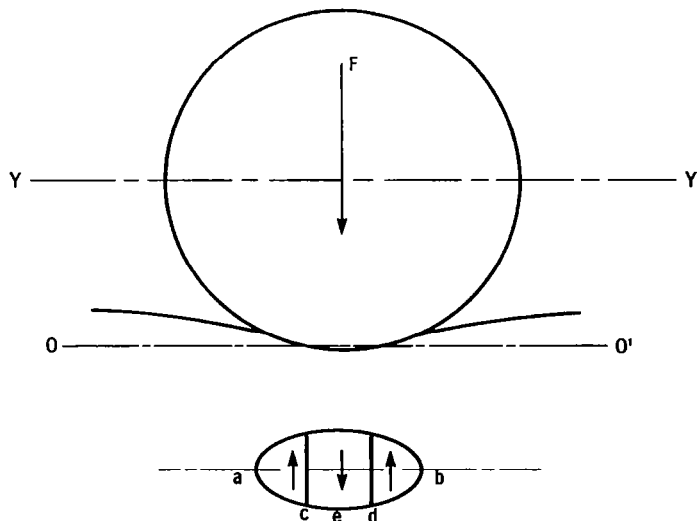


Figure 28. — Differential slip due to curvature of contact ellipse.



interfacial slip. In the contact area, rolling without slip will occur at a specific radius from the  $y$  axis. Where the radius is greater than this radius to the rolling point, slip will occur in one direction; where it is less than the radius to this rolling point, slip will occur in the other direction. In figure 28, the lines to points  $c$  and  $d$  represent the approximate location of the rolling bands, and the arrows shown in the three portions of the contact area represent the directions of interfacial slip when the ball is rolling into the paper.

The location of the two rolling bands relative to the axis of the contact ellipse can be obtained by summing the forces acting on the ball in the direction of rolling. In figure 29 these are

$$2T_b - T_a = \mu F$$

where  $\mu$  is the coefficient of rolling friction. If a Hertzian

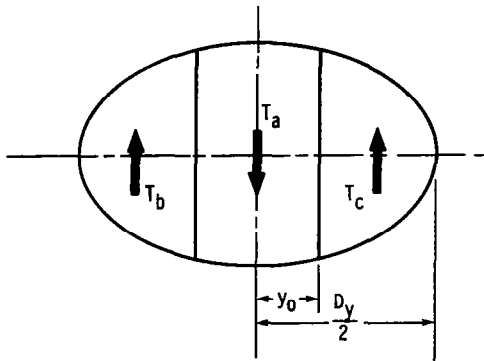


Figure 29. — Friction forces in contact ellipse.

ellipsoidal pressure distribution is assumed, the location of the rolling bands can be determined (Bissson and Anderson, 1964). For bearing steels

$$y_o/D_y \approx 0.174$$

where  $D_y$  is the diameter of the contact ellipse along the  $y$  axis (eq. (40)).

In actuality, all materials are elastic so that areas of no slip as well as areas of microslip exist within the contact as pointed out by Johnson and Tabor (1967-68). Differential strains in the materials in contact will cause slip unless it is prevented by friction. In high-conformity contacts, slip is likely to occur over most of the contact region, as shown in figure 30. The limiting value of friction force  $T$  is

$$T = \frac{0.2 \mu D_y^2 F}{r_{ax}^2}$$

A portion of the elastic energy of compression in rolling is always lost because of hysteresis. The effect of hysteresis losses on rolling resistance has been studied by Tabor (1955). Tabor developed the following expression:

$$T = c_4 \lambda \frac{F D_y}{r_{ax}}$$

where

$$\lambda = \frac{\pi D_y^2 E'}{4 \mu r_{ax}^2 p_m}$$

$p_m$  is the mean pressure within the contact, and  $c_4$  is 1/3

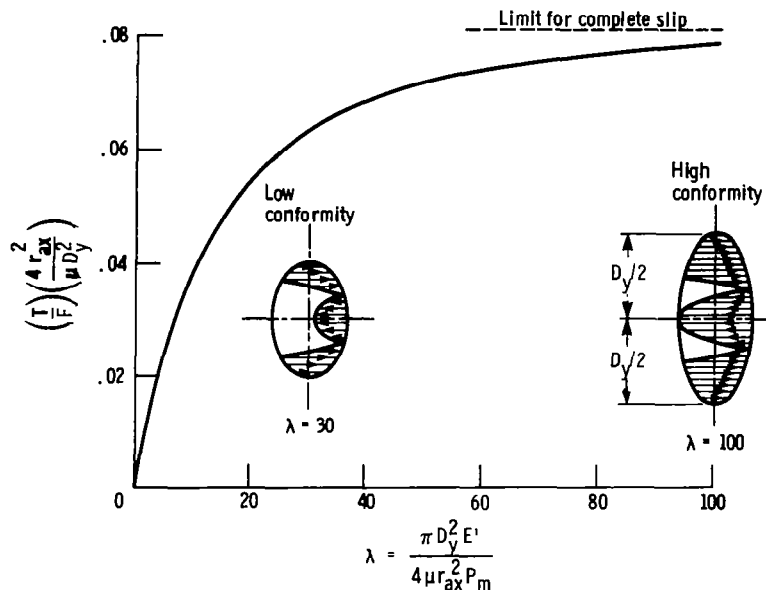


Figure 30. — Frictional resistance of ball in conforming groove.

for rectangular contacts and  $3/32$  for elliptical contacts. Two hard-steel surfaces show a  $\lambda$  of about 1 percent.

Of far greater importance in contributing to frictional losses in rolling-element bearings, especially at high speeds, is ball spinning. Spinning as well as rolling takes place in one or both of the ball-race contacts of a ball bearing. The situation is illustrated in figure 16.

High speeds cause a divergency of the contact angles  $\beta_i$  and  $\beta_o$ . In figure 17(b) the ball is rolling with inner-race control, so that approximately pure rolling takes place at the inner-race contact. The rolling and spinning vectors,  $\omega_r$  and  $\omega_s$ , at the outer-race contact are shown in figure 16. The higher the ratio  $\omega_s/\omega_r$ , the higher the friction losses.

## 9.2 Friction Losses in Rolling-Element Bearings

Some of the factors that affect the magnitude of friction losses in rolling bearings are

- (1) Bearing size
- (2) Bearing type
- (3) Bearing design
- (4) Load (magnitude and type, either thrust or radial)
- (5) Speed
- (6) Oil viscosity
- (7) Oil flow

In a specific bearing, friction losses consist of

(1) Sliding friction losses in the contacts between the rolling elements and the races. These losses include differential slip and slip due to ball spinning. They are complicated by the presence of elastohydrodynamic lubrication films. The shearing of elastohydrodynamic lubrication films, which are extremely thin and contain oil whose viscosity is increased by orders of magnitude above its atmospheric pressure value, accounts for a significant fraction of the friction losses in rolling-element bearings.

(2) Hysteresis losses due to the damping capacity of the race and ball materials

(3) Sliding friction losses between the separator and its locating race surface and between the separator pockets and the rolling elements

(4) Shearing of oil films between the bearing parts and oil churning losses caused by excess lubricant within the bearing

(5) Flinging of oil off the rotating parts of the bearing

Because of the dominant role played in bearing frictional losses by the method of lubrication, there are no quick and easy formulas for computing rolling-element bearing power loss. Coefficients of friction for a particular bearing can vary by a factor of 5 depending on lubrication. A flood-lubricated bearing may consume five times the power of one that is merely wetted by oil-air mist lubrication.

As a rough but useful guide, we can use the friction coefficients given by Palmgren (1959). These values were

computed at a bearing load that will give a life of  $1 \times 10^9$  revolutions for the respective bearings. The friction coefficients for several different bearings are shown here:

Self-aligning ball .....	0.0010
Cylindrical roller, with flange-guided short rollers .....	0.0011
Thrust ball.....	0.0013
Single-row, deep-groove ball .....	0.0015
Tapered and spherical roller, with flange-guided rollers .....	0.0018
Needle roller .....	0.0045

All of these friction coefficients are referenced to the bearing bore.

More accurate estimates of bearing power loss and temperature rise can be obtained by using one or more of the available computer codes that represent the basis for current design methodology for rolling-element bearings. These are discussed in Anderson (1979) and Pirvics (1980) and briefly reviewed later in this report.

## 10. Lubricants and Lubrication Systems

A liquid lubricant has several functions in a rolling-element bearing. It provides the medium for the establishment of separating films between the bearing parts (elastohydrodynamic between the races and rolling elements and hydrodynamic between the cage or separator and its locating surface). It serves as a coolant if circulated through the bearing either to an external heat exchanger or simply brought into contact with the bearing housing and machine casing. A circulating lubricant also serves to flush out wear debris and carry it to a filter where it can be removed from the system. Finally it provides corrosion protection. The different methods of providing liquid lubricant to a bearing are discussed here individually.

### 10.1 Solid Lubrication

An increasing number of rolling-element bearings are lubricated with solid-film lubricants, usually in applications such as extreme temperature or the vacuum of space where conventional liquid lubricants are not suitable.

Success in cryogenic applications where the bearing is cooled by the cryogenic fluid (liquid oxygen or hydrogen) has been achieved with transfer films of polytetrafluoroethylene (Scibbe, 1968). Bonded films of soft metals such as silver, gold and lead applied by ion plating as very thin films (0.2 to 0.3  $\mu\text{m}$ ) have also been used (Todd and Bentall, 1978). Silver, and lead in particular, have found use in bearings used to support the rotating anode in X-ray tubes. Very thin films are required in rolling-





element bearings in order not to significantly alter the bearing internal geometry and to retain the basic mechanical properties of the substrate materials in the Hertzian contacts.

## 10.2 Liquid Lubrication

The great majority of rolling-element bearings are lubricated by liquids. The liquid in greases can be used, or liquid can be supplied to the bearing from either noncirculating or circulating systems.

**Greases.**—The most common and probably least expensive mode of lubrication is grease lubrication. In the strictest sense, a grease is not a liquid, but the liquid or fluid constituent in the grease is the lubricant. Greases consist of a fluid phase of either a petroleum oil or a synthetic oil and a thickener. The most common thickeners are sodium-, calcium-, or lithium-based soaps, although thickeners of inorganic materials such as bentonite clay have been used in synthetic greases. Some discussion of the characteristics and temperature limits of greases is given in Bisson and Anderson (1964) and McCarthy (1973).

Greases are usually retained within the bearing by shields or seals that are an integral part of the assembled bearing. Since there is no recirculating fluid, grease-lubricated bearings must reject their heat by conduction and convection. They are therefore limited in operating speeds to maximum  $d_b N$  values of 0.25 to 0.4 million.

The proper grease for a particular application depends on the temperature, speed, and ambient pressure environment to which the bearing is exposed. McCarthy (1973) presents a comprehensive discussion useful in the selection of a grease; the bearing manufacturer can also recommend the most suitable grease and bearing type.

**Nonrecirculating liquid lubrication systems.**—At low to moderate speeds, where the use of grease lubrication is not suitable, other methods of supplying lubricant to the bearing can be used. These include splash or bath lubrication, wick, oil-ring, and oil-air mist lubrication. Felt wicks can be used to transport oil by capillary action from a nearby reservoir. Oil rings, which are driven by frictional contact with the rotating shaft, run partially immersed in an oil reservoir and feed oil mechanically to the shaft, which is adjacent to the bearing. The bearing may itself be partially immersed in an oil reservoir to splash lubricate itself. All of these methods require very modest ambient temperatures and thermal conditions as well as speed conditions equivalent to a maximum  $d_b N$  of about 0.5 million. The machinery must also remain in a fixed-gravity orientation.

Oil-air mist lubrication supplies atomized oil in an air stream to the bearing, where a reclassifier increases the droplet size, allowing it to condense on the bearing surfaces. Feed rates are low and a portion of the oil flow escapes with the feed air to the atmosphere. Commercial

oil-air mist generators are available for systems ranging from a single bearing to hundreds of bearings. Bearing friction losses and heat generation with mist lubrication are low, but ambient temperatures and cooling requirements must be moderate because oil-air mist systems provide minimal cooling. Many bearings, especially small-bore bearings, are successfully operated at high speeds ( $d_b N$  values to greater than 1 million) with oil-air mist lubrication.

**Jet lubrication.**—In applications where speed or heat rejection requirements are too high, jet lubrication is frequently used to lubricate and control bearing temperatures. A number of variables are critical to achieving not only satisfactory but near optimal performance and bearing operation. These include the placement of the nozzles, the number of nozzles, the jet velocity, the lubricant flow rate, and the scavenging of the lubricant from the bearing and immediate vicinity. The importance of proper jet lubricating system design is shown by Matt and Gianotti (1966). Their results are summarized in figure 31.

Proper placement of the jets should take advantage of any natural pumping ability of the bearings. Figure 32 (Parker, 1980) illustrates jet lubrication of ball and tapered-roller bearings. Centrifugal forces aid in moving the oil through the bearing to cool and lubricate the elements. Directing jets at the radial gaps between the cage and the races achieves maximum penetration of oil into the interior of the bearing. Miyakawa, et al. (1972),

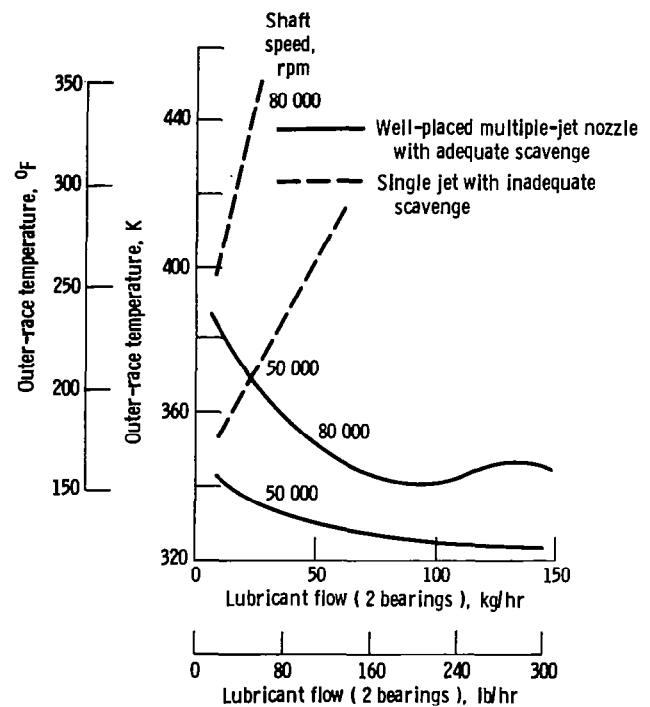


Figure 31.—Effectiveness of proper jet lubrication. Test bearings, 20-mm-bore angular-contact ball bearings; thrust load, 222 N (50 lbf). (From Matt and Gianotti, 1968.)

Anderson, et al. (1954), Zaretsky, et al. (1976), and Parker and Signer (1978) present useful data on the influence of jet placement and velocity on the lubrication of several types of bearings.

**Under-race lubrication.** — As bearing speeds increase, centrifugal effects become more predominant, making it increasingly difficult to effectively lubricate and cool a bearing. The jetted oil is thrown off the sides of the bearing rather than penetrating to the interior. At extremely high  $d_b N$  values (2.4 million and higher), jet lubrication becomes ineffective. Increasing the flow rate only adds to heat generation through increased churning losses. Brown (1970) describes an under-race oiling system used in a turbofan engine for both ball and cylindrical roller bearings. Figure 33 illustrates the technique. The lubricant is directed radially under the bearings. Centrifugal effects assist in pumping oil out through the bearings through suitable slots and holes, which are made a part of both the shaft and mounting system and the bearings themselves. Holes and slots are provided within the bearing to feed oil directly to the ball-race and cage-race contacts.

This lubrication technique has been thoroughly tested for large-bore ball and roller bearings up to 3 million  $d_b N$ . Pertinent data are reported by Signer, et al. (1974), Brown, et al. (1977), Schuller (1979), and Signer and Schuller (1982).

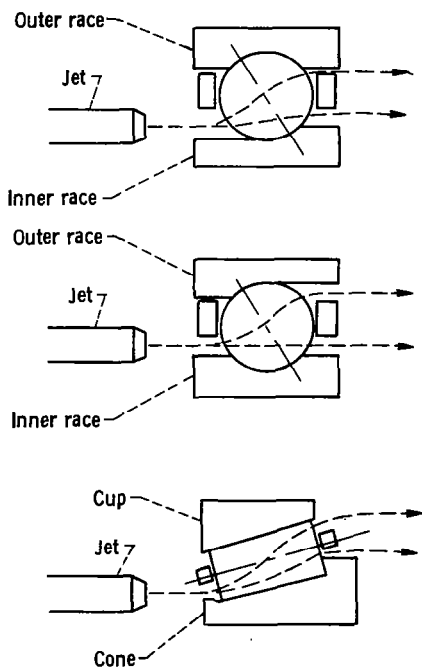


Figure 32. — Placement of jets for ball bearings with relieved rings and tapered-roller bearings.

## 11. Elastohydrodynamic Lubrication

Elastohydrodynamic lubrication is a form of fluid-film lubrication where elastic deformation of the bearing surfaces becomes significant. It is usually associated with highly stressed machine components such as rolling-element bearings. Historically, elastohydrodynamic lubrication may be viewed as one of the major developments in the field of lubrication in the twentieth century. It not only revealed the existence of a previously unsuspected regime of lubrication in highly stressed nonconforming machine elements, but it also brought order to the complete spectrum of lubrication regimes, ranging from boundary to hydrodynamic.

### 11.1 Relevant Equations

The relevant equations used in elastohydrodynamic lubrication are given here.

*Lubrication equation (Reynolds equation)*

$$\frac{\partial}{\partial x} \left( \frac{\rho h^3}{\eta} \frac{\partial p}{\partial x} \right) + \frac{\partial}{\partial y} \left( \frac{\rho h^3}{\eta} \frac{\partial p}{\partial y} \right) = 12u \frac{\partial}{\partial x} (\rho h)$$

where

$$u = (u_a + u_b) / 2$$

*Viscosity variation*

$$\eta = \eta_0 e^{\xi p}$$

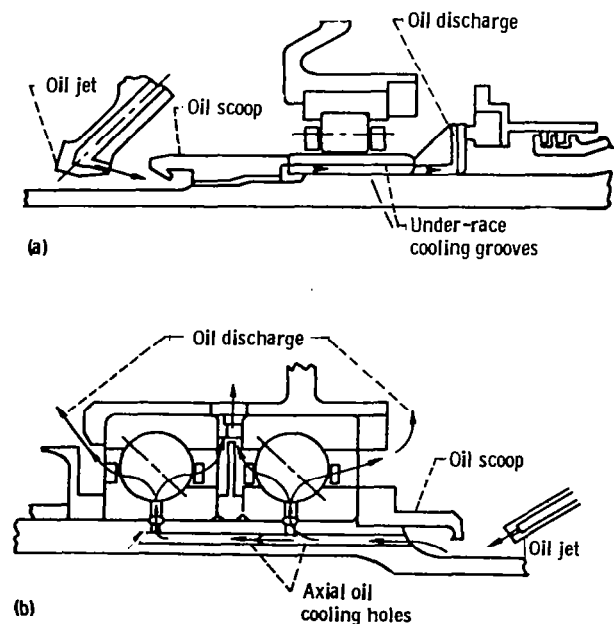


Figure 33. — Under-race oiling system for main shaft bearings on turbofan engine. (a) Cylindrical roller bearing. (b) Ball thrust bearing. (From Brown, 1970.)

where  $\eta_0$  is the coefficient of absolute or dynamic viscosity at atmospheric pressure and  $\xi$  is the pressure-viscosity coefficient of the fluid.

*Density variation (for mineral oils)*

$$\rho = \rho_0 \left( 1 + \frac{0.6 p}{1 + 1.17 p} \right)$$

where  $\rho_0$  is the density at atmospheric conditions.

*Elasticity equation*

$$\delta = \frac{2}{E'} \int \int_A \frac{p(x,y) dx dy}{\sqrt{(x-x_1)^2 + (y-y_1)^2}}$$

where

$$E' = \frac{2}{\frac{1-\nu_a^2}{E_a} + \frac{1-\nu_b^2}{E_b}}$$

*Film thickness equation*

$$h = h_0 + x^2/2R_x + y^2/2R_y + \delta(x,y)$$

where

$$1/R_x = 1/r_{ax} + 1/r_{bx} \quad (69)$$

$$1/R_y = 1/r_{ay} + 1/r_{by} \quad (70)$$

The different radii expressed in equations (69) and (70) are depicted in figure 10.

The elastohydrodynamic lubrication solution therefore requires the calculation of the pressure distribution within the conjunction, at the same time allowing for the effects that this pressure will have on the properties of the fluid and on the geometry of the elastic solids. The solution will also provide the shape of the lubricant film, particularly the minimum clearance between the solids. A detailed description of the elasticity model one could use is given by Dowson and Hamrock (1976), and the complete elastohydrodynamic lubrication theory is given by Hamrock and Dowson (1976).

## 11.2 Dimensionless Grouping

The variables resulting from the elastohydrodynamic lubrication theory are

$E'$	effective elastic modulus, N/m <sup>2</sup>
$F$	normal applied load, N
$h$	film thickness, m
$R_x$	effective radius in $x$ (motion) direction, m
$R_y$	effective radius in $y$ (transverse) direction, m

$u$	mean surface velocity in $x$ direction, m/s
$\xi$	pressure-viscosity coefficient of fluid, m <sup>2</sup> /N
$\eta_0$	atmospheric viscosity, N s/m <sup>2</sup>

From these variables the following five dimensionless groupings can be established:

*Dimensionless film thickness*

$$H = h/R_x$$

*Ellipticity parameter*

$$k = D_y/D_x = (R_y/R_x)^{2/\pi}$$

*Dimensionless load parameter*

$$W = F/E' R_x^2 \quad (71)$$

*Dimensionless speed parameter*

$$U = \eta_0 u / E' R_x \quad (72)$$

*Dimensionless materials parameter*

$$G = \xi E'$$

The dimensionless minimum film thickness can thus be written as a function of the other four parameters

$$H = f(k, U, W, G)$$

The most important practical aspect of elastohydrodynamic lubrication theory is the determination of the minimum film thickness within a conjunction. That is, maintaining a fluid-film thickness of adequate magnitude is extremely important to the operation of machine elements like rolling-element bearings. Specifically, elastohydrodynamic film thickness influences fatigue life, as discussed in section 12.

## 11.3 Minimum-Film-Thickness Formula

By using the numerical procedures outlined in Hamrock and Dowson (1976), the influence of the ellipticity parameter and the dimensionless speed, load, and materials parameters on minimum film thickness has been investigated by Hamrock and Dowson (1977). The ellipticity parameter  $k$  was varied from 1 (a ball-on-plate configuration) to 8 (a configuration approaching a rectangular contact). The dimensionless speed parameter  $U$  was varied over a range of nearly two orders of magnitude, and the dimensionless load parameter  $W$  over a range of one order of magnitude. Situations equivalent to using solid materials of bronze, steel, and silicon nitride and lubricants of paraffinic and naphthenic oils

were considered in the investigation of the role of the dimensionless materials parameter  $G$ . Thirty-four cases were used in generating the minimum-film-thickness formula given here.

$$H_{\min} = 3.63 U^{0.68} G^{0.49} W^{-0.073} (1 - e^{-0.68k}) \quad (74)$$

In this equation the most dominant exponent occurs on the speed parameter, and the exponent on the load parameter is very small and negative. The materials parameter also carries a significant exponent, although the range of this variable in engineering situations is limited.

#### 11.4 Pressure and Film Thickness Plots

A representative contour plot of dimensionless pressure is shown in figure 34 for  $k=1.25$ ,  $U=0.168 \times 10^{-11}$ , and  $G=4522$ . In this figure and in figure 35, the + symbol indicates the center of the Hertzian contact zone. The dimensionless representation of the  $X$  and  $Y$  coordinates causes the actual Hertzian contact ellipse to be a circle regardless of the value of the ellipticity parameter. The Hertzian contact circle is shown by asterisks. On this figure is a key showing the contour labels and each corresponding value of dimensionless pressure. The inlet region is to the left and

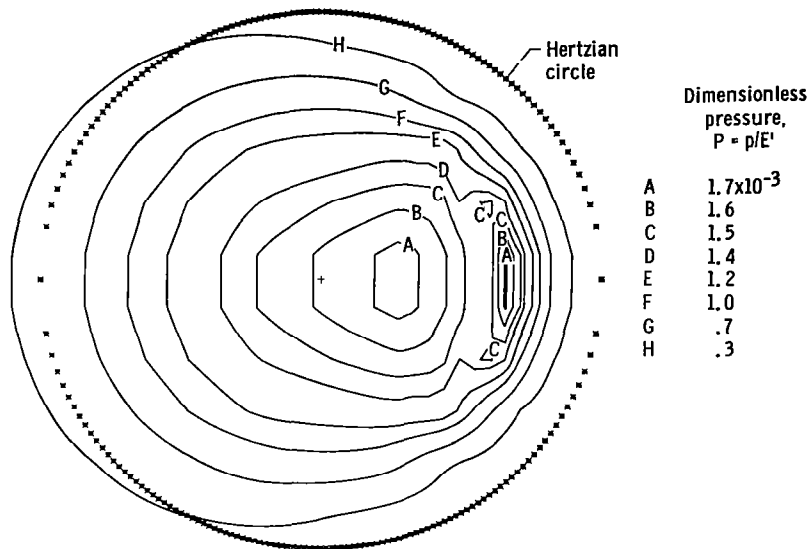


Figure 34. — Contour plot of dimensionless pressure.  $k=1.25$ ;  $U=0.168 \times 10^{-11}$ ;  $W=0.111 \times 10^{-6}$ ;  $G=4522$ .

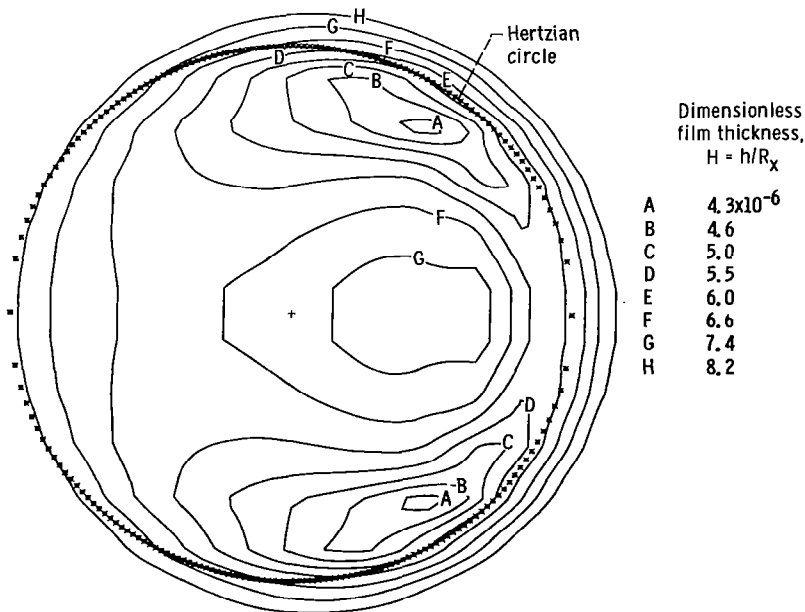


Figure 35. — Contour plot of dimensionless film thickness.  $k=1.25$ ;  $U=0.168 \times 10^{-11}$ ;  $W=0.111 \times 10^{-6}$ ;  $G=4522$ .

the exit region is to the right. The pressure gradient at the exit end of the conjunction is much larger than that in the inlet region. In figure 34 a pressure spike is visible at the exit of the contact.

Contour plots of the film thickness are shown in figure 35 for  $k=1.25$ ,  $U=0.168 \times 10^{-11}$ ,  $W=0.111 \times 10^{-6}$ , and  $G=4522$ . In this figure two minimum regions occur in well-defined side lobes that follow, and are close to, the edge of the Hertzian contact circle. These results produce all the essential features of previously reported experimental observations based on optical interferometry (Cameron and Gohar, 1966).

## 12. Rolling Bearing Fatigue Life

### 12.1 Contact Fatigue Theory

Rolling fatigue is a material failure caused by the application of repeated stresses to a small volume of material. It is a unique failure type. It is essentially a process of seeking out the weakest point at which the first failure will occur. A typical spall is shown in figure 36. We can surmise that on a microscale there will be a wide dispersion in material strength or resistance to fatigue because of inhomogeneities in the material. Because bearing materials are complex alloys, we would not expect them to be homogeneous or equally resistant to failure at all points. Therefore the fatigue process can be expected to be one in which a group of supposedly identical specimens exhibit wide variations in failure time when stressed in the same way. For this reason it is necessary to treat the fatigue process statistically.

To be able to predict how long a particular bearing will run under a specific load, we must have the following two essential pieces of information:

(1) An accurate, quantitative estimate of the life dispersion or scatter

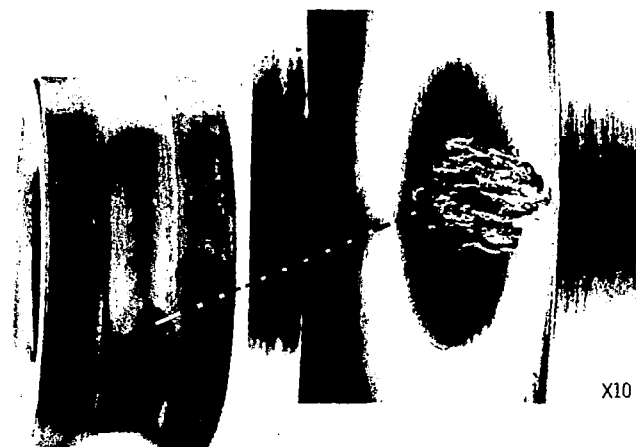


Figure 36. — Typical fatigue spall.

(2) The life at a given survival rate or reliability level. This translates into an expression for the “load capacity,” or the ability of the bearing to endure a given load for a stipulated number of stress cycles or revolutions. If a group of supposedly identical bearings is tested at a specific load and speed, there will be a wide scatter in bearing lives, as shown in figure 37.

### 12.2 The Weibull Distribution

Weibull (1949) postulates that the fatigue lives of a homogeneous group of rolling-element bearings are dispersed according to the following relation:

$$\ln \ln 1/S = e_1 \ln L/A$$

where  $S$  is the probability of survival,  $L$  is the fatigue life, and  $e_1$  and  $A$  are constants. The Weibull distribution results from a statistical theory of strength based on probability theory, where the dependence of strength on volume is explained by the dispersion in material strength. This is the “weakest link” theory.

Consider a volume being stressed that is broken up into  $m$  similar volumes

$$S_1 = 1 - M_1 \quad S_2 = 1 - M_2 \quad S_3 = 1 - M_3 \quad \cdots \quad S_m = 1 - M_m$$

The  $M$ 's represent the probability of failure and the  $S$ 's, the probability of survival. For the entire volume we can write

$$S = S_1 \cdot S_2 \cdot S_3 \cdots S_m$$

Then

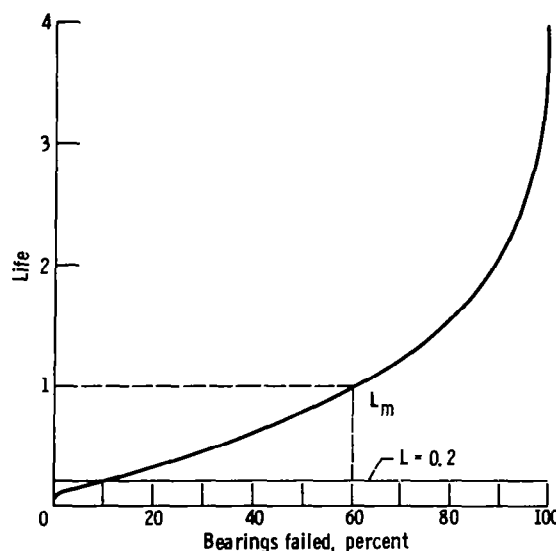


Figure 37. — Distribution of bearing fatigue failures.

$$1 - M = (1 - M_1)(1 - M_2)(1 - M_3) \cdots (1 - M_m)$$

$$1 - M = \prod_{i=1}^m (1 - M_i)$$

$$S = \prod_{i=1}^m (1 - M_i)$$

The probability of a crack starting in the  $i^{\text{th}}$  volume is

$$M_i = f(x) v_i$$

where  $f(x)$  is a function of the stress level, the number of stress cycles, and the depth into the material where the maximum stress occurs and  $v_i$  is the elementary volume. Therefore

$$S = \prod_{i=1}^m [1 - f(x) v_i]$$

$$\ln S = \sum_{i=1}^m \ln [1 - f(x) v_i]$$

Now if  $f(x) v_i \ll 1$ , then  $\ln [1 - f(x) v_i] = -f(x) v_i$  and

$$\ln S = - \sum_{i=1}^m f(x) v_i$$

Let  $v_i \rightarrow 0$ ; then

$$\sum_{i=1}^m f(x) v_i = f(x) dv = f(x) V$$

Lundberg and Palmgren (1947) assume that  $f(x)$  could be expressed as a power function of shear stress  $\tau_0$ , number of stress cycles  $J$ , and depth to the maximum shear stress  $Z_0$ .

$$f(x) = \tau_0^{c_1} J^{c_2} / Z_0^{c_3}$$

They also choose as the stressed volume

$$V = D_y Z_0 l_v$$

Then

$$\ln S = - \frac{\tau_0^{c_1} J^{c_2} D_y l_v}{Z_0^{c_3 - 1}}$$

or

$$\ln 1/S = \frac{\tau_0^{c_1} J^{c_2} D_y l_v}{Z_0^{c_3 - 1}} \quad (75)$$

For a specific bearing and load (e.g., stress)  $\tau_0$ ,  $D_y$ ,  $l_v$ , and  $Z_0$  are all constant so that

$$\ln 1/S \approx J^{c_2}$$

Designating  $J$  as life  $L$  in stress cycles gives

$$\ln 1/S = (L/A)^{c_2}$$

or

$$\ln \ln 1/S = c_2 \ln(L/A) \quad (76)$$

This is the Weibull distribution, which relates probability of survival and life. It has two principal functions. First, bearing fatigue lives plot as a straight line on Weibull coordinates (log log vs. log), so that the life at any reliability level can be determined. Of most interest are the  $L_{10}$  life ( $S=0.9$ ) and the  $L_{50}$  life ( $S=0.5$ ). Bearing load ratings are based on the  $L_{10}$  life. Second, equation (76) can be used to determine what the  $L_{10}$  life must be to obtain a required life at any reliability level. The  $L_{10}$  life is calculated, from the load on the bearing and the bearing dynamic capacity or load rating given in manufacturers' catalogs and engineering journals, by using the equation

$$L = (C/F_e)^m$$

where

- $C$  basic dynamic capacity or load rating
- $F_e$  equivalent bearing load
- $m$  3 for elliptical contacts and 10/3 for rectangular contacts

A typical Weibull plot is shown in figure 38.

### 12.3 Lundberg-Palmgren Theory

The Lundberg-Palmgren theory, on which bearing ratings are based, is expressed by equation (75). The exponents in this equation are determined experimentally from the dispersion of bearing lives and the dependence of life on load, geometry, and bearing size. As a standard of reference, all bearing load ratings are expressed in terms of the specific dynamic capacity  $C$ , which, by definition, is the load that a bearing can carry for 1 million inner-race revolutions with a 90 percent chance of survival.

Factors on which specific dynamic capacity and bearing life depend are

- (1) Size of rolling element
- (2) Number of rolling elements per row
- (3) Number of rows of rolling elements
- (4) Conformity between rolling elements and races
- (5) Contact angle under load
- (6) Material properties
- (7) Lubricant properties

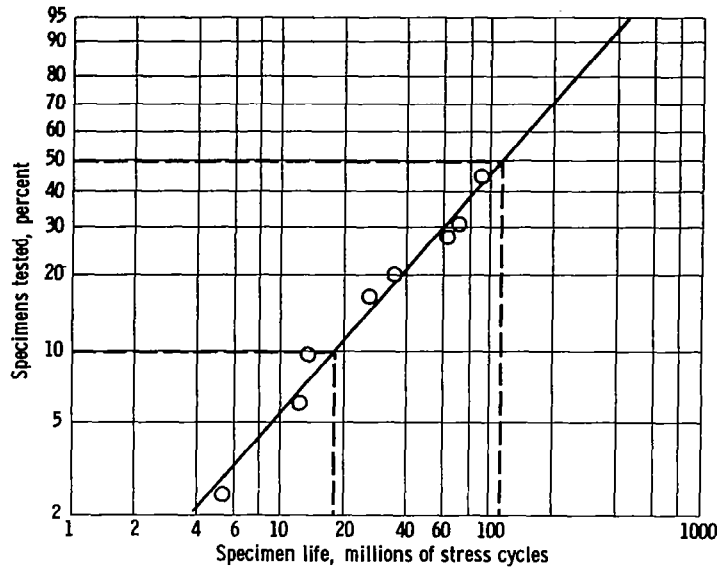


Figure 38. — Typical Weibull plot of bearing fatigue failures.

- (8) Operating temperature
- (9) Operating speed

Only factors (1) to (5) are incorporated in bearing dynamic capacities developed from the Lundberg-Palmgren theory. The remaining factors must be taken into account in the life adjustment factors discussed in section 12.5.

The formulas for specific dynamic capacity as developed by Lundberg-Palmgren (1947, 1952) are as follows:

For radial ball bearings with  $d \leq 25$  mm,

$$C = f_c (i \cos \beta)^{0.7} n^{2/3} \left( \frac{d}{0.0254} \right)^{1.8}$$

where

- $d$  diameter of rolling element, m
- $i$  number of rows of rolling elements
- $n$  number of rolling elements per row
- $\beta$  contact angle
- $f_c$  coefficient dependent on material and bearing type

For radial ball bearings with  $d \geq 25$  mm,

$$C = f_c (i \cos \beta)^{0.7} n^{2/3} \left( \frac{d}{0.0254} \right)^{1.4}$$

For radial roller bearings,

$$C = f_c (i \cos \beta)^{0.78} n^{3/4} \left( \frac{d}{0.0254} \right)^{1.07} \left( \frac{l_t}{0.0254} \right)^{0.78}$$

where  $l_t$  is roller length in meters.

For thrust ball bearings with  $\beta \neq 90^\circ$ ,

$$C = f_c (i \cos \beta)^{0.7} (\tan \beta) n^{2/3} \left( \frac{d}{0.0254} \right)^{1.8}$$

For thrust roller bearings,

$$C = f_c (i \cos \beta)^{0.78} (\tan \beta) n^{3/4} \left( \frac{l_t}{0.0254} \right)^{0.78}$$

For thrust ball bearings with  $\beta = 90^\circ$ ,

$$C = f_c i^{0.7} n^{2/3} \left( \frac{d}{0.0254} \right)^{1.8}$$

For thrust roller bearings with  $\beta = 90^\circ$ ,

$$C = f_c i^{0.78} n^{3/4} \left( \frac{d}{0.0254} \right)^{1.07} \left( \frac{l_t}{0.0254} \right)^{0.78}$$

For ordinary bearing steels such as SAE 52100 with mineral oil lubrication,  $f_c$  can be evaluated by using tables 14 and 15, but a more convenient method is to use tabulated values from the most recent Antifriction Bearing Manufacturers Association (AFBMA) documents on dynamic load ratings and life (ISO, 1976). The value of  $C$  is calculated or determined from bearing manufacturers' catalogs. The equivalent load  $F_e$  can be calculated from the equation

$$F_e = XF_r + YF_t$$

Factors  $X$  and  $Y$  are given in bearing manufacturers' catalogs for specific bearings.

In addition to specific dynamic capacity  $C$ , every bearing has a specific static capacity, usually designated as  $C_0$ . Specific static capacity is defined as the load that, under static conditions, will result in a permanent deformation of 0.0001 times the rolling-element diameter. For some bearings  $C_0$  is less than  $C$ , so it is important to avoid exposing a bearing to a static load that exceeds  $C_0$ . Values of  $C_0$  are given in bearing manufacturers' catalogs.

#### 12.4 The AFBMA Method

Shortly after publication of the Lundberg-Palmgren theory, the AFBMA began efforts to standardize methods for establishing bearing load ratings and making life predictions. Standardized methods of establishing load ratings for ball bearings (AFBMA, 1960a) and roller bearings (AFBMA, 1960b) were devised, based essentially on the Lundberg-Palmgren theory. These early standards are published in their entirety in Jones (1964). In recent years, significant advances have been made in rolling-element bearing material quality and in our understanding of the role of lubrication in bearing life through the development of elastohydrodynamic theory. Therefore the original AFBMA standards in AFBMA (1960a and b) have been updated with life adjustment factors. These factors have been incorporated into ISO (1976), which is discussed in the following section.

#### 12.5 Life Adjustment Factors

A comprehensive study of the factors affecting the fatigue life of bearings, which were not taken account of in the Lundberg-Palmgren theory, is reported in Bamberger (1971). In that reference it was assumed that the various environmental or bearing design factors are multiplicative in their effect on bearing life. The following equation results:

$$L_A = (\bar{D}) (\bar{E}) (\bar{F}) (\bar{G}) (\bar{H}) L_{10}$$

or

$$L_A = (\bar{D}) (\bar{E}) (\bar{F}) (\bar{G}) (\bar{H}) (C/F_e)^m$$

where

- $\bar{D}$  materials factor
- $\bar{E}$  metallurgical processing factor
- $\bar{F}$  lubrication factor
- $\bar{G}$  speed effect factor
- $\bar{H}$  misalignment factor
- $F_e$  bearing equivalent load
- $m$  load-life exponent; either 3 for ball bearings or 10/3 for roller bearings

Factors  $\bar{D}$ ,  $\bar{E}$ , and  $\bar{F}$  are briefly reviewed here. The reader is referred to Bamberger (1971) for a complete discussion of all five life adjustment factors.

**Materials factors  $\bar{D}$  and  $\bar{E}$ .** – For over a century, AISI 52100 steel has been the predominant material for rolling-element bearings. In fact, the basic dynamic capacity as defined by AFMBA in 1949 is based on an air-melted 52100 steel, hardened to at least Rockwell C 58. Since that time, as discussed in section 5.1, better control of air-melting processes and the introduction of vacuum remelting processes have resulted in more homogeneous steels with fewer impurities. Such steels have extended rolling-element bearing fatigue lives to several times the AFBMA or catalog life. Life improvements of 3 to 8 times are not uncommon. Other steel compositions, such as AISI M-1 and AISI M-50, chosen for their higher temperature capabilities and resistance to corrosion, also have shown greater resistance to fatigue pitting when vacuum melting techniques are employed. Case-hardened materials, such as AISI 4620, AISI 4118, and AISI 8620, used primarily for roller bearings, have the advantage of a tough, ductile steel core with a hard, fatigue-resistant surface.

The recommended  $\bar{D}$  factors for various alloys processed by air melting are shown in table 16. Insufficient definitive life data with case-hardened materials were found to recommend  $\bar{D}$  factors for them. It is recommended that the user refer to the bearing manufacturer for the choice of a specific case-hardened material.

The metallurgical processing variables considered in the development of the  $\bar{E}$  factor included melting practice (air and vacuum melting) and metal working (thermo-mechanical working). Thermomechanical working of M-50 has also been shown to result in improved life, but in a practical sense it is costly and still not fully developed as a processing technique. Bamberger (1971) recommend an  $\bar{E}$  factor of 3 for consumable-electrode-vacuum-melted materials.

The translation of these factors into a standard (ISO, 1976) is discussed later.

**Lubrication factor  $\bar{F}$ .** – Until approximately 1960, the role of the lubricant between surfaces in rolling contact was not fully appreciated. Metal-to-metal contact was presumed to occur in all applications with attendant required boundary lubrication. The development of elastohydrodynamic lubrication theory showed that lubricant films of thicknesses of the order of microinches and tens of microinches occur in rolling contact. Since surface finishes are of the same order of magnitude as the lubricant film thicknesses, the significance of rolling-element bearing surface roughnesses to bearing performance became apparent. Tallian (1967) first reported on the importance to bearing life of the ratio of elastohydrodynamic lubrication film thickness to surface roughness. Figure 39 shows life as a percentage of



calculated  $L_{10}$  life as a function of  $\Lambda$ , where

$$\Lambda = h_{\min} / \sqrt{f_a^2 + f_b^2} \quad (77)$$

Figure 40, from Bamberger (1971), presents a curve of the recommended  $F$  factor as a function of the  $\Lambda$  parameter. A mean of the curves presented in Tallian (1967) for ball bearings and in Skurka (1970) for roller bearings is recommended for use. A formula for calculating the minimum film thickness  $h_{\min}$  is given in equation (74).

The results of Bamberger (1971) have not been fully accepted into the current AFBMA standard represented by ISO (1976). The standard presents the following:

- (1) Life and dynamic load rating formulas for radial and thrust ball bearings and radial and thrust roller bearings
  - (2) Tables of  $f_c$  for all cases
  - (3) Tables of  $X$  and  $Y$  factors for calculating equivalent loads
  - (4) Load rating formulas for multirow bearings
  - (5) Life correction factors for high-reliability levels  $a_1$ , materials  $a_2$ , and lubrication or operating conditions  $a_3$
- Procedures for calculating  $a_2$  and  $a_3$  are less than definitive, reflecting the need for additional research, life data, and operating experience.

### 13. Dynamic Analyses and Computer Codes

As has been stated, a precise analysis of rolling bearing kinematics, stresses, deflections, and life can be accomplished only by using a large-scale computer code. Presented here is a very brief discussion of some of the significant analyses that have led to the formulation of modern bearing analytical computer codes. The reader is referred to COSMIC, University of Georgia, Athens, GA 30601, for the public availability of program listings.

#### 13.1 Quasi-Static Analyses

Rolling-element bearing analysis began with the work of Jones on ball bearings (Jones, 1959 and 1960). Jones did his work before there was a general awareness of elastohydrodynamic lubrication and assumed Coulomb friction in the race contacts. This led to the commonly known "race control" theory, which assumes that pure rolling (except for Heathcote interfacial slip) can occur at one of the ball-race contacts. All of the spinning required for dynamic equilibrium of the balls would then take place at the other, or "noncontrolling," race contact. Jones' analysis proved to be quite effective for predicting fatigue life but less useful for predicting cage slip, which usually occurs at high speeds and light loads. Harris (1971b) extended Jones' analysis, retaining the

assumption of Coulomb friction but allowing a frictional resistance to gyroscopic moments at the noncontrolling as well as the controlling race contact. Harris' analysis

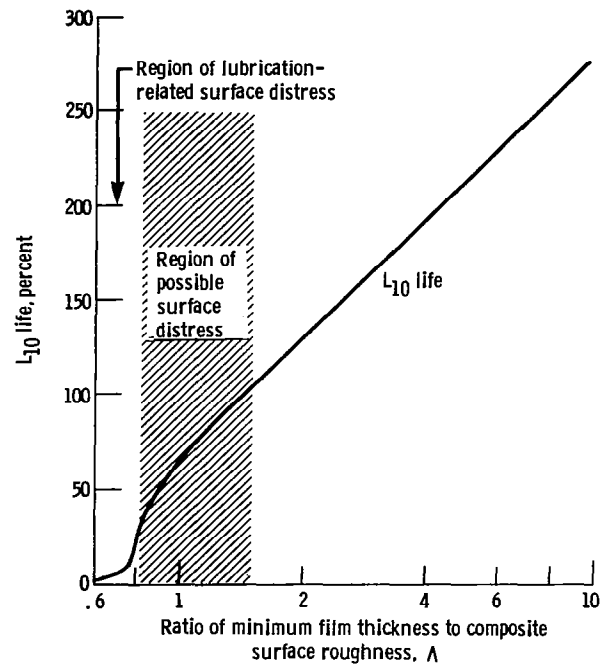


Figure 39. — Group fatigue life  $L_{10}$  as function of  $\Lambda$ . (From Tallian, 1967.)

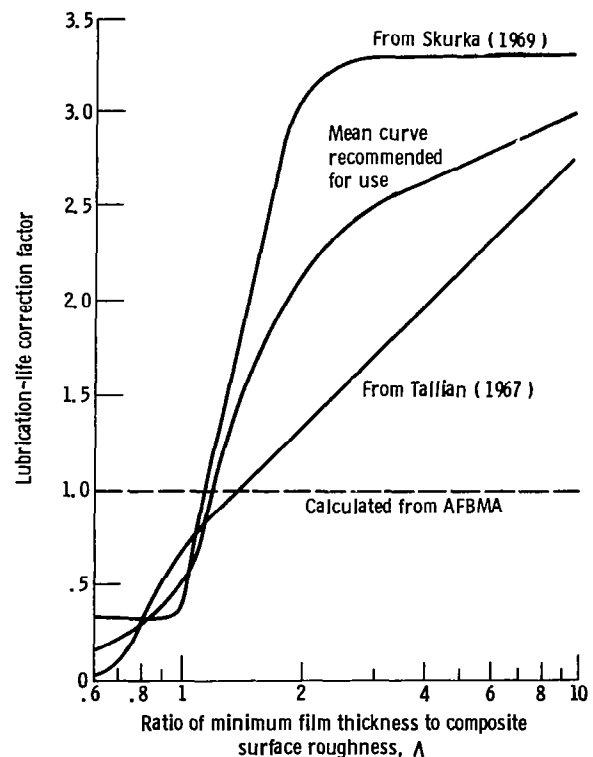


Figure 40. — Lubrication-life correction factor as function of  $\Lambda$ . (From Bamberger, et al., 1971.)

(1971b) is adequate for predicting bearing performance under conditions of dry-film lubrication or whenever there is a complete absence of any elastohydrodynamic film.

Harris (1971a) first incorporated elastohydrodynamic relationships into a ball bearing analysis. A revised version of Harris' computer program, called SHABERTH, was developed that incorporated actual traction data from a disk machine. The program SHABERTH has been expanded until today it encompasses ball, cylindrical roller, and tapered-roller bearings.

Harris (1966) first introduced elastohydrodynamics into a cylindrical roller bearing analysis. His initial analysis has been augmented with more precise viscosity-pressure and temperature relationships and traction data for the lubricant. This has evolved into the program CYBEAN and more recently has been incorporated into SHABERTH. Parallel efforts by Harris' associates have resulted in SPHERBEAN, a program that can be used to predict the performance of spherical roller bearings. These analyses can range from relatively simple force balance and life analyses through a complete thermal analysis of a shaft bearing system in several steps of varying complexity.

### 13.2 Dynamic Analyses

The work of Jones and Harris is categorized as quasi-static because it applies only when steady-state conditions prevail. Under highly transient conditions such as accelerations or decelerations, only a true dynamic analysis will suffice. Walters (1975) made the first attempt at a dynamic analysis to explain cage dynamics in gyro-spin-axis ball bearings. Gupta (1975) solved the generalized differential equations of motion of the ball in an angular-contact ball bearing. Gupta continued his dynamic analyses for both cylindrical roller bearings (1979a and b) and for ball bearings (1979c and d). Gupta's work is available in the program DREB.

## 14. Applications

In this section two applications of the film thickness equations developed throughout this report are presented to illustrate how the fluid-film lubrication conditions in machine elements can be analyzed. Specifically a typical roller and a typical ball bearing problem are considered.

### 14.1 Cylindrical Roller Bearing Problem

The equations for elastohydrodynamic film thickness that have been developed in section 11 relate primarily to elliptical contacts, but they are sufficiently general to allow them to be used with adequate accuracy in line-contact problems, as would be found in a cylindrical

roller bearing. Therefore the minimum elastohydrodynamic film thicknesses on the inner and outer races of a cylindrical roller bearing with the following dimensions are calculated:

Inner-race diameter, $d_i$ , mm	.....64 (0.064m)
Outer-race diameter, $d_o$ , mm	.....96 (0.096m)
Diameter of cylindrical rollers, $d$ , mm	.....16 (0.016m)
Axial length of cylindrical rollers, $l$ , mm	.....16 (0.016m)
Number of rollers in complete bearing, $n$	.....9

A bearing of this kind might well experience the following operating conditions:

Radial load, $F_r$ , N	.....10 800
Inner-race angular velocity, $\beta_i$ , rad/s	.....524
Outer-race angular velocity, $\beta_o$ , rad/s	.....0
Lubricant viscosity at atmospheric pressure at operating temperature of bearings, $\eta_0$ , N s/m <sup>2</sup>	.....0.01
Viscosity-pressure coefficient, $\xi$ , m <sup>2</sup> /N	..... $2.2 \times 10^{-8}$
Modulus of elasticity for both rollers and races, $E$ , N/m <sup>2</sup>	..... $2.075 \times 10^{11}$
Poisson's ratio, $\nu$	.....0.03

**Calculation.** – From equation (59), the most heavily loaded roller can be expressed as

$$F_{\max} = 4F_r/n = 4(10\,800\text{ N})/9 = 4800\text{ N} \quad (59)$$

Therefore, the radial load per unit length on the most heavily loaded roller is

$$F'_{\max} = 4800\text{ N}/0.016\text{ m} = 0.3\text{ MN/m} \quad (59)$$

From figure 41 we can write the radii of curvature as

$$r_{ax} = 0.008\text{ m}, r_{ay} = \infty$$

$$r_{bx,i} = 0.032\text{ m}, r_{by,i} = \infty$$

$$r_{bx,o} = 0.048\text{ m}, r_{by,o} = \infty$$

Then

$$1/R_{x,i} = 1/0.008 + 1/0.032 = 5/0.032 \quad (21)$$

giving  $R_{x,i} = 0.0064\text{ m}$ ,

$$1/R_{x,o} = 1/0.008 - 1/0.048 = 5/0.048 \quad (21)$$

giving  $R_{x,o} = 0.0096\text{ m}$ , and

$$\frac{1}{R_{y,i}} = \frac{1}{R_{y,o}} = \frac{1}{\infty} + \frac{1}{\infty} = 0 \quad (22)$$

giving  $R_{y,i} = R_{y,o} = \infty$ .

From the input information, the effective modulus of elasticity can be written as

$$E' = \frac{2}{\frac{1-\nu_a^2}{E_a} + \frac{1-\nu_b^2}{E_b}} = 2.28 \times 10^{11} \text{ N/m}^2 \quad (43)$$

For pure rolling, the surface velocity  $u$  relative to the lubricated conjunctions for a cylindrical roller is

$$u = |\omega_i - \omega_o| (d_e^2 - d^2) / 4d_e \quad (33)$$

where  $d_e$  is the pitch diameter and  $d$  is the roller diameter.

$$d_e = (d_o + d_i) / 2 = (0.096 + 0.064) / 2 = 0.08 \text{ m} \quad (1)$$

Hence

$$u = \frac{0.082 - 0.162}{4 \times 0.08} |524 - 0| = 10.061 \text{ m/s} \quad (33)$$

The dimensionless speed, materials, and load parameters for the inner- and outer-race conjunctions thus become

$$U_i = \frac{\eta_0 u}{E' R_{x,i}} = \frac{0.01 \times 10.061}{2.28 \times 10^{11} \times 0.0064} = 6.895 \times 10^{-11} \quad (72)$$

$$G_i = \xi E' = 5016 \quad (73)$$

$$W_i = \frac{F}{E' (R_{x,i})^2} = \frac{4800}{2.28 \times 10^{11} \times (0.0064)^2} = 5.140 \times 10^{-4} \quad (71)$$

$$U_o = \frac{\eta_0 u}{E' R_{x,o}} = \frac{0.01 \times 10.061}{2.28 \times 10^{11} \times 0.0096} = 4.597 \times 10^{-11} \quad (72)$$

$$G_o = \xi E' = 5016 \quad (73)$$

$$W_o = \frac{F}{E' (R_{x,o})^2} = \frac{4800}{2.28 \times 10^{11} \times (0.0096)^2} = 2.284 \times 10^{-4} \quad (71)$$

The appropriate elliptical-contact elastohydrodynamic film thickness equation for a fully flooded conjunction is developed in section 11.3 and recorded as equation (74):

$$H_{\min} = h_{\min} / R_x = 3.63 U^{0.68} G^{0.49} W^{-0.073} (1 - e^{-0.68k}) \quad (74)$$

In the case of a roller bearing,  $k = \infty$  and this equation reduces to

$$H_{\min} = 3.63 U^{0.68} G^{0.49} W^{-0.073}$$

The dimensionless film thickness for the *roller-inner-race* conjunction is

$$\begin{aligned} H_{\min} &= h_{\min} / R_{x,i} \\ &= 3.63 \times 1.231 \times 10^{-7} \times 65.04 \times 1.738 \\ &= 50.5 \times 10^{-6} \end{aligned}$$

and hence

$$h_{\min} = 0.0064 \times 50.5 \times 10^{-6} = 0.32 \text{ } \mu\text{m}$$

The dimensionless film thickness for the *roller-outer-race* conjunction is

$$\begin{aligned} H_{\min} &= h_{\min} / R_{x,o} \\ &= 3.63 \times 9.343 \times 10^{-8} \times 65.04 \times 1.844 \\ &= 40.7 \times 10^{-6} \end{aligned}$$

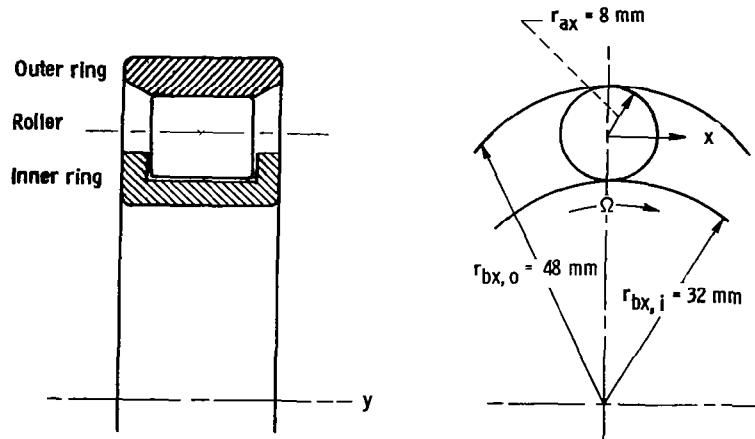


Figure 41. — Roller bearing example.  $r_{ay} = r_{by,i} = r_{by,o} = \infty$ .

and hence

$$h_{\min} = 0.0096 \times 40.7 \times 10^{-6} = 0.39 \mu\text{m}$$

It is clear from these calculations that the smaller minimum film thickness in the bearing occurs at the roller-inner-race conjunction, where the geometrical conformity is less favorable. It was found that, if the ratio of minimum film thickness to composite surface roughness is greater than 3, an adequate elasto-hydrodynamic film is maintained. This implies that a composite surface roughness of less than  $0.1 \mu\text{m}$  is needed to assure that an elasto-hydrodynamic film is maintained.

#### 14.2 Radial Ball Bearing Problem

Consider a single-row, radial, deep-groove ball bearing with the following dimensions:

Inner-race diameter, $d_i$ , m	0.052291
Outer-race diameter, $d_o$ , m	0.077706
Ball diameter, $d$ , m	0.012700
Number of balls in complete bearing, $n$	9
Inner-groove radius, $r_i$ , m	0.006604
Outer-groove radius, $r_o$ , m	0.006604
Contact angle, $\beta$ , deg	0
rms surface finish of balls, $f_b$ , $\mu\text{m}$	0.0625
rms surface finish of races, $f_a$ , $\mu\text{m}$	0.0175

A bearing of this kind might well experience the following operating conditions:

Radial load, $F_r$ , N	8900
Inner-race angular velocity, $\beta_i$ , rad/s	400
Outer-race angular velocity, $\beta_o$ , rad/s	0
Lubricant viscosity at atmospheric pressure and effective operating temperature of bearing, $\eta_0$ , N s/m <sup>2</sup>	0.04
Viscosity-pressure coefficient, $\xi$ , m <sup>2</sup> /N	$2.3 \times 10^{-8}$
Modulus of elasticity for both balls and races, $E$ , N/m <sup>2</sup>	$2 \times 10^{11}$
Poisson's ratio for both balls and races, $\nu$	0.3

The essential features of the geometry of the inner and outer conjunctions (figs. 5 and 11) can be ascertained as follows:

Pitch diameter (eq. (1))

$$d_e = 0.5(d_o + d_i) = 0.065 \text{ m}$$

Diametral clearance (eq. (2))

$$P_d = d_o - d_i - 2d = 1.5 \times 10^{-5} \text{ m}$$

Race conformity (eq. (3))

$$f_i = f_o = r/d = 0.52$$

Equivalent radius (eq. (23))

$$R_{x,i} = d(d_e - d)/2d_e = 0.00511 \text{ m}$$

Equivalent radius (eq. (25))

$$R_{x,o} = d(d_e + d)/2d_e = 0.00759 \text{ m}$$

Equivalent radius (eq. (24))

$$R_{y,i} = f_i d / (2f_i - 1) = 0.165 \text{ m}$$

Equivalent radius (eq. (26))

$$R_{y,o} = f_o d / (2f_o - 1) = 0.165 \text{ m}$$

The curvature sum

$$1/R_i = 1/R_{x,i} + 1/R_{y,i} = 201.76 \quad (19)$$

gives  $R_i = 4.956 \times 10^{-3} \text{ m}$ , and the curvature sum

$$1/R_o = 1/R_{x,o} + 1/R_{y,o} = 137.81 \quad (19)$$

gives  $R_o = 7.256 \times 10^{-3} \text{ m}$ . Also,  $\alpha_i = R_{y,i}/R_{x,i} = 32.35$  and  $\alpha_o = R_{y,o}/R_{x,o} = 21.74$ .

The nature of the Hertzian contact conditions can now be assessed.

Ellipticity parameters

$$\left. \begin{aligned} \bar{k}_i &= \alpha_i^2 / \pi = 9.42 \\ \bar{k}_o &= \alpha_o^2 / \pi = 7.09 \end{aligned} \right\} \quad (37)$$

Elliptic integrals

$$\left. \begin{aligned} q &= \pi/2 - 1 \\ \bar{\epsilon}_i &= 1 + q/\alpha_i = 1.0188 \\ \bar{\epsilon}_o &= 1 + q/\alpha_o = 1.0278 \end{aligned} \right\} \quad (38)$$

$$\left. \begin{aligned} \bar{\mathcal{F}}_i &= \frac{\pi}{2} + q \ln \alpha_i = 3.6205 \\ \bar{\mathcal{F}}_o &= \frac{\pi}{2} + q \ln \alpha_o = 3.3823 \end{aligned} \right\} \quad (39)$$

The effective elastic modulus  $E'$  is given by

$$E' = \frac{2}{\frac{1-\nu_a^2}{E_a} + \frac{1-\nu_b^2}{E_b}} = 2.198 \times 10^{11} \text{ N/m}^2$$

To determine the load carried by the most heavily loaded ball in the bearing, it is necessary to adopt an iterative procedure based on the calculation of local static compression and the analysis presented in section 8. Stribeck (1901) found that the value of  $Z$  was about 4.37 in the expression

$$F_{\max} = ZF_r/n \quad (57)$$

where

$F_{\max}$  load on most heavily loaded ball  
 $F_r$  radial load on bearing  
 $n$  number of balls

However, it is customary to adopt a value of  $Z=5$  in simple calculations in order to produce a conservative design, and this value will be used to begin the iterative procedure.

*Stage 1.* Assume  $Z=5$ . Then

$$F_{\max} = 5F_r/9 = 5/9 \times 8900 = 4944 \text{ N} \quad (57)$$

The maximum local elastic compression is

$$\delta_i = \mathcal{F}_i \left[ \left( \frac{9}{2\varepsilon_i R_i} \right) \left( \frac{F_{\max}}{\pi k_i E'} \right)^2 \right]^{1/3} = 2.902 \times 10^{-5} \text{ m} \quad (42)$$

$$\delta_o = \mathcal{F}_o \left[ \left( \frac{9}{2\varepsilon_o R_o} \right) \left( \frac{F_{\max}}{\pi k_o E'} \right)^2 \right]^{1/3} = 2.877 \times 10^{-5} \text{ m}$$

The sum of the local compressions on the inner and outer races is

$$\delta = \delta_i + \delta_o = 5.779 \times 10^{-5} \text{ m}$$

A better value for  $Z$  can now be obtained from

$$Z = \frac{\pi(1 - P_d/2\delta)^{3/2}}{2.491 \left\{ \left[ 1 + \left( \frac{1 - P_d/2\delta}{1.23} \right)^2 \right]^{1/2} - 1 \right\}}$$

since  $P_d/2\delta = (1.5 \times 10^{-5})/(5.779 \times 10^{-5}) = 0.1298$ .

Thus, from equation (30)

$$Z = 4.551$$

*Stage 2*

$$Z = 4.551$$

$$F_{\max} = (4.551 \times 8900)/9 = 4500 \text{ N}$$

$$\delta_i = 2.725 \times 10^{-5} \text{ m}$$

$$\delta_o = 2.702 \times 10^{-5} \text{ m}$$

$$\delta = 5.427 \times 10^{-5} \text{ m}$$

$$P_d/2\delta = 0.1382$$

Thus

$$Z = 4.565$$

*Stage 3*

$$Z = 4.565$$

$$F_{\max} = (4.565 \times 8900)/9 = 4514 \text{ N}$$

$$\delta_i = 2.731 \times 10^{-5} \text{ m}$$

$$\delta_o = 2.708 \times 10^{-5} \text{ m}$$

$$\delta = 5.439 \times 10^{-5} \text{ m}$$

$$P_d/2\delta = 0.1379$$

and hence

$$Z = 4.564$$

This value is very close to the previous value from stage 2 of 4.565, and a further iteration confirms its accuracy.

*Stage 4*

$$Z = 4.564$$

$$F_{\max} = (4.564 \times 8900)/9 = 4513 \text{ N}$$

$$\delta_i = 2.731 \times 10^{-5} \text{ m}$$

$$\delta_o = 2.707 \times 10^{-5} \text{ m}$$

$$\delta = 5.438 \times 10^{-5} \text{ m}$$

$$P_d/2\delta = 0.1379$$

and hence

$$Z = 4.564$$

The load on the most heavily loaded ball is thus 4513 N.

**Elastohydrodynamic minimum film thickness.** – For pure rolling

$$u = |\omega_o - \omega_i|(d_e^2 - d^2)/4d_e = 6.252 \text{ m/s} \quad (33)$$

The dimensionless speed, materials, and load parameters for the inner- and outer-race conjunctions thus become

$$\begin{aligned} U_i &= \frac{\eta_0 u}{E' R_{x,i}} \\ &= \frac{0.04 \times 6.252}{2.198 \times 10^{11} \times 5.11 \times 10^{-3}} = 2.227 \times 10^{-10} \end{aligned} \quad (72)$$

$$G_i = \xi E' = 2.3 \times 10^{-8} \times 2.198 \times 10^{11} = 5055 \quad (73)$$

$$\begin{aligned} W_i &= \frac{F}{E' (R_{x,i})^2} \\ &= \frac{4513}{2.198 \times 10^{11} \times (5.11)^2 \times 10^{-6}} = 7.863 \times 10^{-4} \end{aligned} \quad (71)$$

$$\begin{aligned} U_o &= \frac{\eta_0 u}{E' R_{x,o}} \\ &= \frac{0.04 \times 6.252}{2.198 \times 10^{11} \times 7.59 \times 10^{-3}} = 1.499 \times 10^{-10} \end{aligned} \quad (72)$$

$$G_o = \xi E' = 2.3 \times 10^{-8} \times 2.198 \times 10^{11} = 5055 \quad (73)$$

$$\begin{aligned} W_o &= \frac{F}{E' (R_{x,o})^2} \\ &= \frac{4513}{2.198 \times 10^{11} \times (7.59)^2 \times 10^{-6}} = 3.564 \times 10^{-4} \end{aligned} \quad (71)$$

The dimensionless minimum elastohydrodynamic film thickness in a fully flooded elliptical contact is given by equation (74).

$$\begin{aligned} H_{\min} &= h_{\min}/R_x \\ &= 3.63 U^{0.68} G^{0.49} W^{-0.073} (1 - e^{-0.68k}) \end{aligned} \quad (74)$$

*Ball-inner-race conjunction*

$$\begin{aligned} (H_{\min})_i &= 3.63 \times 2.732 \times 10^{-7} \times 65.29 \\ &\quad \times 1.685 \times 0.9983 \\ &= 1.09 \times 10^{-4} \end{aligned} \quad (74)$$

Thus

$$(h_{\min})_i = 1.09 \times 10^{-4} R_{x,i} = 0.557 \text{ } \mu\text{m}$$

The lubrication factor  $\Lambda$  discussed in section 12.5 was found to play a significant role in determining the fatigue life of rolling-element bearings. In this case

$$\begin{aligned} \Lambda_i &= \frac{(h_{\min})_i}{\sqrt{f_a^2 + f_b^2}} \\ &= \frac{0.557 \times 10^{-6}}{[(0.175)^2 + (0.06225)^2]^{1/2} \times 10^{-6}} = 3.00 \end{aligned} \quad (77)$$

*Ball-outer-race conjunction*

$$\begin{aligned} (H_{\min})_o &= (h_{\min})_o/R_{x,o} \\ &= 3.63 U_o^{0.68} G_o^{0.49} W_o^{-0.073} (1 - e^{-0.68k_o}) \\ &= 3.63 \times 2.087 \times 10^{-7} \times 65.29 \\ &\quad \times 1.785 \times 0.9919 \\ &= 0.876 \times 10^{-4} \end{aligned} \quad (74)$$

Thus

$$(h_{\min})_o = 0.876 \times 10^{-4} R_{x,o} = 0.665 \text{ } \mu\text{m}$$

In this case, the lubrication factor  $\Lambda$  is given by

$$\Lambda = \frac{0.665 \times 10^{-6}}{[(0.175)^2 + (0.0625)^2]^{1/2} \times 10^{-6}} = 3.58 \quad (77)$$

Once again, it is evident that the smaller minimum film thickness occurs between the most heavily loaded ball and the inner race. However, in this case the minimum elastohydrodynamic film thickness is about three times the composite surface roughness, and the bearing lubrication can be deemed to be entirely satisfactory. Indeed it is clear from figure 40 that very little

improvement in the lubrication factor  $F$  and thus in the fatigue life of the bearing could be achieved by further improving the minimum film thickness and hence  $\Lambda$ .









## References

- AFBMA (1960a) "Method of Evaluating Load Ratings for Roller Bearings," AFBMA Standard System No. 11 (Anti-Friction Bearings Manufacturers Association, Inc., New York, N.Y.).
- AFBMA (1960b) "Method of Evaluating Load Ratings for Ball Bearings," AFBMA Standard System No. 9, Revision No. 4 (Anti-Friction Bearing Manufacturers Association, Inc., New York, N.Y.).
- Anderson, N. E. and Zaretsky, E. V. (1975) "Short-Term Hot Hardness Characteristics of Five Case-Hardened Steels," NASA TN D-8031.
- Anderson, W. J. (1970) "Elastohydrodynamic Lubrication Theory as a Design Parameter for Rolling Element Bearings," ASME Paper 70-DE-19.
- Anderson, W. J. (1979) "Practical Impact of Elastohydrodynamic Lubrication," in *Proceedings of Fifth Leeds-Lyon Symposium in Tribology on "Elastohydrodynamics and Related Topics,"* D. Dowson, C. M. Taylor, M. Godet, and D. Berthe, eds., Mechanical Engineering Publication, Bury St. Edmunds, Suffolk, England, pp. 217-226.
- Anderson, W. J., Macks, E. J., and Nemeth, Z. N. (1954) "Comparison of Performance of Experimental and Conventional Cage Designs and Materials for 75-Millimeter-Bore Cylindrical Roller Bearings at High Speeds," NACA TR-1177.
- Bamberger, E. N. (1970) "Effect of Materials-Metallurgy Viewpoint," in *Interdisciplinary Approach to the Lubrication of Concentrated Contacts*, P. M. Ku, ed., NASA SP-237, 1970.
- Bamberger, E. N. (1971) *Life Adjustment Factors for Ball and Roller Bearings—An Engineering Design Guide*, American Society for Mechanical Engineers, New York, N.Y.
- Bamberger, E. N., Zaretsky, E. V., and Signer, H. (1976) "Endurance and Failure Characteristics of Main-Shaft Jet Engine Bearings at  $3 \times 10^6$  DN," ASME Trans., Journal of Lubrication Technology, vol. 98, series F, no. 4, pp. 580-585.
- Bamberger, E. N., et al. (1980) "Materials for Rolling Element Bearings," in *Bearing Design—Historical Aspects, Present Technology and Future Problems*, W. J. Anderson, ed., American Society of Mechanical Engineers, New York, N.Y. pp. 1-46.
- Bisson, E. E. and Anderson, W. J. (1964) *Advanced Bearing Technology*, NASA SP-38.
- Brown, P. F. (1970) "Bearings and Dampers for Advanced Jet Engines," SAE Paper 700318.
- Brown, P. F., Dobek, L. C., Hsing, F. C., and Miner, J. R. (1977) "Mainshaft High Speed Cylindrical Roller Bearings for Gas Engines," PWA-FR-8615, Pratt & Whitney Group, West Palm Beach, Fla.
- Cameron, A. and Gohar, R. (1966) "Theoretical and Experimental Studies of the Oil Film in Lubricated Point Contact," Proc. R. Soc. London, ser. A, vol. 291, pp. 520-536.
- Cundill, R. T. and Giordano, F. (1982) "Lightweight Materials for Rolling Elements in Aircraft Bearings," In *Problems in Bearing and Lubrication*, AGARD Conference Preprint No. 323, AGARD NATO, Paris, France, pp. 6-1 to 6-10.
- Dowson, D. and Hamrock, B. J. (1976) "Numerical Evaluation of the Surface Deformation of Elastic Solids Subjected to a Hertzian Contact Stress," ASLE Transaction, vol. 19, no. 4, pp. 279-286.
- ESDU (1965) "General Guide to the Choice of Journal Bearing Type," Engineering Science Data Unit, Item 65007, Institution of Mechanical Engineers, London, England.
- ESDU (1967) "General Guide to the Choice of Thrust Bearing Type," Engineering Science Data Unit, Item 67033, Institution of Mechanical Engineers, London, England.
- ESDU (1978) "Contact Stresses," Engineering Science Data Unit, Item 78035, Institution of Mechanical Engineers, London, England.
- Gupta, P. K. (1975) "Transient Ball Motion and Skid in Ball Bearings," ASME Journal of Lubrication Technology, vol. 97, no. 2, pp. 261-269.
- Gupta, P. K. (1979a) "Dynamics of Rolling Element Bearings—Part I, Cylindrical Roller Bearings Analysis," ASME Journal of Lubrication Technology, vol. 101, no. 3, pp. 293-304.
- Gupta, P. K. (1979b) "Dynamics of Rolling Element Bearings—Part II, Cylindrical Roller Bearing Results," ASME Journal of Lubrication Technology, vol. 101, no. 3, pp. 305-311.
- Gupta, P. K. (1979c) "Dynamics of Rolling Element Bearings—Part III, Ball Bearing Analysis," ASME Journal of Lubrication Technology, vol. 101, no. 3, pp. 312-318.
- Gupta, P. K. (1979d) "Dynamics of Rolling Element Bearings—Part IV, Ball Bearing Results," ASME Journal of Lubrication Technology, vol. 101, no. 3, pp. 319-326.
- Hamrock, B. J. and Anderson, W. J. (1973) "Analysis of an Arched Outer-Race Ball Bearing Considering Centrifugal Forces," ASME Journal of Lubrication Technology, vol. 95, no. 3, pp. 265-276.
- Hamrock, B. J. and Brewster, D. (1982) "Simplified Solution for Stresses and Deformations," ASME Journal of Lubrication Technology.
- Hamrock, B. J. and Dowson, D. (1976) "Isothermal Elastohydrodynamic Lubrication of Point Contacts, Part I—Theoretical Formulation," ASME Journal of Lubrication Technology, vol. 98, no. 22, pp. 223-229.
- Hamrock, B. J. and Dowson, D. (1977) "Isothermal Elastohydrodynamic Lubrication of Point Contacts, Part III—Fully Flooded Results," ASME Journal of Lubrication Technology, vol. 99, no. 2, pp. 264-276.
- Hamrock, B. J. and Dowson, D. (1981) *Ball Bearing Lubrication—The Elastohydrodynamics of Elliptical Contacts*, Wiley, New York, N.Y.
- Harris, T. A. (1966) "An Analytical Method to Predict Skidding in High Speed Roller Bearings," ASLE Transactions, vol. 9, pp. 229-241.
- Harris, T. A. (1971a) "An Analytical Method to Predict Skidding in Thrust-Loaded, Angular-Contact Ball Bearings," ASME Journal of Lubrication Technology, vol. 93, no. 1, pp. 17-24.
- Harris, T. A. (1971b) "Ball Motion in Thrust-Loaded, Angular Contact Bearings with Coulomb Friction," ASME Journal of Lubrication Technology, vol. 93, no. 1, pp. 32-38.
- Heathcote, H. L. (1921) "The Ball Bearing in the Making, Under Test and in Service," Proceedings of the Institute of Automotive Engineers, London, England, vol. 15, pp. 569-702.
- Hertz, H. (1881) "The Contact of Elastic Solids," J. Reine Angew. Math., vol. 92, pp. 156-171.
- ISO (1976) "Rolling Bearings, Dynamic Load Ratings and Rating Life," ISO/TC4/JC8, Revision of ISOR281. Issued by International Organization for Standardization, Technical Committee ISO/TC4.
- Johnson, K. L. and Tabor, D. (1967-68) "Rolling Friction," Proceedings of the Institution of Mechanical Engineers, vol. 182, part 3A, pp. 168-172.
- Jones, A. B. (1946) "Analysis of Stresses and Deflections," New Departure Engineering Data, General Motors Corp., Bristol, Conn.

- Jones, A. B. (1959) "Ball Motion and Sliding Friction in Ball Bearings," ASME Journal of Basic Engineering, vol. 81, no. 1, pp. 1-12.
- Jones, A. B. (1960) "A General Theory for Elastically Constrained Ball and Radial Roller Bearings Under Arbitrary Load and Speed Conditions," ASME Journal of Basic Engineering, vol. 82, no. 2, pp. 309-320.
- Jones, A. B. (1964) "The Mathematical Theory of Rolling Element Bearings," in *Mechanical Design and Systems Handbook*, H. A. Rothbart, ed., McGraw-Hill, New York, N.Y. pp. 13-1 to 13-76.
- Lundberg, G. and Palmgren, A. (1947) "Dynamic Capacity of Rolling Bearings," Acta Polytechnica, Mechanical Engineering Series, vol. I, no. 3.
- Lundberg, G. and Palmgren, A. (1952) "Dynamic Capacity of Rolling Bearings," Acta Polytechnica, Mechanical Engineering Series, vol. II, no. 4.
- Matt, R. J. and Gianotti, R. J. (1966) "Performance of High Speed Ball Bearings with Jet Oil Lubrication," Lubrication Engineering, vol. 22, no. 8, pp. 316-326.
- McCarthy, P. R. (1973) "Greases," in *Interdisciplinary Approach to Liquid Lubricant Technology*, P. M. Ku, ed., NASA SP-318, pp. 137-185.
- Miyakawa, Y., Seki, K., and Yokoyama, M. (1972) "Study on the Performance of Ball Bearings at High  $DN$  Values," NAL-TR-284, National Aerospace Lab., Tokyo, Japan. (NASA TTF-15017, 1973.)
- Palmgren, A. (1959) *Ball and Roller Bearing Engineering*, third ed., SKF Industries, Inc. Philadelphia, Pa.
- Parker, R. J. (1980) "Lubrication of Rolling Element Bearings," in *Bearing Design—Historical Aspects, Present Technology and Future Problems*, W. J. Anderson, ed., American Society of Mechanical Engineers, New York, N.Y., pp. 87-110.
- Parker, R. J. and Signer, H. R. (1978) "Lubrication of High-Speed, Large Bore Tapered-Roller Bearings," ASME Journal of Lubrication Technology, vol. 100, no. 1, pp. 31-38.
- Pirvics, J. (1980) "Numerical Analysis Techniques and Design Methodology for Rolling Element Bearing Load Support Systems," in *Bearing Design—Historical Aspects, Present Technology and Future Problems*, W. J. Anderson, ed., American Society of Mechanical Engineers, New York, N.Y., pp. 47-86.
- Reynolds, O. (1875) "On Rolling Friction," Philosophical Transactions of the Royal Society (London), part 1, vol. 166, pp. 155-174.
- Schuller, F. T. (1979) "Operating Characteristics of a Large-Bore Roller Bearing to Speed of  $3 \times 10^6 DN$ ," NASA TP-1413.
- Scibbe, H. W. (1968) "Bearing and Seal for Cryogenic Fluids," SAE Paper 680550.
- Sibley, L. W. (1982) "Silicon Nitride Bearing Elements for High Speed High Temperature Applications," AGARD Conference Proceedings no. 323, AGARD, NATO, Paris, France.
- Signer, H. R., Bamberger, E. N., and Zaretsky, E. V. (1974) "Parametric Study of the Lubrication of Thrust Loaded 120-mm Bore Ball Bearings to 3 Million  $DN$ ," ASME Journal of Lubrication Technology, vol. 96, no. 3, pp. 515-524.
- Signer, H. R. and Schuller, F. T. (1982) "Lubrication of 35-Millimeter-Bore Ball Bearings of Several Designs at Speeds to 2.5 Million  $DN$ ," In *Problems in Bearing and Lubrication*, AGARD Conference Preprint no. 323, AGARD NATO, Paris, France, pp. 8-1 to 8-15.
- Skurka, J. C. (1970) "Elastohydrodynamic Lubrication of Roller Bearings," ASME Journal of Lubrication Technology, vol. 92, no. 2, pp. 281-291.
- Stribeck, R. (1901) "Kugellager fur beliebige Belastungen," Z. Ver. dt. Ing., vol. 45, no. 3, pp. 73-125.
- Tabor, D. (1955) "The Mechanism of Rolling Friction. II. The Elastic Range," Proceedings of the Royal Society (London), part A, vol. 229, pp. 198-220.
- Tallian, T. E. (1967) "On Competing Failure Modes in Rolling Contact," Transactions ASLE, vol. 10, pp. 418-439.
- Todd, M. J. and Bentall, R. H. (1978) "Lead Film Lubrication in Vacuum," Proceedings of 2nd ASLE International Conference on Solid Lubrication, pp. 148-157.
- Walters, C. T. (1975) "The Dynamics of Ball Bearings," ASME Journal of Lubrication Technology, vol. 93, no. 1, pp. 1-10.
- Weibull, W. (1949) "A Statistical Representation of Fatigue Failures in Solids," Transactions Royal Institute of Technology, Stockholm, vol. 27.
- Zaretsky, E. V. and Anderson, W. J. (1966) "Material Properties and Processing Variables and Their Effect on Rolling-Element Fatigue," NASA TM X-52226.
- Zaretsky, E. V., Signer, H., and Bamberger, E. N. (1976) "Operating Limitations of High-Speed Jet-Lubricated Ball Bearings," ASME Journal of Lubrication Technology, vol. 98, no. 1, pp. 32-39.








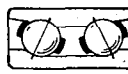

TABLE 1. - CHARACTERISTICS OF REPRESENTATIVE RADIAL BALL BEARINGS

Type	Approximate range of bore sizes, mm		Relative capacity		Limiting speed factor	Tolerance to misalignment
	Minimum	Maximum	Radial	Thrust		
Conrad or deep groove 	3	1060	1.00	<sup>a</sup> 0.7	1.0	±0°15'
Maximum capacity or filling notch 	10	130	1.2-1.4	<sup>a</sup> 0.2	1.0	±0°3'
Magneto or counterbored outer 	3	200	0.9-1.3	<sup>b</sup> 0.5-0.9	1.0	±0°5'
Airframe or aircraft control 	4.826	31.75	High static capacity	<sup>a</sup> 0.5	0.2	0°
Self-aligning, internal 	5	120	0.7	<sup>b</sup> 0.2	1.0	±2°30'
Self-aligning, external 	-----	-----	1.0	<sup>a</sup> 0.7	1.0	High
Double row, maximum 	6	110	1.5	<sup>a</sup> 0.2	1.0	±0°3'
Double row, deep groove 	6	110	1.5	<sup>a</sup> 1.4	1.0	0°

<sup>a</sup>Two directions.

<sup>b</sup>One direction.

TABLE 2. - CHARACTERISTICS OF REPRESENTATIVE ANGULAR-CONTACT BALL BEARINGS

Type	Approximate range of bore sizes, mm		Relative capacity		Limiting speed factor	Tolerance to misalignment
	Minimum	Maximum	Radial	Thrust		
One-directional thrust 	10	320	<sup>b</sup> 1.00-1.15	<sup>a, b</sup> 1.5-2.3	<sup>b</sup> 1.1-3.0	$\pm 0^{\circ} 2'$
Duplex, back to back 	10	320	1.85	<sup>c</sup> 1.5	3.0	0°
Duplex, face to face 	10	320	1.85	<sup>c</sup> 1.5	3.0	0°
Duplex, tandem 	10	320	1.85	<sup>a</sup> 2.4	3.0	0°
Two-directional or split ring 	10	110	1.15	<sup>c</sup> 1.5	3.0	$\pm 0^{\circ} 2'$
Double row 	10	140	1.5	<sup>c</sup> 1.85	0.8	0°
Double row, maximum 	10	110	1.65	<sup>a</sup> 0.5 <sup>d</sup> 1.5	0.7	0°




<sup>a</sup>One direction.

<sup>b</sup>Depends on contact angle.

<sup>c</sup>Two directions.

<sup>d</sup>In other direction.

TABLE 3. - CHARACTERISTICS OF REPRESENTATIVE THRUST BALL BEARINGS



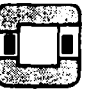






Type	Approximate range of bore sizes, mm		Relative capacity		Limiting speed factor	Tolerance to misalignment
	Minimum	Maximum	Radial	Thrust		
One directional, flat race 	6.45	88.9	0	<sup>a</sup> 0.7	0.10	<sup>b</sup> 0°
One directional, grooved race 	6.45	1180	0	<sup>a</sup> 1.5	0.30	0°
Two directional, grooved race 	15	220	0	<sup>c</sup> 1.5	0.30	0°

<sup>a</sup>One direction.

<sup>b</sup>Accepts eccentricity.

<sup>c</sup>Two directions.





TABLE 4. - CHARACTERISTICS OF REPRESENTATIVE CYLINDRICAL ROLLER BEARINGS

Type	Approximate range of bore sizes, mm		Relative capacity		Limiting speed factor	Tolerance to misalignment
	Minimum	Maximum	Radial	Thrust		
Separable outer ring, nonlocating (RN, RIN) 	10	320	1.55	0	1.20	$\pm 0^{\circ}5'$
Separable inner ring, nonlocating (RU, RIU) 	12	500	1.55	0	1.20	$\pm 0^{\circ}5'$
Separable outer ring, one-direction locating (RF, RIF) 	40	177.8	1.55	<sup>a</sup> Locating	1.15	$\pm 0^{\circ}5'$
Separable inner ring, one-direction locating (RJ, RIJ) 	12	320	1.55	<sup>a</sup> Locating	1.15	$\pm 0^{\circ}5'$
Self-contained, two-direction locating 	12	100	1.35	<sup>b</sup> Locating	1.15	$\pm 0^{\circ}5'$
Separable inner ring, two-direction locating (RT, RIT) 	20	320	1.55	<sup>b</sup> Locating	1.15	$\pm 0^{\circ}5'$
Nonlocating, full complement (RK, RIK) 	17	75	2.10	0	0.20	$\pm 0^{\circ}5'$
Double row, separable outer ring, nonlocating (RD) 	30	1060	1.85	0	1.00	0°
Double row, separable inner ring, nonlocating 	70	1060	1.85	0	1.00	0°

<sup>a</sup>One direction.

<sup>b</sup>Two directions.

TABLE 5. - CHARACTERISTICS OF REPRESENTATIVE SPHERICAL ROLLER BEARINGS

Type	Approximate range of bore sizes, mm		Relative capacity		Limiting speed factor	Tolerance to misalignment
	Minimum	Maximum	Radial	Thrust		
Single row, barrel or convex 	20	320	2.10	0.20	0.50	$\pm 2^\circ$
Double row, barrel or convex 	25	1250	2.40	0.70	0.50	$\pm 1^\circ 30'$
Thrust 	85	360	<sup>a</sup> 0.10 <sup>b</sup> 0.10	<sup>a</sup> 1.80 <sup>b</sup> 2.40	0.35-0.50	$\pm 3^\circ$
Double row, concave 	50	130	2.40	0.70	0.50	$\pm 1^\circ 30'$

<sup>a</sup>Symmetric rollers.

<sup>b</sup>Asymmetric rollers.

TABLE 6. - CHARACTERISTICS OF STANDARDIZED DOUBLE-ROW, SPHERICAL ROLLER BEARINGS




Type	Roller design	Retainer design	Roller guidance	Roller-race contact
SLB 	Symmetric	Machined, roller piloted	Retainer pockets	Modified line, both races
SC 	Symmetric	Stamped, race piloted	Floating guide ring	Modified line, both races
SD 	Asymmetric	Machined, race piloted	Inner-ring center rib	Line contact, outer; point contact, inner

TABLE 7. - CHARACTERISTICS OF SPHERICAL ROLLER BEARINGS

Series	Types	Approximate range of bore sizes, mm		Approximate relative capacity <sup>a</sup>		Limiting speed factor
		Minimum	Maximum	Radial	Thrust	
202	Single-row barrel	20	320	1.0	0.11	0.5
203	Single-row barrel	20	240	1.7	.18	.5
204	Single-row barrel	25	110	2.1	.22	.4
212	SLB	35	75	1.0	.26	.6
213	SLB	30	70	1.7	.53	↓
22, 22K	SLB, SC, SD	30	320	1.7	.46	↓
23, 23K	SLB, SC, SD	40	280	2.7	1.0	↓
30, 30K	SLB, SC, SD	120	1250	1.2	.29	.7
31, 31K	SLB, SC, SD	110	1250	1.7	.54	.6
32, 32K	SLB, SC, SD	100	850	2.1	.78	.6
39, 39K	SD	120	1250	.7	.18	.7
40, 40K	SD	180	250	1.5	----	.7

<sup>a</sup>Load capacities are comparative within the various series of spherical roller bearings only. For a given envelope size, a spherical roller bearing has a radial capacity approximately equal to that of a cylindrical roller bearing.

TABLE 8. - CHARACTERISTICS OF REPRESENTATIVE TAPERED ROLLER BEARINGS







Type	Subtype	Approximate range of bore sizes, mm	
		Minimum	Maximum
Single row (TS)  	TST - Tapered bore TSS - Steep angle TS - Pin cage TSE, TSK - keyway cones TSF, TSSF - flanged cup TSG - steering gear (without cone)	8 24 16 12 8	1690 430 1270 ---- 380 1070 ----
Two row, double cone, single cups (TDI)  	TDIK, TDIT, TDITP - tapered bore TDIE, TDIKE - slotted double cone TDIS - steep angle	30 30 24 55	1200 860 690 520
Two row, double cup, single cones, adjustable (TDO)  	TDO TDOS - steep angle	8 20	1830 1430
Two row, double cup, single cones, nonadjustable (TNA)  	TNA TNASW - slotted cones TNASWE - extended cone rib TNASWH - slotted cones, sealed TNADA, TNHDADX - self-aligning cup AD	20 30 20 8 ---	60 260 305 70 ----
Four row, cup adjusted (TQO)  	TQO, TQOT - tapered bore	70 250	1500 1500
Four row, cup adjusted (TQI)  	TQIT - tapered bore	---	----

TABLE 9. - CHARACTERISTICS OF REPRESENTATIVE NEEDLE ROLLER BEARINGS


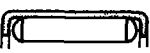


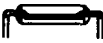


Type	Bore sizes, mm		Relative load capacity		Limiting speed factor	Misalignment tolerance
	Minimum	Maximum	Dynamic	Static		
Drawn cup, needle  Open end      Closed end	3	185	High	Moderate	0.3	Low
Drawn cup, needle, grease retained 	4	25	High	Moderate	0.3	Low
Drawn cup, roller  Open end      Closed end	5	70	Moderate	Moderate	0.9	Moderate
Heavy-duty roller 	16	235	Very high	Moderate	1.0	Moderate
Caged roller 	12	100	Very high	High	1.0	Moderate
Cam follower 	12	150	Moderate to high	Moderate to high	0.3-0.9	Low
Needle thrust 	6	105	Very high	Very high	0.7	Low

TABLE 10. - TYPICAL CHEMICAL COMPOSITIONS OF SELECTED BEARING STEELS (FROM BAMBERGER, 1980)

Designation	Alloying element, wt%											
	C	P (max)	S (max)	Mn	Si	Cr	V	W	Mo	Co	Cb	Ni
SAE 52100	1.00	0.025	0.025	0.35	0.30	1.45	----	----	----	----	----	----
MHT <sup>a</sup>	1.03	.025	.025	.35	.35	1.50	----	----	----	----	----	----
AISI M-1	.80	.030	.030	.30	.30	4.00	1.00	1.50	8.00	----	----	----
AISI M-2	.83			.30	.30	3.85	1.90	6.15	5.00	----	----	----
AISI M-10	.85			.25	.30	4.00	2.00	----	8.00	----	----	----
AISI M-50	.80			.30	.25	4.00	1.00	----	4.25	----	----	----
T-1 (18-4-1)	.70			.30	.25	4.00	1.00	18.0	----	----	----	----
T15	1.52	.010	.004	.26	.25	4.70	4.90	12.5	.20	5.10	----	----
440C	1.03	.018	.014	.48	.41	17.30	.14	----	.50	----	----	----
AMS 5749	1.15	.012	.004	.50	.30	14.50	1.20	----	4.00	----	----	----
Vasco Matrix II	.53	.014	.013	.12	.21	4.13	1.08	1.40	4.80	7.81	----	0.10
CRB-7	1.10	.016	.003	.43	.31	14.00	1.03	----	2.02	----	0.32	----
AISI 9310 <sup>b</sup>	.10	.006	.001	.54	.28	1.18	----	----	.11	----	----	3.15
CBS 600 <sup>b</sup>	.19	.007	.014	.61	1.05	1.50	----	----	.94	----	----	.18
CBS 1000M <sup>b</sup>	.14	.018	.019	.48	.43	1.12	----	----	4.77	----	----	2.94
Vasco X-2 <sup>b</sup>	.14	.011	.011	.24	.94	4.76	.45	1.40	1.40	.03	----	.10

<sup>a</sup>Also contains 1.36% Al.

<sup>b</sup>Carburizing grades.



TABLE 11. - COMPARISON OF NUMERICALLY DETERMINED VALUES WITH CURVE-FIT VALUES FOR GEOMETRICALLY DEPENDENT VARIABLES

[ $R_x = 1.0$  cm.]

Radius-of-curvature ratio, $\alpha$	Ellipticity parameter, $k$	Ellipticity		Complete elliptic integral of first kind			Complete elliptic integral of second kind		
		$\bar{k}$	Percent error, $e$	$\mathcal{E}$	$\bar{\mathcal{E}}$	Percent error, $e$	$\mathcal{E}$	$\bar{\mathcal{E}}$	Percent error, $e$
1.00	1.0000	1.0000	0	1.5708	1.5708	0	1.5708	1.5708	0
1.25	1.1604	1.1526	.66	1.6897	1.6892	-.50	1.4643	1.4566	.52
1.50	1.3101	1.2945	1.19	1.7898	1.8022	-.70	1.3911	1.3805	.76
1.75	1.4514	1.4280	1.61	1.8761	1.8902	-.75	1.3378	1.3262	.87
2.00	1.5858	1.5547	1.96	1.9521	1.9664	-.73	1.2972	1.2854	.91
3.00	2.0720	2.0125	2.87	2.1883	2.1979	-.44	1.2002	1.1903	.83
4.00	2.5007	2.4170	3.35	2.3595	2.3621	-.11	1.1506	1.1427	.69
5.00	2.8902	2.7860	3.61	2.4937	2.4895	.17	1.1205	1.1142	.57
6.00	3.2505	3.1289	3.74	2.6040	2.5935	.40	1.1004	1.0951	.48
7.00	3.5878	3.4515	3.80	2.6975	2.6815	.59	1.0859	1.0815	.40
8.00	3.9065	3.7577	3.81	2.7786	2.7577	.75	1.0751	1.0713	.35
9.00	4.2096	4.0503	3.78	2.8502	2.8250	.88	1.0666	1.0634	.30
10.00	4.4994	4.3313	3.74	2.9142	2.8851	1.00	1.0599	1.0571	.26
15.00	5.7996	5.6069	3.32	3.1603	3.1165	1.38	1.0397	1.0381	.15
20.00	6.9287	6.7338	2.81	3.3342	3.2807	1.60	1.0296	1.0285	.10
25.00	7.9440	7.7617	2.29	3.4685	3.4081	1.74	1.0236	1.0228	.07
30.00	8.8762	8.7170	1.79	3.5779	3.5122	1.84	1.0196	1.0190	.05
35.00	9.7442	9.6158	1.32	3.6700	3.6002	1.90	1.0167	1.0163	.04
40.00	10.5605	10.4689	.87	3.7496	3.6764	1.95	1.0146	1.0143	.03
45.00	11.3340	11.2841	.44	3.8196	3.7436	1.99	1.0129	1.0127	.02
50.00	12.0711	12.0670	.03	3.8821	3.8038	2.02	1.0116	1.0114	.02
60.00	13.4557	13.5521	-.72	3.9898	3.9078	2.06	1.0096	1.0095	.01
70.00	14.7430	14.9495	-1.40	4.0806	3.9958	2.08	1.0082	1.0082	.01
80.00	15.9522	16.2759	-2.03	4.1590	4.0720	2.09	1.0072	1.0071	.01
90.00	17.0969	17.5432	-2.61	4.2280	4.1393	2.10	1.0064	1.0063	0
100.00	18.1871	18.7603	-3.15	4.2895	4.1994	2.10	1.0057	1.0057	0

TABLE 12. - SIMPLIFIED EQUATIONS

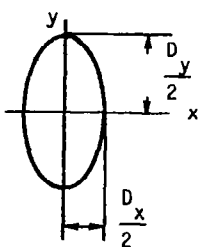
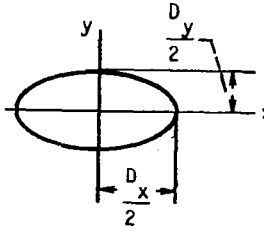
	
<p style="text-align: center;"><math>\alpha \geq 1</math></p> <p style="text-align: center;"><math>\bar{k} = \alpha^{2/\pi}</math></p> <p style="text-align: center;"><math>\bar{\nu} = \frac{\pi}{2} + q \ln \alpha</math></p> <p style="text-align: center;">where <math>q = \frac{\pi}{2} - 1</math></p> <p style="text-align: center;"><math>\bar{\rho} = 1 + \frac{q}{\alpha}</math></p> <p style="text-align: center;"><math>D_y = 2 \left( \frac{6k^2 \rho FR}{\pi E'} \right)^{1/3}</math></p> <p style="text-align: center;">where <math>R^{-1} = R_x^{-1} + R_y^{-1}</math></p> <p style="text-align: center;"><math>D_x = 2 \left( \frac{6 \rho FR}{\pi k E'} \right)^{1/3}</math></p> <p style="text-align: center;"><math>\delta = \rho \left[ \left( \frac{4.5}{\rho R} \right) \left( \frac{F}{\pi k E'} \right)^2 \right]^{1/3}</math></p>	<p style="text-align: center;"><math>\alpha &lt; 1</math></p> <p style="text-align: center;"><math>\bar{k} = \frac{2}{\alpha^{2/\pi}}</math></p> <p style="text-align: center;"><math>\bar{\nu} = \frac{\pi}{2} + q \ln \alpha</math></p> <p style="text-align: center;">where <math>q = \frac{\pi}{2} - 1</math></p> <p style="text-align: center;"><math>\bar{\rho} = 1 + q\alpha</math></p> <p style="text-align: center;"><math>D_y = 2 \left( \frac{6k \rho FR}{\pi E'} \right)^{1/3}</math></p> <p style="text-align: center;">where <math>R^{-1} = R_x^{-1} + R_y^{-1}</math></p> <p style="text-align: center;"><math>D_x = 2 \left( \frac{6 \rho FR}{\pi E' k^2} \right)^{1/3}</math></p> <p style="text-align: center;"><math>\delta = \rho \left[ \left( \frac{4.5}{\rho R} \right) \left( \frac{Fk}{\pi E'} \right)^2 \right]^{1/3}</math></p>

TABLE 13. - PRACTICAL APPLICATIONS FOR DIFFERING CONFORMITIES

[ $E' = 2.197 \times 10^7 \text{ N/cm}^2$ .]

Contact parameters	Wheel on rail	Ball on plane	Ball - outer-race contact
F	$1.00 \times 10^5 \text{ N}$	222.4111 N	222.4111 N
$r_{ax}$	50.1900 cm	0.6350 cm	0.6350 cm
$r_{ay}$	$\infty$	0.6350 cm	0.6350 cm
$r_{bx}$	$\infty$	$\infty$	-3.8900 cm
$r_{by}$	30.0000 cm	$\infty$	-0.6600 cm
$\alpha$	0.5977	1.0000	22.0905
k	0.7099	1.0000	7.3649
$\bar{k}$	0.7206	1.0000	7.1738
$\epsilon$	1.3526	1.5708	1.0267
$\bar{\epsilon}$	1.3412	1.5708	1.0258
$\epsilon$	1.8508	1.5708	3.3941
$\bar{\epsilon}$	1.8645	1.5708	3.3375
$D_y$	1.0783 cm	0.0426 cm	0.1842 cm
$\bar{D}_y$	1.0807 cm	0.0426 cm	0.1810 cm
$D_x$	1.5190 cm	0.0426 cm	0.0250 cm
$\bar{D}_x$	1.4997 cm	0.0426 cm	0.0252 cm
$\delta$	0.0106 cm	$7.13 \times 10^{-4} \text{ cm}$	$3.56 \times 10^{-4} \text{ cm}$
$\bar{\delta}$	0.0108 cm	$7.13 \times 10^{-4} \text{ cm}$	$3.57 \times 10^{-4} \text{ cm}$
$\sigma_{\max}$	$1.166 \times 10^5 \text{ N/cm}^2$	$2.34 \times 10^5 \text{ N/cm}^2$	$9.22 \times 10^4 \text{ N/cm}^2$
$\bar{\sigma}_{\max}$	$1.1784 \times 10^5 \text{ N/cm}^2$	$2.34 \times 10^5 \text{ N/cm}^2$	$9.30 \times 10^4 \text{ N/cm}^2$

TABLE 14. - CAPACITY FORMULAS FOR RECTANGULAR AND ELLIPTICAL CONTACTS

[Units in kg and mm.]

Function	Elliptical contact of ball bearings			Rectangular contact of roller bearings		
C	$f_c f_a i^{0.7} N^{2/3} d^{1.8}$			$f_c f_a i^{7/9} N^{3/4} d^{29/27} l_{t,i}^{7/9}$		
$f_c$	$g_c f_1 f_2 \left( \frac{d_i}{d_i - d} \right)^{0.41}$			$g_c f_1 f_2$		
$g_c$	$\left[ 1 + \left( \frac{C_i}{C_o} \right)^{10/8} \right]^{-0.8}$			$\left[ 1 + \left( \frac{C_i}{C_o} \right)^{9/2} \right]^{-2/9}$		
$C_i/C_o$	$f_3 \left[ \frac{d_i(d_o - d)}{d_o(d_i - d)} \right]^{0.41}$			$f_3 \left( \frac{l_{t,i}}{l_{t,o}} \right)^{7/9}$		
	Radial	Thrust		Radial	Thrust	
		$\beta \neq 90^\circ$	$\beta = 90^\circ$		$\beta \neq 90^\circ$	$\beta = 90^\circ$
$\gamma$	$\frac{d \cos \beta}{d_e}$		$\frac{d}{d_e}$	$\frac{d \cos \beta}{d_e}$		$\frac{d}{d_e}$
$f_a$	$(\cos \beta)^{0.7}$	$(\cos \beta)^{0.7} \tan \beta$	1	$(\cos \beta)^{7/9}$	$(\cos \beta)^{7/9} \tan \beta$	1
$f_1$	3.7-4.1	6-10		18-25	36-60	
$f_2$	$\frac{\gamma^{0.3}(1-\gamma)^{1.39}}{(1+\gamma)^{1/3}}$		$\gamma^{0.3}$	$\frac{\gamma^{2/9}(1-\gamma)^{29/27}}{(1+\gamma)^{1/3}}$		$\gamma^{2/9}$
$f_3$	$104f_4$	$f_4$	1	$1.14 f_4$	$f_4$	1
$f_4$	$\left( \frac{1-\gamma}{1+\gamma} \right)^{1.72}$			$\left( \frac{1-\gamma}{1+\gamma} \right)^{38/37}$		

TABLE 15. - CAPACITY FORMULAS FOR MIXED RECTANGULAR AND ELLIPTICAL CONTACTS

$$[C = C_i[1 + (C_i/C_o)^4]^{1/4}; \text{ units in kg and mm.}]$$

Function	Radial bearing		Thrust bearing		Radial bearing		Thrust bearing	
			$\beta \neq 90^\circ$	$\beta = 90^\circ$			$\beta \neq 90^\circ$	$\beta = 90^\circ$
	Inner race				Outer race			
$\gamma$	$\frac{d \cos \beta}{d_e}$		$\frac{d}{d_e}$		$\frac{d \cos \beta}{d_e}$		$\frac{d}{d_e}$	
	Rectangular contact $C_i$				Elliptical contact $C_o$			
$C_i$ or $C_o$	$f_1 f_2 f_a i^{7/9} N^{3/4} D^{29/27} l_{t,i}^{7/9}$				$f_1 f_2 f_a \left( \frac{2R}{D} \frac{r_o}{r_o - R} \right)^{0.41} i^{0.7} N^{2/3} D^{1.8}$			
$f_a$	$(\cos \beta)^{7/9}$	$(\cos \beta)^{7/9} \tan \beta$	1		$(\cos \beta)^{0.7}$	$(\cos \beta)^{0.7} \tan \beta$	1	
$f_1$	18-25		36-60		3.5-3.9		6-10	
$f_2$	$\frac{\gamma^{2/9} (1 - \gamma)^{29/27}}{(1 + \gamma)^{1/3}}$		$\gamma^{3/9}$		$\frac{\gamma^{0.3} (1 + \gamma)^{1.39}}{(1 - \gamma)^{1/3}}$		$\gamma^{0.3}$	
	Point contact $C_i$				Line contact $C_o$			
$C_i$ or $C_o$	$f_1 f_2 f_a \left( \frac{2R}{D} \frac{r_i}{r_i - R} \right)^{0.41} i^{0.7} N^{2/3} d^{1.8}$				$f_1 f_2 f_a i^{7/9} N^{3/4} d^{29/27} l_{t,o}^{7.9}$			
$f_a$	$(\cos \alpha)^{0.7}$	$(\cos \alpha)^{0.7} \tan \alpha$	1		$(\cos \alpha)^{7/9}$	$(\cos \alpha)^{7/9} \tan \alpha$	1	
$f_1$	3.7-4.1		6-10		15-22		36-60	
$f_2$	$\frac{\gamma^{0.3} (1 - \gamma)^{1.39}}{(1 + \gamma)^{1/3}}$		$\gamma^{0.3}$		$\frac{\gamma^{2/9} (1 + \gamma)^{29/27}}{(1 - \gamma)^{1/3}}$		$\gamma^{2/9}$	

TABLE 16. - MATERIAL FACTOR  
FOR THROUGH-HARDENED  
BEARING MATERIALS

[From Bamberger, et al.,  
1971; air-melted mate-  
rials assumed.]

Material	$\tilde{D}$ -Factor
52100	2.0
M-1	.6
M-2	.6
M-10	2.0
M-50	2.0
T-1	.6
Halmo	2.0
M-42	.2
WB 49	.6
440C	0.6-0.8

1. Report No. NASA RP-1105	2. Government Accession No.	3. Recipient's Catalog No.	
4. Title and Subtitle <b>ROLLING-ELEMENT BEARINGS</b>		5. Report Date June 1983	6. Performing Organization Code <b>505-32-42</b>
		8. Performing Organization Report No. <b>E-1440</b>	10. Work Unit No.
7. Author(s) <b>Bernard J. Hamrock and William J. Anderson</b>		11. Contract or Grant No.	
9. Performing Organization Name and Address <b>National Aeronautics and Space Administration Lewis Research Center Cleveland, Ohio 44135</b>		13. Type of Report and Period Covered <b>Reference Publication</b>	
		14. Sponsoring Agency Code	
12. Sponsoring Agency Name and Address <b>National Aeronautics and Space Administration Washington, D. C. 20546</b>		15. Supplementary Notes <b>Bernard J. Hamrock, Lewis Research Center; William J. Anderson, Consulting Engineer - Bearings and Lubrication, North Olmsted, Ohio. Published as Chapter 33 in Mechanical Design and Systems Handbook, McGraw-Hill Book Co., 1983.</b>	
16. Abstract Rolling-element bearings are a precision, yet simple, machine element of great utility. This report draws together the current understanding of rolling-element bearings. A brief history of rolling-element bearings is reviewed in the introduction, and subsequent sections describe the types of rolling-element bearings, their geometry and kinematics, as well as the materials they are made from and the manufacturing processes they involve. Unloaded and unlubricated rolling-element bearings are considered in Sections 1 to 6, loaded but unlubricated rolling-element bearings are considered in Sections 7 to 9, and loaded and lubricated rolling-element bearings are considered in Sections 10 to 14. The recognition and understanding of elasto-hydrodynamic lubrication, covered briefly in Sections 11, 12, and 14, represents one of the major developments in rolling-element bearings since the last edition of the Mechanical Design and Systems Handbook was published in 1964.			
17. Key Words (Suggested by Author(s)) Fatigue life; Elastohydrodynamic lubrication; Ball and roller bearings; Materials and manufacturing processes; Contact stresses and deformations; Static load capacity; Rolling friction and friction in bearings; Lubricants and lubrication systems		18. Distribution Statement <b>Unclassified - unlimited STAR Category 37</b>	
19. Security Classif. (of this report) <b>Unclassified</b>	20. Security Classif. (of this page) <b>Unclassified</b>	21. No. of Pages <b>59</b>	22. Price* <b>A02</b>